

ขั้นตอนวิธีเชิงตัวเลขสำหรับปัญหาการไหลผ่านของ
ของไหลอุดมคติที่ยุบตัวไม่ได้

นางเพียงพบ มนต์นวลปรางค์

วิทยานิพนธ์นี้เป็นส่วนหนึ่งของการศึกษาตามหลักสูตรปริญญาวิทยาศาสตรดุษฎีบัณฑิต

สาขาวิชาคณิตศาสตร์ประยุกต์

มหาวิทยาลัยเทคโนโลยีสุรนารี

ปีการศึกษา 2544

ISBN 974-533-036-1

**NUMERICAL ALGORITHMS FOR FLOWING-
THROUGH PROBLEM OF AN IDEAL
INCOMPRESSIBLE FLUID**

Ms. Peiangpob Mounnumprang

A Thesis Submitted in Partial Fulfillment of the Requirements
for the Degree of Doctor of Philosophy in Applied Mathematics
Suranaree University of Technology
Academic Year 2001
ISBN 974-533-036-1

**NUMERICAL ALGORITHMS FOR FLOWING-
THROUGH PROBLEM OF AN IDEAL
INCOMPRESSIBLE FLUID**

Suranaree University of Technology Council has approved this thesis submitted in partial fulfillment of the requirements for a Doctoral Degree.

Thesis Examining Committee

(Assoc. Prof. Dr. Prapasri Asawakun)
Chairman

(Assoc. Prof. Dr. Nikolay Moshkin)
Thesis Advisor

(Assoc. Prof. Dr. Tawit Chitsomboon)
Member

(Asst. Prof. Dr. Jack Asavanant)
Member

(Prof. Dr. Sergey Meleshko)
Member

(Assoc. Prof. Dr. Tawit Chitsomboon)
Vice Rector for Academic Affairs

(Assoc. Prof. Dr. Prasart Suebka)
Dean of the Institute of Science

เพียงพบ มนต์นวลปรางค์: ขั้นตอนวิธีเชิงตัวเลขสำหรับปัญหาการไหลผ่าน
ของของไหลอุดมคติที่ยุบตัวไม่ได้ (NUMERICAL ALGORITHMS FOR
FLOWING-THROUGH PROBLEM OF AN IDEAL INCOMPRESSIBLE
FLUID)

อ. ที่ปรึกษา: Assoc. Prof. Dr. Nikolay Moshkin, 126 หน้า

ISBN 974-533-036-1

วิทยานิพนธ์ฉบับนี้ เป็นการเสนองานวิจัยเกี่ยวกับ ขั้นตอนวิธีการเชิงตัวเลข สำหรับการไหลของของไหลอุดมคติที่ยุบตัวไม่ได้ ที่ไหลผ่านตลอดโดเมน ซึ่งมีช่องการไหลเข้า ไหลออก และ ส่วนที่ของไหลไม่สามารถไหลซึมผ่านขอบเขตของโดเมน กับสมการออยเลอร์ โดยใช้วิธีผลต่าง สืบเนื่อง สำหรับผลงานวิจัยฉบับนี้ ได้แสดงผลการวิจัยด้วยรูปภาพ ให้เห็นถึงรูปทรงต่างๆ กับเงื่อนไขขอบเขตสำหรับการไหลของของไหลที่แตกต่างกัน 3 กรณี ดังนี้

กรณีที่ 1 เมื่อกำหนดตัวประกอบเส้นสัมผัสของความเร็วหมุนวน และตัวประกอบแนวฉาก ของเวกเตอร์ความเร็ว ในส่วนของขอบเขตของโดเมนที่ของไหลมีการไหลเข้า และตัวประกอบแนวฉากของความเร็ว ในส่วนของขอบเขตของโดเมนที่ของไหลมีการไหลออก

กรณีที่ 2 เมื่อกำหนดตัวประกอบทั้งหมดของเวกเตอร์ความเร็ว ในส่วนของขอบเขตของโดเมนที่ของไหลมีการไหลเข้า และตัวประกอบแนวฉากของเวกเตอร์ความเร็ว ในส่วนของขอบเขตของโดเมนที่ของไหลมีการไหลออก

กรณีที่ 3 เหมือนกับกรณีที่ 2 เมื่อกำหนดตัวประกอบทั้งหมดของเวกเตอร์ความเร็ว ในส่วนของขอบเขตของโดเมนที่ของไหลมีการไหลเข้า และความดัน ในส่วนของขอบเขตของโดเมนที่ของไหลมีการไหลออก

สาขาวิชาคณิตศาสตร์

ปีการศึกษา 2544

ลายมือชื่อนักศึกษา.....

ลายมือชื่ออาจารย์ที่ปรึกษา.....

NUMERICAL ALGORITHMS FOR FLOWING-THROUGH PROBLEM
OF AN IDEAL INCOMPRESSIBLE FLUID
THESIS ADVISOR: ASSOC. PROF. DR. NIKOLAY MOSHKIN, Ph.D.
126 PP. ISBN 974-533-036-1

NUMERICAL ALGORITHM / FLOWING-THROUGH / IDEAL / INCOM-
PRESSIBLE FLUID / IMPERMEABLE / FINITE-DIFFERENCE / EULER
EQUATIONS / VORTICITY

This thesis is involved with a numerical method for an ideal incompressible fluid flow through a bounded domain with inflow, outflow and impermeable parts of the boundary. The finite-difference scheme is used to solve the Euler equations for certain geometries of flow domain and boundary conditions. The numerical algorithms can be useful in predicting flows for three different kinds of boundary conditions on inflow and outflow parts of the channel boundary.

In the first case it is given the tangent components of vorticity and normal component of the velocity vector on the inflow parts of domain boundary and only the normal component of the velocity vector on the outflow parts of channel boundary.

In the second case is given the whole vector of the velocity on inflow parts of domain boundaries and only the normal component of the velocity vector on the outflow parts of channel boundary.

In the third case the boundary condition on the inflow parts of the domain boundary is the same as in the second case and on the outflow parts only the pressure is given.

School of Mathematics

Student _____

Academic Year 2001

Advisor _____

Acknowledgements

I would like to express my sincere gratitude to my advisor Assoc. Prof. Dr. Nikolay P. Moshkin, School of Mathematics, Institute of Science, Suranaree University of Technology for his kind guidance and support throughout the course of this research. I have been working under his invaluable supervision for about five years and have had many unique research experiences which I will cherish throughout my life.

I am also very grateful to and would like to thank the Chairman of the School of Mathematics of Suranaree University of Technology, Assoc. Prof. Dr. Prapasri Asawakun and all the lecturers who taught and helped me during my study in Suranaree University of Technology. They are Assoc. Prof. Dr. Suwan Tangmanee, Assoc. Prof. Dr. Pairote Sattayatham, Prof. Dr. Sergey V. Meleshko, Assoc. Prof. Dr. B.I. Kvasov, Asst. Prof. Dr. Eckart Schulz and Asst. Prof. Dr. Arjuna Chaiyasena for their help, advice and support.

I want to express my appreciation to Anirut Laudsong, Paladorn Suwanapho, Apichai Hematulin, Asst. Prof. Supot Witayangkurn, Jessada Tantannuch, Dr. Wei Wei, Mana Kaomek and Anusorn Ruchirabha for their invaluable professional guidance and friendly encouragement.

In addition, I wish to express my special thanks to Rajabhat Institute Petchburiwittayalongkorn and Government of France for offering the scholarship which enabled me to continue my advanced studies in Suranaree University of Technology, Thailand.

Peiangpob Mounnumprang

Contents

| | Page |
|---|------------|
| Abstract in Thai | I |
| Abstract in English | II |
| Acknowledgements | III |
| Contents | IV |
| List of Tables | VI |
| List of Figures | VII |
| Chapter | |
| I Introduction | 1 |
| 1.1 Purpose and Background of the Research | 1 |
| 1.2 General Considerations on the Euler Equations | 2 |
| 1.2.1 The Equation of Motion of an Ideal Incompressible Fluid | 2 |
| 1.2.2 Vorticity and Stream Function | 3 |
| 1.2.3 Conservation Laws | 5 |
| 1.2.4 Potential and Irrotational Flows | 7 |
| 1.2.5 Historical Comments | 8 |
| 1.2.6 Existence and Uniqueness of the Solution | 9 |
| 1.2.7 Comment (Existence and Uniqueness) | 9 |
| 1.3 Mathematical Formulation of Flowing-Through Problems . . | 10 |
| 1.4 Review of Literatures | 12 |
| 1.4.1 Theoretical Investigation of Initial Boundary Value Problems for Euler Equations | 12 |
| 1.4.2 Analyzing Numerical Schemes | 13 |
| 1.5 Survey of the Thesis | 14 |
| II Numerical Methods for Steady Flowing-Through Problems: Problem 2 and Problem 3 | 16 |
| 2.1 Introduction | 16 |
| 2.2 Mathematical Formulation | 16 |
| 2.2.1 The Euler Equations in Terms of New Unknown Func- tion $w(x, y)$ and $q(x, y)$ | 18 |

Contents (Continued)

| Chapter | Page |
|--|---|
| 2.2.2 | Transformation from Cartesian Coordinates (x,y) to Generalized Curvilinear Coordinates (φ, ψ) 21 |
| 2.2.3 | The Equations in New Generalized Curvilinear Coordinates (φ, ψ) 24 |
| 2.3 | Discretization of the Equations and the Solution Procedure . 32 |
| 2.3.1 | The Method of Block SOR 38 |
| 2.3.2 | The Method of Stabilizing Corrections 40 |
| 2.3.3 | Interpretation and Presentation of Results of Numerical Calculations 40 |
| 2.4 | Results and Discussions 44 |
| 2.4.1 | 90 Degree Elbow with Contraction 44 |
| 2.4.2 | Convergence of Numerical Algorithm 45 |
| 2.4.3 | Numerical Results for 90 Degree Elbow with Contraction 49 |
| 2.4.4 | Numerical Results for Two-Dimensional Channel with Curved Walls 58 |
| 2.4.5 | Numerical Results for α Degree Elbow 73 |
| 2.5 | Conclusions 75 |
| III Numerical Methods for Steady Flowing-Through Problem: | |
| | Problem 1 80 |
| 3.1 | Introduction 80 |
| 3.2 | Mathematical Statement of the Problem 80 |
| 3.3 | Problem in Two-Dimensional Generalized Curvilinear Coordinates 81 |
| 3.4 | Relations between Metric and Differential Equations 82 |
| 3.5 | Discretization of the Equations and the Solution Procedure . 85 |
| 3.6 | Convergence, Results and Discussions 89 |
| 3.6.1 | Euler Equations with Exact Solution 89 |
| 3.6.2 | Flowing Through a Channel with Curved Walls 94 |
| 3.7 | Conclusions 111 |
| IV Conclusions 112 | |
| References 115 | |
| Appendix | |
| A. | Examples of MAPLE Program. 120 |
| Curriculum Vitae 126 | |

List of Tables

| Table | Page |
|--|------|
| 2.1 Convergence to exact solution. The results of numerical simulations for different grids for 90 degree elbow. | 46 |
| 2.2 Rate of convergence of numerical algorithm. | 47 |
| 2.3 The choice of the relaxation parameter. The results of numerical calculations for the case of 90 degree elbow with $x_0 = 2.0$, $y_0 = 2.0$, $R_1 = 1.0$, $R_2 = 2.0$, $\frac{R_2 - R_1}{R_2} = \frac{1}{2}$ | 48 |
| 2.4 Detailed description of data of numerical simulations for 90 degree elbow with contraction. Tolerance criteria $\epsilon_\phi = 10^{-4}$, $\epsilon_w = 10^{-4}$, $\epsilon_q = 10^{-4}$ | 49 |
| 2.5 The maximum of $ \varphi_{C'D'}(\psi) $ for different length of exit for 90 degree elbow with contraction, $y_0 = 2$, $R_1 = 1$, $R_2 = 2$ | 57 |
| 2.6 Results of numerical simulations for different grids. | 59 |
| 2.7 Choices of the relaxation parameter for channel with curved walls $x_{1t} = 1.0$, $x_{2t} = 2.0$, $x_{Lt} = 5.0$, $h_t = 0.0$, $x_{1d} = 2.0$, $x_{2d} = 3.0$, $x_{Ld} = 5.0$, $h_d = 0.05$ | 60 |
| 2.8 Detailed description of results of numerical simulations with tolerances criteria $\epsilon_\phi = 10^{-4}$, $\epsilon_w = 10^{-4}$, $\epsilon_q = 10^{-4}$. Channel with curve walls. | 61 |
| 2.9 Detailed descriptions of numerical experiments on different grids for α degree elbow with $L_{x_0} = 2.0$, $y_0 = 2.0$, $R_1 = 1.0$, $R_2 = 2.0$ | 74 |
| 3.1 Absolute errors of stream function and vorticity and rate of convergence for test problem (3.6.5). | 92 |
| 3.2 Absolute errors of stream function and vorticity and rate of convergence for test problem (3.6.9). | 92 |
| 3.3 Computed error parameters, sensitivity. | 97 |

List of Figures

| Figure | Page |
|--|------|
| 1.1 Evolving in time of closed curve. | 6 |
| 1.2 Normal vector on surface. | 7 |
| 1.3 | 8 |
| 1.4 Sketch of a domain. | 11 |
| 2.1 Sketch of a physical domain. | 17 |
| 2.2 Physical and computational domain. | 21 |
| 2.3 Domain $A'B'C'D'$ for problem 3'. | 30 |
| 2.4 Domain $A'B'C'D'$ for problem 2'. | 31 |
| 2.5 Sketch of finite difference grid. | 34 |
| 2.6 Flowchart of the iterative process. | 38 |
| 2.7 Computational stencil for finite difference equation (2.3.5). | 39 |
| 2.8 Sketch of an elbow-shaped domain and coordinates. | 45 |
| 2.9 Pressure contours for 90 degree elbow with contraction, $\frac{R_2-R_1}{R_2} = \frac{2}{3}$ | 51 |
| 2.10 Pressure contours for 90 degree elbow with contraction, $\frac{R_2-R_1}{R_2} = \frac{1}{2}$ | 51 |
| 2.11 Pressure contours for 90 degree elbow with contraction, $\frac{R_2-R_1}{R_2} = \frac{1}{3}$ | 52 |
| 2.12 Pressure contours for 90 degree elbow with contraction, $\frac{R_2-R_1}{R_2} = \frac{1}{3}$ | 52 |
| 2.13 Colored graphics of pressure contours for 90 degree elbow with contraction, $\frac{R_2-R_1}{R_2} = \frac{2}{3}$ | 53 |
| 2.14 Colored graphics of pressure contours for 90 degree elbow with contraction, $\frac{R_2-R_1}{R_2} = \frac{1}{2}$ | 53 |
| 2.15 Colored graphics of pressure contours for 90 degree elbow with contraction, $\frac{R_2-R_1}{R_2} = \frac{1}{3}$ | 54 |
| 2.16 Colored graphics of pressure contours for 90 degree elbow with contraction, $\frac{R_2-R_1}{R_2} = \frac{1}{3}$ | 54 |
| 2.17 Velocity vectors for 90 degree elbow with contraction, $\frac{R_2-R_1}{R_2} = \frac{2}{3}$ | 55 |
| 2.18 Streamlines for 90 degree elbow with contraction, $\frac{R_2-R_1}{R_2} = \frac{2}{3}$ | 55 |
| 2.19 Pressure as a function of φ along streamlines $\psi = -1, -0.5, 0$ for 90 degree elbow with contraction, $\frac{R_2-R_1}{R_2} = \frac{2}{3}, R_1 = 1, R_2 = 3, x_0 = 2, y_0 = 2, P_{CD} = 2$ | 56 |
| 2.20 Modulus of the velocity vector as a function of φ along streamline $\psi = -1, -0.5, 0$ for 90 degree elbow with contraction, $\frac{R_2-R_1}{R_2} = \frac{2}{3}, R_1 = 1, R_2 = 3, x_0 = 2, y_0 = 2, P_{CD} = 2$ | 56 |
| 2.21 Graph of $C'D'$ boundary for 90 degree elbow with contraction, $\frac{R_2-R_1}{R_2} = \frac{2}{3}, R_1 = 1, R_2 = 3, x_0 = 2, y_0 = 2, P_{CD} = 2$ | 57 |

List of Figures (Continued)

| Figure | Page |
|---|------|
| 2.22 Physical domain. | 58 |
| 2.23 Pressure contours by T. W. Roberts et al. Contour increment $\Delta P = 0.01$ | 62 |
| 2.24 Pressure contours for channel with curved walls. Results of numerical simulations for $x_{1d} = 1$, $x_{2d} = 2$, $x_{Ld} = 3$, $h_d = 0.05$, $N1 = 97$, $N2 = 33$. Contour increment $\Delta P = 0.01$ | 62 |
| 2.25 Pressure contours for channel with curved walls. Results of numerical simulations for $x_{1t} = 0$, $x_{2t} = 0$, $x_{Lt} = 3$, $h_t = 0$, $x_{1d} = 1$, $x_{2d} = 2$, $x_{Ld} = 3$, $h_d = 0.04$, $N1 = 41$, $N2 = 41$ | 63 |
| 2.26 Pressure contours for channel with curved walls. Results of numerical simulations for $x_{1t} = 0$, $x_{2t} = 0$, $x_{Lt} = 3$, $h_t = 0$, $x_{1d} = 1$, $x_{2d} = 2$, $x_{Ld} = 3$, $h_d = 0.1$, $N1 = 41$, $N2 = 41$ | 63 |
| 2.27 Pressure contours for channel with curved walls. Results of numerical simulations for $x_{1t} = 0$, $x_{2t} = 0$, $x_{Lt} = 3$, $h_t = 0$, $x_{1d} = 1$, $x_{2d} = 2$, $x_{Ld} = 3$, $h_d = -0.07$, $N1 = 41$, $N2 = 41$ | 64 |
| 2.28 Pressure contours for channel with curved walls. Results of numerical simulations for $x_{1t} = 0$, $x_{2t} = 0$, $x_{Lt} = 3$, $h_t = 0$, $x_{1d} = 1.5$, $x_{2d} = 2.5$, $x_{Ld} = 3$, $h_d = -0.03$, $N1 = 41$, $N2 = 41$ | 64 |
| 2.29 Pressure contours for channel with curved walls. Results of numerical simulations for $x_{1t} = 2$, $x_{2t} = 3$, $x_{Lt} = 5$, $h_t = -0.1$, $x_{1d} = 2$, $x_{2d} = 3$, $x_{Ld} = 5$, $h_d = 0.1$, $N1 = 41$, $N2 = 41$ | 65 |
| 2.30 Pressure contours for channel with curved walls. Results of numerical simulations for $x_{1t} = 2$, $x_{2t} = 3$, $x_{Lt} = 5$, $h_t = -0.1$, $x_{1d} = 2.5$, $x_{2d} = 3.5$, $x_{Ld} = 5$, $h_d = 0.1$, $N1 = 41$, $N2 = 41$ | 65 |
| 2.31 Pressure contours for channel with curved walls. Results of numerical simulations for $x_{1t} = 1$, $x_{2t} = 2$, $x_{Lt} = 5$, $h_t = -0.03$, $x_{1d} = 2$, $x_{2d} = 3$, $x_{Ld} = 5$, $h_d = 0.03$, $N1 = 61$, $N2 = 61$ | 66 |
| 2.32 Pressure contours for channel with curved walls. Results of numerical simulations for $x_{1t} = 1$, $x_{2t} = 2$, $x_{Lt} = 5$, $h_t = -0.1$, $x_{1d} = 3$, $x_{2d} = 4$, $x_{Ld} = 5$, $h_d = 0.1$, $N1 = 41$, $N2 = 41$ | 66 |
| 2.33 Pressure contours for channel with curved walls. Results of numerical simulations for $x_{1t} = 2$, $x_{2t} = 3$, $x_{Lt} = 5$, $h_t = 0.2$, $x_{1d} = 2$, $x_{2d} = 3$, $x_{Ld} = 5$, $h_d = -0.2$, $N1 = 61$, $N2 = 61$ | 67 |
| 2.34 Pressure contours for channel with curved walls. Results of numerical simulations for $x_{1t} = 2$, $x_{2t} = 3$, $x_{Lt} = 5$, $h_t = 0.1$, $x_{1d} = 2$, $x_{2d} = 3$, $x_{Ld} = 5$, $h_d = -0.1$, $N1 = 41$, $N2 = 41$ | 67 |
| 2.35 Pressure contours for channel with curved walls. Results of numerical simulations for $x_{1t} = 2$, $x_{2t} = 3$, $x_{Lt} = 5$, $h_t = 0.05$, $x_{1d} = 2.5$, $x_{2d} = 3.5$, $x_{Ld} = 5$, $h_d = -0.05$, $N1 = 41$, $N2 = 41$ | 68 |

List of Figures (Continued)

| Figure | Page |
|---|------|
| 2.36 Pressure contours for channel with curved walls. Results of numerical simulations for $x_{1t} = 2$, $x_{2t} = 3$, $x_{Lt} = 5$, $h_t = 0.05$, $x_{1d} = 3$, $x_{2d} = 4$, $x_{Ld} = 5$, $h_d = -0.05$, $N_1 = 41$, $N_2 = 41$ | 68 |
| 2.37 Pressure contours for channel with curved walls. Results of numerical simulations for $x_{1t} = 2$, $x_{2t} = 3$, $x_{Lt} = 5$, $h_t = -0.1$, $x_{1d} = 2$, $x_{2d} = 3$, $x_{Ld} = 5$, $h_d = -0.1$, $N_1 = 41$, $N_2 = 41$ | 69 |
| 2.38 Pressure contours for channel with curved walls. Results of numerical simulations for $x_{1t} = 2$, $x_{2t} = 3$, $x_{Lt} = 5$, $h_t = -0.1$, $x_{1d} = 2.5$, $x_{2d} = 3.5$, $x_{Ld} = 5$, $h_d = -0.1$, $N_1 = 41$, $N_2 = 41$ | 69 |
| 2.39 Streamlines for channel with curved walls. Results of numerical simulations for $x_{1t} = 1$, $x_{2t} = 2$, $x_{Lt} = 5$, $h_t = -0.1$, $x_{1d} = 2$, $x_{2d} = 3$, $x_{Ld} = 5$, $h_d = 0.1$, $N_1 = 21$, $N_2 = 21$ | 70 |
| 2.40 Streamlines for channel with curved walls. Results of numerical simulations for $x_{1t} = 2$, $x_{2t} = 3$, $x_{Lt} = 5$, $h_t = 0.2$, $x_{1d} = 2$, $x_{2d} = 3$, $x_{Ld} = 5$, $h_d = -0.2$, $N_1 = 21$, $N_2 = 21$ | 70 |
| 2.41 Velocity vectors for channel with curved walls. Results of numerical simulations for $x_{1t} = 1$, $x_{2t} = 2$, $x_{Lt} = 5$, $h_t = -0.1$, $x_{1d} = 2$, $x_{2d} = 3$, $x_{Ld} = 5$, $h_d = 0.1$, $N_1 = 21$, $N_2 = 21$ | 71 |
| 2.42 Velocity vectors for channel with curved walls. Results of numerical simulations for $x_{1t} = 2$, $x_{2t} = 3$, $x_{Lt} = 5$, $h_t = 0.2$, $x_{1d} = 2$, $x_{2d} = 3$, $x_{Ld} = 5$, $h_d = -0.2$, $N_1 = 21$, $N_2 = 21$ | 71 |
| 2.43 Colored graphics of pressure contours for channel with curved walls. Results of numerical simulations for $x_{1t} = 1$, $x_{2t} = 2$, $x_{Lt} = 5$, $h_t = -0.1$, $x_{1d} = 2$, $x_{2d} = 3$, $x_{Ld} = 5$, $h_d = 0.1$, $N_1 = 61$, $N_2 = 61$ | 72 |
| 2.44 Colored graphics of pressure contours for channel with curved walls. Results of numerical simulations for $x_{1t} = 2$, $x_{2t} = 3$, $x_{Lt} = 5$, $h_t = 0.2$, $x_{1d} = 2$, $x_{2d} = 3$, $x_{Ld} = 5$, $h_d = -0.2$, $N_1 = 61$, $N_2 = 61$ | 72 |
| 2.45 Geometry of α° elbow channel. | 73 |
| 2.46 Pressure contours for channel with curved walls. Results of numerical simulations for $R_1 = 1$, $R_2 = 2$, $L_{x0} = 2$, $y_0 = 2$, $\alpha = \pi/2$, $N_1 = 41$, $N_2 = 41$ | 76 |
| 2.47 Pressure contours for channel with curved walls. Results of numerical simulations for $R_1 = 1$, $R_2 = 2$, $L_{x0} = 2$, $y_0 = 2$, $\alpha = 3\pi/4$, $N_1 = 21$, $N_2 = 21$ | 76 |
| 2.48 Pressure contours for channel with curved walls. Results of numerical simulations for $R_1 = 1$, $R_2 = 2$, $L_{x0} = 2$, $y_0 = 2$, $\alpha = \pi$, $N_1 = 21$, $N_2 = 21$ | 77 |

List of Figures (Continued)

| Figure | Page |
|---|------|
| 2.49 Pressure contours for channel with curved walls. Results of numerical simulations for $R_1 = 1$, $R_2 = 2$, $L_{x0} = 2$, $y_0 = 2$, $\alpha = 5\pi/4$, $N_1 = 21$, $N_2 = 21$ | 77 |
| 2.50 Colored graphics of pressure contours for channel with curved walls. Results of numerical simulations for $R_1 = 1$, $R_2 = 2$, $L_{x0} = 2$, $y_0 = 2$, $\alpha = \pi/2$, $N_1 = 41$, $N_2 = 41$ | 78 |
| 2.51 Colored graphics of pressure contours for channel with curved walls. Results of numerical simulations for $R_1 = 1$, $R_2 = 2$, $L_{x0} = 2$, $y_0 = 2$, $\alpha = 3\pi/4$, $N_1 = 21$, $N_2 = 21$ | 78 |
| 2.52 Colored graphics of pressure contours for channel with curved walls. Results of numerical simulations for $R_1 = 1$, $R_2 = 2$, $L_{x0} = 2$, $y_0 = 2$, $\alpha = \pi$, $N_1 = 21$, $N_2 = 21$ | 79 |
| 2.53 Colored graphics of pressure contours for channel with curved walls. Results of numerical simulations for $R_1 = 1$, $R_2 = 2$, $L_{x0} = 2$, $y_0 = 2$, $\alpha = 5\pi/4$, $N_1 = 21$, $N_2 = 21$ | 79 |
| 3.1 Physical and computational domain. | 82 |
| 3.2 Computational domain. | 86 |
| 3.3 Stencil of the finite-difference equation for ω | 88 |
| 3.4 Flow domain of the test problem. | 90 |
| 3.5 Pressure contours for solution (3.6.5) | 93 |
| 3.6 Pressure contours for solution (3.6.9) | 93 |
| 3.7 Pressure along lower boundary for solution (3.6.5) | 93 |
| 3.8 Pressure along lower boundary for solution (3.6.9) | 93 |
| 3.9 Pressure along section $x = 0.25$ for solution (3.6.5) | 93 |
| 3.10 Pressure along section $x = 0.25$ for solution (3.6.9) | 93 |
| 3.11 Sketch of channel with curved walls. | 95 |
| 3.12 Pressure at line $x = 1.5$. Numerical solutions computed on four grids with $h_1 = 1/20$, $h_2 = h_1/2$, $h_3 = h_1/4$, $h_4 = h_1/8$ | 98 |
| 3.13 Pressure contours for $a_\omega = 0$, $K = 1$ | 101 |
| 3.14 Pressure contours for $a_\omega = 0.1$, $K = 1$ | 101 |
| 3.15 Pressure contours for $a_\omega = 1.0$, $K = 1$ | 101 |
| 3.16 Pressure contours for $a_\omega = 1.0$, $K = 2$ | 102 |
| 3.17 Pressure contours for $a_\omega = 5.0$, $K = 1$ | 102 |
| 3.18 Pressure contours for $a_\omega = 5.0$, $K = 2$ | 102 |
| 3.19 Isolines $\psi = \text{constant}$ for the values of the levels vary from 0 to 1.0 with interval 0.0625. $a_\omega = 5.0$, $K = 1$ | 103 |
| 3.20 Isolines $\psi = \text{constant}$ for the values of the levels vary from 0 to 1.0 with interval 0.0625. $a_\omega = 5.0$, $K = 2$ | 103 |

List of Figures (Continued)

| Figure | Page |
|---|------|
| 3.21 The pressure along lower boundary of channel with $x_d = 3.0$, $x_{d1} = 1.0$, $x_{d2} = 2.0$, $h_d = 0.05$. $a_\omega = 0.0; 0.1; 1.0$; $K = 1$ | 104 |
| 3.22 The pressure along lower boundary of channel with $x_d = 3.0$, $x_{d1} = 1.0$, $x_{d2} = 2.0$, $h_d = 0.05$. $a_\omega = 0.1$; $K = 1$; 2. | 104 |
| 3.23 The pressure along section $x = 1.5$ of channel with $x_d = 3.0$, $x_{d1} = 1.0$, $x_{d2} = 2.0$, $h_d = 0.05$. $a_\omega = 0.0; 0.1; 1.0$ $K = 1$ | 105 |
| 3.24 The pressure along section $x = 1.5$ of channel with $x_d = 3.0$, $x_{d1} = 1.0$, $x_{d2} = 2.0$, $h_d = 0.05$. $a_\omega = 1.0$ $K = 1$; 2. | 105 |
| 3.25 Pressure contours for $a_\omega = 0.0$, $K = 1$ | 106 |
| 3.26 Pressure contours for $a_\omega = 0.1$, $K = 1$ | 106 |
| 3.27 Pressure contours for $a_\omega = 1.0$, $K = 1$ | 106 |
| 3.28 Pressure contours for $a_\omega = 1.0$, $K = 2$ | 107 |
| 3.29 Pressure contours for $a_\omega = 5.0$, $K = 1$ | 107 |
| 3.30 Pressure contours for $a_\omega = 5.0$, $K = 2$ | 107 |
| 3.31 Isolines $\psi = \text{constant}$ for the values of the levels vary from 0 to 1.0 with interval 0.0625. $a_\omega = 5.0$, $K = 1$ | 108 |
| 3.32 Isolines $\psi = \text{constant}$ for the values of the levels vary from 0 to 1.0 with interval 0.0625. $a_\omega = 5.0$, $K = 2$ | 108 |
| 3.33 The pressure along lower boundary of channel with $x_d = 3.0$, $x_{d1} = 1.0$, $x_{d2} = 2.0$, $h_d = 0.3$. $a_\omega = 0; 0.1; 1.0$; $K = 1$ | 109 |
| 3.34 The pressure along lower boundary of channel with $x_d = 3.0$, $x_{d1} = 1.0$, $x_{d2} = 2.0$, $h_d = 0.3$. $a_\omega = 1.0$; $K = 1$; 2. | 109 |
| 3.35 The pressure along section $x = 1.5$ of channel with $x_d = 3.0$, $x_{d1} = 1.0$, $x_{d2} = 2.0$, $h_d = 0.3$. $a_\omega = 0; 0.1; 1.0$, $K = 1$ | 110 |
| 3.36 The pressure along section $x = 1.5$ of channel with $x_d = 3.0$, $x_{d1} = 1.0$, $x_{d2} = 2.0$, $h_d = 0.3$. $a_\omega = 1.0$, $K = 1$; 2. | 110 |

Chapter I

Introduction

1.1 Purpose and Background of the Research

One of the main problems of fluid dynamics is the motion of fluid in a given domain whose boundaries do not only consist of solid impermeable parts but also the inflow and outflow parts. We will call such kind of problem as the “flowing-through” problem.

Many flow properties can be described by the inviscid approximation (for example, determination of the pressure distribution). The inviscid flows in which the viscosity forces can be neglected play an important role in fluid mechanics. In many cases, the hypothesis of incompressibility is a good approach of the real process in gas. The Euler equations for an incompressible ideal fluid are a classical model of hydrodynamics. The Euler equations can be interpreted as the limit of the Navier-Stokes equations of vanishing viscosity, and their character is hyperbolic in the unsteady cases.

The purpose of this thesis is to develop a numerical method for the Euler equations of an ideal homogeneous incompressible fluid flows when the boundary of the domain includes the inflow, the outflow and the impermeable parts as well.

Theoretical investigation of initial boundary value problems for the Euler equations was initiated by N. M. Gunter (1927) and L. Lichtenstein (1929). These authors obtained basic results for the cases when the liquid filled the whole space, or a container with impermeable walls, and when the vector of mass forces was potential. However, the demonstration that the boundary value problem for the Euler equations of an ideal fluid is well-posed, is quite difficult even for the problem considered in small time intervals. The results obtained in this field are mostly local in time. It was N. E. Kochin (1956) who first studied the flowing-through problem in a model formulation, in which the boundary conditions at the entrance were formulated for a velocity vortex. The two-dimensional non-stationary problem with a given vortex at the inlet part was studied by V. I. Yudovich (1964). A. V. Kazhikhov *et al.* (1980) proved the short time existence results for non-stationary problem of an ideal liquid flow through a bounded domain, in case the total vector of velocity is given on the inflow parts of the boundary, while its normal component is given on the outflow parts of the boundary.

The numerical methods for the solution of the Euler equations of an ideal

incompressible fluid flow through a bounded domain with the inflow and outflow parts of boundaries have not yet been considered in detail. The goal of this thesis is to study the numerical methods for approximating solutions of such flowing-through problems.

1.2 General Considerations on the Euler Equations

This section has an introductory nature, wherein we discuss the fundamental equations describing the motion of an incompressible nonviscous fluid and formulate some elementary properties.

1.2.1 The Equation of Motion of an Ideal Incompressible Fluid

Fluid mechanics does not study the dynamics of the individual molecules constituting the fluid. We want to investigate the gross behavior of many of molecules. For this purpose, we assume the fluid as a continuum, a point of which is a very small portion of the real fluid. This small volume, a point in our mathematical description, will be called *fluid particle* or element of fluid.

Let D be a region in two- or three- dimensional space filled with a fluid. Let $\mathbf{X} = (X^1, X^2, X^3)$, $\mathbf{X} \in D$ be the coordinates of the fluid particle at time $t = 0$. Let $\mathbf{x} = (x^1, x^2, x^3)$, $\mathbf{x} \in D$ be the coordinates of the same fluid particle at time t . Then an incompressible motion is, by definition, a function

$$\mathbf{x} = \varphi(\mathbf{X}, t) \quad (\text{or } x^i = \varphi^i(\mathbf{X}, t)) \quad (1.2.1)$$

such that:

- a) φ is invertible;
- b) φ and φ^{-1} are smooth enough so that the main operations of calculus may be performed on them;
- c) $\mathbf{X} = \varphi(\mathbf{X}, 0)$, $\varphi(\mathbf{X}, t_1 + t_2) = \varphi(\varphi(\mathbf{X}, t_1), t_2)$.

If \mathbf{X} is fixed and t is changed, then equation (1.2.1) determines a *trajectory* of fluid particle P which initially placed at point \mathbf{X} . From another side, If t is fixed, then equation (1.2.1) determines the transformation of the fluid domain at time $t = 0$ to the fluid domain at time $t = t_1$.

In spite of the fact that (1.2.1) determines the fluid motion, it is also important to study the time evolution at given point $\mathbf{x} \in D$ of the density field $\rho(\mathbf{x}, t)$, velocity field $\mathbf{u} = \mathbf{u}(\mathbf{x}, t)$ and so on.

The derivation of the fluid motion equations is based on three basic principles:

- I: mass is neither created or destroyed,
- II: the rate of change of momentum of a portion of the fluid equals the force applied to it (*Newton's second law*),
- III: energy is neither created nor destroyed.

By the law of conservation of mass together with the condition of incompressibility, we have

$$\operatorname{div} \mathbf{u}(\mathbf{x}, t) \equiv \nabla \cdot \mathbf{u}(\mathbf{x}, t) = 0, \quad \forall \mathbf{x} \in D, t \in \mathbb{R}. \quad (1.2.2)$$

Equation (1.2.2) is called the *continuity equation* for incompressible flows.

Let us define an *ideal fluid* as one with the following property: for any motion of the fluid, there is a function $P(\mathbf{x}, t)$ called the *pressure* such that if S is a surface in the fluid with a chosen unit normal \mathbf{n} , the force of stress exerted across the surface S per unit area at $\mathbf{x} \in S$ at time t is $P(\mathbf{x}, t) \cdot \mathbf{n}$. By Newton's second law (force = mass \otimes acceleration), we got the differential equation of the law of balance of momentum.

$$\rho \left(\frac{\partial \mathbf{u}}{\partial t} + (\mathbf{u} \cdot \nabla) \mathbf{u} \right) = -\nabla P + \rho \mathbf{f} \quad (1.2.3)$$

where $\mathbf{f} = \mathbf{f}(\mathbf{x}, t)$ is external force per unity volume.

Equation (1.2.3), together with the equation (1.2.2) form the *Euler equations* for an ideal (or perfect) incompressible fluid.

Remarks:

1. In the present research, we will assume the density to be always constant (for simplicity $\rho \equiv 1$).
2. When \mathbf{f} is a potential force ($\mathbf{f} = -\nabla U$ for some scalar field U), we can modify equation (1.2.3) to

$$\frac{\partial \mathbf{u}}{\partial t} + (\mathbf{u} \cdot \nabla) \mathbf{u} = -\nabla P \quad (1.2.4)$$

with P replaced by $P + U$.

Later on, we will assume the absence of external forces.

1.2.2 Vorticity and Stream Function

There are two different points of view on fluid motion. Fixing time in equation (1.2.1), we have studied the motion of the fluid by following the evolution of a single particle (the Lagrangian point of view). On the contrary, in the Euler equations, the velocity field $\mathbf{u} = \mathbf{u}(\mathbf{x}, t)$ is the unknown quantity. This means that we fixed a point \mathbf{x} and follow the time evolution of the particle that at time t passes through \mathbf{x} (the Eulerian point of view).

The two points of view are related. If we know all the trajectories of the fluid particles, it is possible to find the velocity field by a simple differentiation. More complicated is the inverse problem. In fact, knowing $\mathbf{u} = \mathbf{u}(\mathbf{x}, t)$, we can find the motion of each particle of fluid by solving the initial value problem for ordinary differential equation,

$$\begin{aligned}\frac{d\varphi(\mathbf{x}, t)}{dt} &= \mathbf{u}(\mathbf{x}, t), \\ \varphi(\mathbf{x}, 0) &= \mathbf{X}.\end{aligned}$$

The lines that are tangent in any point to the velocity field, $\mathbf{u} = \mathbf{u}(\mathbf{x})$, are called *streamlines* or *flow lines*. They vary in time and they are constant in time for steady motion. In this case, the streamlines coincide with trajectories of the particles.

A fundamental concept of fluid motion analysis is the concept of the *vorticity field* $\boldsymbol{\omega}(\mathbf{x})$. By definition

$$\boldsymbol{\omega} \equiv \text{curl } \mathbf{u} = \nabla \times \mathbf{u}. \quad (1.2.5)$$

The vorticity field $\boldsymbol{\omega}(\mathbf{x})$ gives a measure of how the fluid is rotating. The vorticity field is an important tool in studying the behavior of fluids. The Euler equations can be expressed in terms of vorticity. Using the following vector identity

$$\frac{1}{2}\nabla\mathbf{u}^2 = \mathbf{u} \times \text{curl } \mathbf{u} + (\mathbf{u} \cdot \nabla)\mathbf{u}, \quad (1.2.6)$$

the Euler equations can be written as

$$\frac{\partial\mathbf{u}}{\partial t} + \frac{1}{2}\nabla\mathbf{u}^2 - \mathbf{u} \times \text{curl } \mathbf{u} = -\nabla P.$$

Taking the curl of both sides

$$\frac{\partial\boldsymbol{\omega}}{\partial t} - \text{curl}(\mathbf{u} \times \boldsymbol{\omega}) = 0$$

Since

$$\text{curl}(\mathbf{u} \times \boldsymbol{\omega}) = (\boldsymbol{\omega} \cdot \nabla)\mathbf{u} - \boldsymbol{\omega}(\nabla \cdot \mathbf{u}) - (\mathbf{u} \cdot \nabla)\boldsymbol{\omega} + \mathbf{u}(\nabla \cdot \boldsymbol{\omega}).$$

We finally obtain

$$\frac{\partial\boldsymbol{\omega}}{\partial t} + (\mathbf{u} \cdot \nabla)\boldsymbol{\omega} = (\boldsymbol{\omega} \cdot \nabla)\mathbf{u}. \quad (1.2.7)$$

However, to study the Euler equations in form (1.2.7), it is necessary to reconstruct the velocity field \mathbf{u} from the vorticity. In other words, we have to solve the following equation in unknown quantity \mathbf{u} :

$$\begin{aligned}\text{curl } \mathbf{u} &= \boldsymbol{\omega}, \quad \boldsymbol{\omega} \in C(D), \\ \nabla \cdot \mathbf{u} &= 0.\end{aligned}$$

In two dimension (1.2.7) becomes much simpler. Namely, in the presence of a planar symmetry

$$\mathbf{u} = (u_1, u_2, 0), \quad u_i = u_i(x_1, x_2)$$

only the third component of the vorticity $\omega_3 = \omega$ is present and the right-hand side of (1.2.7) vanishes. Therefore, the Euler equations for the vorticity in two dimensions becomes

$$\frac{\partial \omega}{\partial t} + (\mathbf{u} \cdot \nabla) \omega = 0. \quad (1.2.8)$$

Notice that (1.2.8) implies the conservation of the vorticity along the trajectories.

1.2.3 Conservation Laws

The energy conservation is the first conservation law valid for the ideal fluid. The *energy*, defined as

$$E = \frac{1}{2} \int_D \mathbf{u}^2 d\mathbf{x} \quad (1.2.9)$$

is conserved during the motion because in mathematical model there is no mechanism of dissipation: the fluid has neither internal friction nor friction with boundaries.

Theorem 1.2.1. *Let $D \subset \mathbb{R}^3$ be a bounded domain and let \mathbf{u} be a solution of the Euler equations with conservative external forces*

$$\frac{\partial \mathbf{u}}{\partial t} + (\mathbf{u} \cdot \nabla) \mathbf{u} = -\nabla(P + U)$$

where $U = U(\mathbf{x}, t)$ is a known function then

$$\frac{d}{dt} E = 0.$$

Remark: The energy conservation law can be extended to unbounded domains. In this case, E is finite if \mathbf{u} decays at infinity fast enough.

For a stationary flow, the energy conservation assumes a very significant form.

Theorem 1.2.2. (Bernoulli) *In an ideal fluid in stationary motion under the action of conservative force with potential U independent of time, the quantity*

$$\varepsilon = \frac{1}{2} \mathbf{u}^2 + (P + U)$$

is constant along the streamlines.

This theorem says that ε remains constant along the streamlines, but in general varies when we pass from one streamline to another. On the contrary, when the velocity field is irrotational, the value of ε does not depend on the choice of the streamline, as follows from:

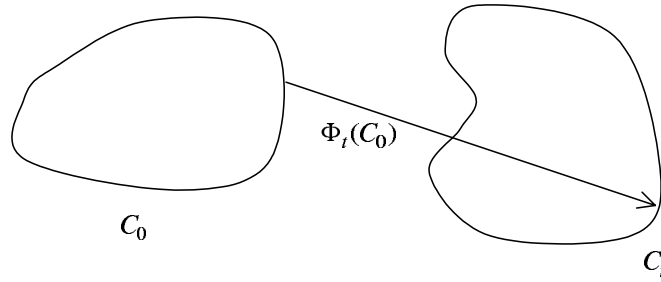


Figure 1.1: Evolving in time of closed curve.

Theorem 1.2.3. (Bernoulli, irrotational flow). Consider an ideal fluid in a stationary irrotational motion in a domain D , under the action of a conservative force with potential U independent of time. Then the quantity

$$\varepsilon = \frac{1}{2}\mathbf{u}^2 + (P + U)$$

is constant.

Remark: The Bernoulli theorems tell us that in the absence of external forces the pressure is greatest when the velocity is smallest and vice-versa. In particular, in a narrowing pipeline the continuity equation implies that, when the pipeline has a smaller section, the velocity must be greater. The Bernoulli theorem ensures that the pressure is smaller.

We proceed now to analyze some conservation laws involving the vorticity. In a fluid motion according to the Euler equations, different layers of the fluid cannot interact between themselves via friction forces. So it is not possible to give rise to or to change the rotation of an ideal fluid. This fact must be reflected in a conservation law involving the vorticity field. This law is expressed by the Kelvin theorem.

Let C_t be a closed curve evolving in time according to the fluid flow (see Figure 1.1)

$$C_t = \phi_t(C_0)$$

We consider the circulation

$$\Gamma(C_t) = \oint_{C_t} \mathbf{u}(t)dl$$

where dl is the infinitesimal element of line in C_t . Then

Theorem 1.2.4. (Kelvin)

$$\frac{d}{dt}\Gamma(C_t) = 0$$

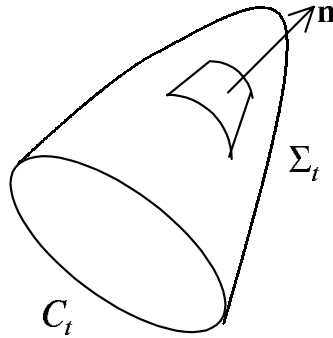


Figure 1.2: Normal vector on surface.

Remark: In terms of the vorticity field the Kelvin theorem has the following consequence: the vorticity flux through a surface Σ_t moving with the fluid

$$\int_{\Sigma_t} \boldsymbol{\omega} \cdot \mathbf{n} d\sigma$$

(\mathbf{n} denotes the normal to surface (Figure. 1.3)) remains constant in time. This follows by the Stokes theorem.

1.2.4 Potential and Irrotational Flows

The *irrotational flows* are flows in which the vorticity vanishes every where. A particular example is given by the so-called *potential flows*, those for which there exists a function $\varphi(\mathbf{x}, t)$, such that

$$\mathbf{u}(\mathbf{x}, t) = \nabla\varphi(\mathbf{x}, t). \quad (1.2.10)$$

Clearly any potential flow is also irrotational. (It follows directly by vector identity $\text{curl}(\text{grad } \varphi) \equiv 0$.) The converse is not true: although, it is possible to find, for any irrotational flow, a function φ satisfying (1.2.10), in general, it may be multivalued for a nonsimply connected domain since it can assume many different values depending on the number of loops around the holes.

The interest in studying irrotational divergence-free flows lies in the fact that they are a stationary solution of the Euler equations. To verify this statement, we assume that $\mathbf{u} = \mathbf{u}(t)$ is a solution of the equations

$$\nabla \cdot \mathbf{u} = 0, \quad \text{curl } \mathbf{u} = 0 \quad (1.2.11)$$

in a domain $D \subset \mathbb{R}^d$, $d = 2, 3$.

From equation (1.2.6), we know that

$$(\mathbf{u} \cdot \nabla)\mathbf{u} = \frac{1}{2}\nabla\mathbf{u}^2 \quad (1.2.12)$$

and so, for boundary conditions do not depend on time, we have a stationary solution of the Euler equations, with the pressure $P = -\frac{1}{2}\mathbf{u}^2$.

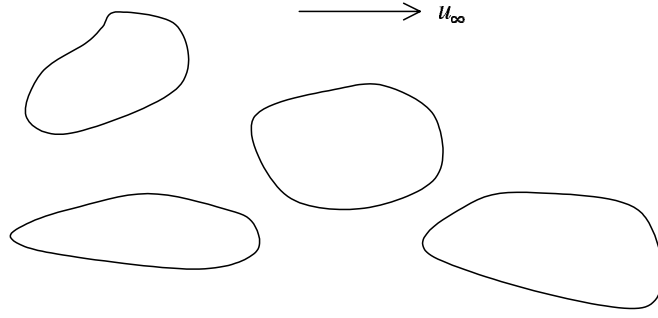


Figure 1.3:

In some problems the boundary conditions depend on time, for instance, when the wall of the region moves with a given law. The Euler equations become (by using (1.2.10) and (1.2.11))

$$\nabla \left(\frac{\partial \varphi}{\partial t} + \frac{1}{2} |\nabla \varphi|^2 + P \right) = 0$$

hence

$$\frac{\partial \varphi}{\partial t} + \frac{1}{2} |\nabla \varphi|^2 + P = \text{constant} \quad (1.2.13)$$

Remark: In a bounded, simply connected domain, all the irrotational flows reduce to the trivial one: $\mathbf{u} = 0$.

So in order to have a nontrivial irrotational field, we must consider either nonsimply connected or unbounded domains. Very important in the applications are so-called *external domain*. They are defined as the complement of a finite union of simply connected bounded regions. A domain as in Figure 1.3 has a different topological structure in two and in three dimensions. In fact, it is simply connected in three dimensions and so $\mathbf{u} = \nabla \varphi$ where φ is a harmonic function satisfying the boundary conditions $\frac{\partial \varphi}{\partial \mathbf{n}} = 0$ on ∂D . Specifying the asymptotic behavior

$$\lim_{\|\mathbf{x}\| \rightarrow \infty} \mathbf{u}(\mathbf{x}) = U_\infty.$$

We have a unique potential flow (following the uniqueness of the Neumann problem)

In two dimensions, such a domain is not simply connected and the irrotational flows are not necessary potential flows.

1.2.5 Historical Comments

The equations of motion of an ideal fluid were derived by L. Euler (1755). Several mathematicians and physicists, for instance, Bernoulli, d'Alembert, Lagrange, Cauchy, Helmholtz, Kelvin and others, have contributed to further developments of the theory. For more detail of the deduction and properties of

the Euler equations (not necessary for incompressible flows) consult the classical books in fluid mechanics such as C.K. Batchelor (1970), J. Serrin (1959), A.J. Chorin (1997), L.D. Landau (1968), H. Lamb (1932).

1.2.6 Existence and Uniqueness of the Solution

In this section, we discuss the problem of the existence and uniqueness of the solutions of the Euler equations. The Euler equations are nonlinear equations. This implies that the construction of its solutions may be a nontrivial task.

The first problem, we meet in the study of a differential equation is to establish an existence and uniqueness theorem for the solutions. This problem is of obvious interest: if a mathematical model of the real world is described by a differential equation, the proof of the existence of a large enough class of solutions is a first verification of the validity of the model. Once the existence of the solutions is ensured, we would like there to be only one solution having a given value at a given instant. If not, the physical state of the system at a time t , could not be uniquely determined by the differential equation itself and the knowledge of the state of the system at a previous time $t_0 < t$. In other words, we would like the Cauchy (initial value) problem associated with our differential equation to be *well-posed*: that is, to have a unique solution with smooth dependence on the initial data.

Once, we have positively answered these questions about uniqueness and existence, we must develop methodologies and algorithms (implementable numerically if possible) that allow, at least in principle, the approximate calculation of the solution. In the case of the Euler equations, we have satisfactory answers in two dimensions. In three dimensions, the theory is much more difficult and it is possible that the solutions may develop singularities in a finite time. Therefore, we confine ourselves to an existence and uniqueness theorem local in time only.

In two dimensions, we are able to construct a solution for any time C. Marchioro (1994). An existence and uniqueness theorem for the solution of the Euler equations in three dimensions for short times was proven, see for instance C. Marchioro (1994).

The shortness of the time in which the solution is constructed depends on the a priori estimates (valid for short times only).

1.2.7 Comment (Existence and Uniqueness)

The solution of the initial value problem associated with the Euler equations, in two dimensions for arbitrary times and in three dimensions for short times has long been known. There is a large literature on the subject. We mention only W. Wolibuer (1933), V.I. Yudowich (1963), T. Kato (1972) for two-dimensional existence theorem and D. Ebin (1970), T. Kato (1972), R. Temam (1975), R. Temam (1976), R. Temam (1986), T. Kato (1988) for the three-dimensional case.

1.3 Mathematical Formulation of Flowing-Through Problems

We will present here the three kinds of well-posed boundary value problems for the Euler equations of an ideal incompressible fluid flow through a bounded domain. In our explanation, we follow A. V. Kazhikhov, *et al.* (1980).

Let Ω be a bounded domain in \mathbb{R}^3 whose boundary Γ consists of three parts. Parts of the inflow are denoted by Γ_l^1 . Parts of the outflow are denoted by Γ_m^2 . The part of the impermeable boundary is denoted by Γ^0 . Each component of Γ_α^i is a sufficiently smooth surface. Boundaries Γ_l^1 and Γ_m^2 do not touch each other and the intersection of Γ^0 with Γ_l^1 and Γ_m^2 occurs at a straight angle or a right angle.

Let $\mathbf{x} = (x_1, x_2, x_3)$ denote the Cartesian coordinates of points of Ω , t — the time, $t \in [0, T]$, $\mathbf{u} = (u_1, u_2, u_3)$ — the velocity vector, $\boldsymbol{\omega} = (\omega_1, \omega_2, \omega_3)$ — the vorticity vector, P — the pressure divided by the constant density of the fluid, \mathbf{f} — the vector of mass forces, $Q = \Omega \times (0, T)$, $S^i = \Gamma^i \times (0, T)$, $i = 0, 1, 2$; \mathbf{n} — the unit vector of the outward normal to Γ , and $\boldsymbol{\tau}_2$ and $\boldsymbol{\tau}_3$ linearly independent vectors tangent to Γ^i , $i = 1, 2$.

The motion of a homogeneous ideal incompressible fluid is described by the Euler equations (see, for example, C. K. Batchelor (1979)).

$$\frac{\partial \mathbf{u}}{\partial t} + (\mathbf{u} \cdot \nabla) \mathbf{u} + \nabla P = \mathbf{f}, \quad (1.3.1)$$

$$\nabla \cdot \mathbf{u} = 0, \quad (\mathbf{x}, t) \in Q.$$

At $t = 0$, the velocity field is given by

$$\mathbf{u}|_{t=0} = \mathbf{u}^0(x), \quad (1.3.2)$$

$$\nabla \cdot \mathbf{u}^0 = 0, \quad \mathbf{x} \in \Omega.$$

A typical boundary condition on the solid parts is imposed by prescribing the value of the normal component of velocity vector as

$$(\mathbf{u} \cdot \mathbf{n}) = 0, \quad (\mathbf{x}, t) \in S^0, \quad (1.3.3)$$

and we assume that on the inflow parts of the boundary Γ_l^1 , the normal component of the velocity is given as well,

$$(\mathbf{u} \cdot \mathbf{n}) = g_1 < 0, \quad (\mathbf{x}, t) \in S^1. \quad (1.3.4)$$

Additional boundary conditions must be imposed at the inflow and the outflow parts of the boundary in order to have a well-posed problem. These boundary conditions may vary. We will name the three different kinds of boundary value problems to be considered in this thesis as problem 1, problem 2 and problem 3.

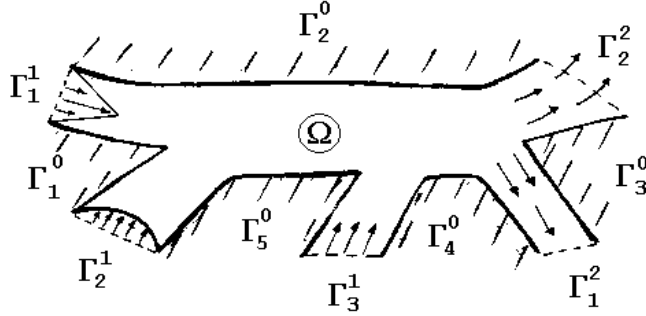


Figure 1.4: Sketch of a domain.

Problem 1:

The additional boundary conditions are the following :

Two tangent components of the vorticity vector are given on the inflow parts of the boundary S_l^1 and the normal component of the velocity vector is given on the outflow parts of the boundary S_m^2 . The whole formulation for problem 1 is therefore as follows:

Find a solution of equation (1.3.1) in the domain Q with initial conditions (1.3.2) and the following boundary conditions

$$\begin{aligned}
 S^0 : \quad & (\mathbf{u} \cdot \mathbf{n}) = 0, \quad (\mathbf{x}, t) \in S^0, \\
 S_l^1 : \quad & (\mathbf{u} \cdot \mathbf{n}) = g_l < 0, \quad (\boldsymbol{\omega} \cdot \boldsymbol{\tau}_i) = h_i, \quad i = 2, 3, \quad (\mathbf{x}, t) \in S_l^1, \quad l = 1, 2, \dots, \\
 S_m^2 : \quad & (\mathbf{u} \cdot \mathbf{n}) = l > 0, \quad (\mathbf{x}, t) \in S_m^2, \quad m = 1, 2, 3, \dots
 \end{aligned}
 \tag{1.3.5}$$

Problem 2:

The additional boundary conditions are the following:

Both tangent components of velocity are prescribed on the inflow parts S_l^1 and the pressure is given on S_m^2 together with a condition on the sign of the normal component of the velocity vector. The whole formulation for problem 2 is therefore as follows:

Find a solution of equation (1.3.1) in domain Q with initial conditions (1.3.2) and the following boundary conditions

$$\begin{aligned}
 S^0 : \quad & (\mathbf{u} \cdot \mathbf{n}) = 0, \quad (\mathbf{x}, t) \in S^0, \\
 S_l^1 : \quad & (\mathbf{u} \cdot \mathbf{n}) = g_l < 0, \quad (\mathbf{u} \cdot \boldsymbol{\tau}_i) = g_i, \quad i = 2, 3, \quad (\mathbf{x}, t) \in S_l^1, \quad l = 1, 2, \dots, \\
 S_m^2 : \quad & (\mathbf{u} \cdot \mathbf{n}) > 0; \quad P = P_2, \quad (\mathbf{x}, t) \in S_m^2, \quad m = 1, 2, 3, \dots
 \end{aligned}
 \tag{1.3.6}$$

Problem 3:

The additional boundary conditions are the following:

Both tangent components of velocity are prescribed on the inflow parts S_l^1 and the normal component of the velocity vector is given on the outflow parts of the boundary S_m^2 . The whole formulation for problem 3 is therefore as follows:

Find a solution of equation (1.3.1) in domain Q with initial conditions (1.3.2) and the following boundary conditions

$$\begin{aligned} S^0 : \quad & (\mathbf{u} \cdot \mathbf{n}) = 0, \quad (\mathbf{x}, t) \in S^0, \\ S_l^1 : \quad & (\mathbf{u} \cdot \mathbf{n}) = g_1 < 0, \quad (\mathbf{u} \cdot \boldsymbol{\tau}_i) = g_i, \quad i = 2, 3, \quad (\mathbf{x}, t) \in S_l^1, \quad l = 1, 2, \dots, \\ S_m^2 : \quad & (\mathbf{u} \cdot \mathbf{n}) = l > 0, \quad (\mathbf{x}, t) \in S_m^2, \quad m = 1, 2, 3, \dots \end{aligned} \tag{1.3.7}$$

1.4 Review of Literatures

In this section, we present a brief review of literatures associated with the well-posed initial boundary value problems and analyze the numerical schemes for the Euler equations in the cases of incompressible fluid.

1.4.1 Theoretical Investigation of Initial Boundary Value Problems for Euler Equations

The equations governing the flow of an incompressible fluid of null viscosity called also ideal fluid have been known for more than 100 years and detailed description of this mathematical model is available for example in the book of C. K. Batchelor (1970).

In each case, the set of boundary conditions supplementing the differential equations has to be studied very carefully. The treatment of boundary conditions is strictly related to the theoretical problem of the closure of the Euler equations, i.e. defining the set of boundary conditions that, together with the initial conditions, can ensure, at least locally, a stable (well-posed) solution.

The investigation of the initial boundary problems of Euler equations was developed in the work of N. M. Gunter (1927), L. Lichtenstein (1929), W. Wolinder (1933), O. A. Laduzenskaya (1975), V. N. Yudovich (1964), T. Kato (1975), H. S. Swann (1970), R. Temam (1975) and N. E. Kochin (1950). There are sufficiently complete results for the case when fluid motion occurs within the whole space or within the volume bounded by impermeable boundaries. The situation is completely different in two dimensions and in three dimensions. The incompressible Euler equations in three dimensions are far from being understood. If the dimension is equal to two, the Cauchy problem for the incompressible Euler equations is much better understood. The fundamental series of work written by R. J. Di Perna and A. Majda (1988,1987) on this subject include a more complete discussion of the background of this issue.

It is of interest to study the problem of fluid flow through a bounded domain with the impermeable, inflow, and outflow parts of the boundary. This

situation is not only very mathematically interesting but also corresponding to various relevant physical situations. The first result for such kind of problems was obtained by N. E. Kochin (1956). Two-dimensional unsteady problems was considered by V. I. Yudovich (1964). A. V. Kazhikhov and V. V. Ragulin (1980) studied the existence and uniqueness of the boundary value problem when on the inflow parts of the boundary was prescribed by three components of velocity or normal component of velocity and two tangent components of vorticity and on the outflow parts of the boundary was prescribed by a normal component of velocity or pressure.

1.4.2 Analyzing Numerical Schemes

Due to the large variety of situations for which numerical schemes are needed, there is a wide literature on the subject a detailed analysis of which is beyond the scope of this research. Here, we will give only a short review.

A lot of research activities are devoted to analyze the numerical schemes for the Euler equations. In general, most of the techniques are consistent with non-steady flow solutions. Special emphasis is on steady flow solutions that play an important role for assessing the validity of any computational technique, especially in the multidimensional cases. Time marching approaches allow any (steady) fluid dynamics flow problem to be formulated as a pseudo-unsteady one, where the time is to be interpreted as an evolutionary coordinate such that the use of a time marching strategy is equivalent to an iterative process, whose convergence is indeed equivalent to the existence of a steady state, A. Jameson (1983), R. Peyret and T. D. Taylor (1983) and C. Hirsch (1990).

Inspite of the complexity of the Euler equations, the analysis and the design of most of successful numerical approaches are in connection with the progress of the numerical treatment of simple linear and non-linear model equations, such as the (one-dimensional) advection-diffusion equation. The milestones for the modern development of numerical schemes for solving the ideal fluid flow equations are the R. Courant-E. Isaacson-M. Rees (Courant et al., 1952), and Lax-Wendroff (1960, 1964) schemes, together with the theory of Lax (Lax and Wendroff (1960, 1964) and Lax (1972)).

Further development is necessary in order to extend the theoretical results obtained by Lax and others for one-dimensional non-linear problems to multidimensional situations. A critical survey of such effort with the emphasis on the Euler and the Navier-Stokes equations has been done by Gunzburger (1996) (see R. Peyret (1996)).

Many schemes have been derived from the Lax-Wendroff scheme, the most popular being R. W. MacCormack's (1969) (and its variants), which dated back to the 1960s. Several methods have been proposed, by assuming the separability of space and time discretization. These give rise to such (rather general) classifications: explicit or implicit schemes; single- or multistep methods as far as time integration is concerned; centered or uncentered (so called upwind methods) schemes when referring to space discretization.

In the last 5-10 years, different categories of schemes preventing the generation of numerical oscillations have been proposed (and successfully employed) following the Flux Corrected Transport (FCT) concept developed by Boris and Book(1973): the Total Variation Diminishing (TVD) concept first developed by A. Harten(1983), with the recent interpretation of A. Jameson (1983) as a Local Extremum Diminishing (LED) principle A. Jameson (1983), the Monotone Upstream Discretization MUSCL concept of B. Van Leer (1977,1979),etc.

In each case, the set of boundary conditions supplementing the different equations has to be studied very carefully.

The treatment of boundary conditions is strictly related to the theoretical problem of the closure of Euler and/or Navier–Stokes equations, i.e. defining the set of boundary conditions that, together with the initial conditions, can ensure, at least locally, a stable (well-posed) solution.

Recent work on the treatment of boundary conditions by J. C. Strikwerda(1977), C. Hirsch(1990) and T. J. Poinsot and S. K. Lele(1992), has focused on the aspect on time-dependent boundary conditions in order to properly account for the interaction between inner and outer phenomena.

1.5 Survey of the Thesis

Several numerical schemes have been proposed for the calculation of incompressible inviscid flows around the body or within an enclosed domain. However, the present study will concentrate almost exclusively on “flowing-through” problem in which the governing equations are the steady Euler equations. Two quite distinct numerical methods will be considered: the first one is based on the transformation of the Euler equations to new unknown functions and new independent variables. The new unknown functions are the flow angle and the modulus of the velocity vector. The new independent variables are similar to the stream function and the potential. The second method is based on the classical stream function vorticity formulation of the Euler equations.

Chapter 2 is developed to study the two-dimensional steady “flowing-through” problem 2 and two-dimensional steady “flowing-through” problem 3. The Euler equations governing two-dimensional flows are expressed in terms of two scalar unknowns which are the flow angle and the modulus of the velocity vector. The curvilinear physical domain is mapped onto a rectangular domain in new independent variables which are similar to a stream function and a potential. The new system of three equations consists of one elliptic equation and the other two equations of hyperbolic type. The difficulty of finding the solution of this system is that we have to deal with the Goursat boundary value problem in which the boundary conditions for the hyperbolic system are prescribed at the characteristics. An iterative method is constructed to obtain the numerical solution. Hyperbolic system of the equations is solved by the method of characteristic and elliptic equation is solved by the block SOR method. The convergence of algorithm is demonstrated by comparison of calculation results on a sequence of grids.

Chapter 3 discusses the “flowing-through” problem 1 in which the normal component of the velocity vector and the tangent components of the vorticity vector are given on the inflow part of the domain boundary. We utilize the non-primitive variable formulation of the Euler equations for two-dimensional flows. The nonprimitive variables are the stream function ψ and the vorticity ω . A system of two equations is solved by the iterative method. Either the block SOR method or the Stabilizing Correction method is used to solve the elliptic equation for the stream function. The upwind approximation of convective terms is applied to find the solution of the vorticity transport equation. We describe the computational techniques for determining realistic estimate of error constant and the order of convergence of a numerical algorithm. We use these techniques to estimate the convergence constant, of the algorithm developed in this thesis. The application of the algorithm is then demonstrated for an ideal incompressible fluid flow through a channel with curved walls. Strong dependence of the pressure field on the boundary condition for vorticity is found .

In Chapter 4, the thesis is briefly reviewed and the conclusions are given.

Chapter II

Numerical Methods for Steady Flowing-Through Problems: Problem 2 and Problem 3

2.1 Introduction

In this Chapter, we study numerical methods for the solution of the “flowing-through” problems in which the governing equations are the steady Euler equations of an ideal incompressible fluid. The numerical methods are developed for fluid flow through domain with an inflow and outflow parts of the domain boundary. The two kinds of boundary value problems which having relation with problem 2 and problem 3 described in section 1.3 are studied.

We rewrite the Euler equations in terms of new unknown functions and transform it to a new curvilinear coordinate system. We solve the Euler equations by an iterative process. The convergence of the numerical algorithms is established numerically by calculation in a sequence of grids. The properties of algorithm is demonstrated for a flow of an ideal incompressible fluid through the elbow channel and the channel with curvilinear boundaries in the two-dimensional case. The main idea of a transformation and an iterative algorithm is to separate the governing equations into two subsystems, one is hyperbolic and another is elliptic. The idea of such transformation was considered by I.L. Osipov et al. (1978).

2.2 Mathematical Formulation

The fundamental equations of the two-dimensional steady incompressible ideal fluid flow are the Euler equations:

$$u \frac{\partial u}{\partial x} + v \frac{\partial u}{\partial y} = - \frac{\partial P}{\partial x}, \quad (2.2.1)$$

$$u \frac{\partial v}{\partial x} + v \frac{\partial v}{\partial y} = - \frac{\partial P}{\partial y}, \quad (2.2.2)$$

$$\frac{\partial u}{\partial x} + \frac{\partial v}{\partial y} = 0, \quad (2.2.3)$$

where $u(x, y)$ and $v(x, y)$ are components of the velocity vector in the x and y directions respectively, $P(x, y)$ is the pressure of a fluid. Without loss of generality, we set the density equal to one ($\rho = 1$).

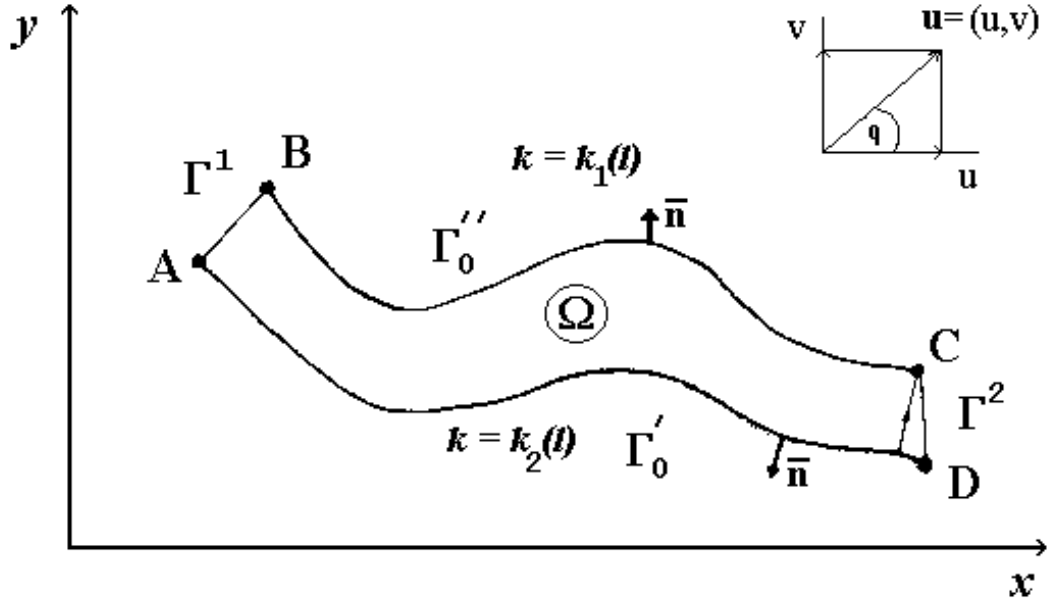


Figure 2.1: Sketch of a physical domain.

Let us assume that flow occurs in the domain Ω depicted in Figure 2.1. We assume that the solid impermeable boundaries Γ_0' and Γ_0'' are described by curves which are given by equations in the natural form

$$k = k_i(l), \quad i = 1, 2,$$

where k is the curvature and l is a natural parameter of curve.

It is convenient to rewrite the Euler equations in terms of new unknown functions $w(x, y)$ and $q(x, y)$ which are determined by the relations $u = w(x, y) \cos q(x, y)$ and $v = w(x, y) \sin q(x, y)$. Actually, $w(x, y)$ is the modulus of the velocity vector and $q(x, y)$ is the angle between the direction of the velocity vector and the Ox axis. We will call q as the flow angle. In this Chapter, we study numerical methods for two kinds of the boundary value problems.

Problem 3':

Find the solution of equations (2.2.1)–(2.2.3) with the following boundary conditions:

Impermeable boundaries AD and BC: $(x, y) \in \Gamma_0' \cup \Gamma_0''$

$$\mathbf{u} \cdot \mathbf{n} = 0. \quad (2.2.4)$$

Inflow part AB: $(x, y) \in \Gamma^1$

$$\begin{aligned} q &= q_1(x, y), \\ w &= w_1(x, y). \end{aligned} \quad (2.2.5)$$

Outflow part CD: $(x, y) \in \Gamma^2$

$$q = q_2(x, y). \quad (2.2.6)$$

Problem 2':

Find the solution of equations (2.2.1)–(2.2.3) with the following boundary conditions:

Impermeable boundaries AD and BC: $(x, y) \in \Gamma'_0 \cup \Gamma''_0$

$$\mathbf{u} \cdot \mathbf{n} = 0. \quad (2.2.7)$$

Inflow part AB: $(x, y) \in \Gamma^1$

$$\begin{aligned} q &= q_1(x, y), \\ w &= w_1(x, y). \end{aligned} \quad (2.2.8)$$

Outflow part CD: $(x, y) \in \Gamma^2$

$$\begin{aligned} P &= P_2(x, y), \\ \mathbf{u} \cdot \mathbf{n} &> 0. \end{aligned} \quad (2.2.9)$$

The problem 2' differs from the problem 3' in the boundary conditions on the outflow part CD . On CD , only pressure and condition for sign of normal component of the velocity vector are given.

2.2.1 The Euler Equations in Terms of New Unknown Function $w(x, y)$ and $q(x, y)$

In the study of the two-dimensional flow, the incompressible Euler equations can be formulated in a convenient alternative manner, by introducing two scalar variables in place of the primitive variables the velocity \bar{u} and the pressure P . The vorticity-stream function formulation has been a popular tools of computing two-dimensional incompressible flows (see, for example, P.J. Roache (1976), L. Quartapelle (1993)). Sometimes, it is convenient to use another two scalar variables which are differed from vorticity and stream function (see, for example, I.L. Osipov (1978)). In this section, we will use the modulus of the velocity and the flow angle (angle between the direction of velocity vector and the direction of Ox axis) as two new unknown functions instead the primitive variables.

We eliminate the pressure from the Euler equations by eliminating the mixed derivatives. Taking the derivatives in equations (2.2.1) and (2.2.2) with respect to y and x , respectively, we obtain

$$\left(\frac{\partial u}{\partial y}\right) \left(\frac{\partial u}{\partial x}\right) + u \frac{\partial^2 u}{\partial x \partial y} + \left(\frac{\partial v}{\partial y}\right) \left(\frac{\partial u}{\partial y}\right) + v \frac{\partial^2 u}{\partial y^2} = -\frac{\partial^2 P}{\partial x \partial y},$$

$$\left(\frac{\partial u}{\partial x}\right)\left(\frac{\partial v}{\partial x}\right) + u\frac{\partial^2 v}{\partial x^2} + \left(\frac{\partial v}{\partial x}\right)\left(\frac{\partial v}{\partial y}\right) + v\frac{\partial^2 v}{\partial x\partial y} = -\frac{\partial^2 P}{\partial y\partial x}.$$

Then, we eliminate the terms containing the pressure by subtracting these two equations and use the condition

$$\frac{\partial^2 P}{\partial x\partial y} = \frac{\partial^2 P}{\partial y\partial x}.$$

We have

$$\begin{aligned} & \left(\frac{\partial u}{\partial y}\right)\left(\frac{\partial u}{\partial x}\right) + u\frac{\partial^2 u}{\partial x\partial y} + \left(\frac{\partial v}{\partial y}\right)\left(\frac{\partial u}{\partial y}\right) + v\frac{\partial^2 u}{\partial y^2} \\ & - \left(\frac{\partial u}{\partial x}\right)\left(\frac{\partial v}{\partial x}\right) - u\frac{\partial^2 v}{\partial x^2} - \left(\frac{\partial v}{\partial x}\right)\left(\frac{\partial v}{\partial y}\right) - v\frac{\partial^2 v}{\partial x\partial y} = 0. \end{aligned} \quad (2.2.10)$$

Substitution of $u = w(x, y) \cos q(x, y)$ and $v = w(x, y) \sin q(x, y)$ into continuity equation (2.2.3) yields

$$\frac{\partial w}{\partial x} \cos q - w \sin q \frac{\partial q}{\partial x} + \frac{\partial w}{\partial y} \sin q + w \cos q \frac{\partial q}{\partial y} = 0. \quad (2.2.11)$$

On the other hand, substitution of the expressions $u = w(x, y) \cos q(x, y)$ and $v = w(x, y) \sin q(x, y)$ into equation (2.2.10) gives us the following equation

$$\begin{aligned} & -4 \cos q w \sin q \frac{\partial w}{\partial y} \frac{\partial q}{\partial x} - 4 w \cos q \sin q \left(\frac{\partial q}{\partial y}\right) \left(\frac{\partial w}{\partial x}\right) - 4 w (\cos q)^2 \left(\frac{\partial w}{\partial x}\right) \frac{\partial q}{\partial x} \\ & + 2 w^2 \cos q \sin q \left(\frac{\partial q}{\partial x}\right)^2 - w \cos q \sin q \left(\frac{\partial^2 w}{\partial x^2}\right) - 4 w^2 (\cos q)^2 \left(\frac{\partial q}{\partial y}\right) \left(\frac{\partial q}{\partial x}\right) \\ & - 2 w^2 \cos q \sin q \frac{\partial^2 q}{\partial x\partial y} + 4 w (\cos q)^2 \left(\frac{\partial q}{\partial y}\right) \left(\frac{\partial w}{\partial y}\right) - 2 w^2 \cos q \sin q \left(\frac{\partial q}{\partial y}\right)^2 \\ & + w \cos q \sin q \frac{\partial^2 w}{\partial y^2} - w^2 \frac{\partial^2 q}{\partial y^2} - \left(\frac{\partial w}{\partial y}\right) \left(\frac{\partial w}{\partial x}\right) - w \frac{\partial^2 w}{\partial x\partial y} + 2 (\cos q) \left(\frac{\partial w}{\partial y}\right)^2 \frac{\partial w}{\partial x} \\ & + 2 w (\cos q)^2 \frac{\partial^2 w}{\partial x\partial y} + \cos q \sin q \left(\frac{\partial w}{\partial y}\right)^2 - \cos q \sin q \left(\frac{\partial w}{\partial x}\right)^2 - w^2 (\cos q)^2 \frac{\partial^2 q}{\partial x^2} \\ & + w^2 (\cos q)^2 \left(\frac{\partial^2 q}{\partial y^2}\right) + 2 w^2 \left(\frac{\partial q}{\partial y}\right) \left(\frac{\partial q}{\partial x}\right) + w \left(\frac{\partial w}{\partial x}\right) \left(\frac{\partial q}{\partial x}\right) - 3 w \left(\frac{\partial q}{\partial y}\right) \left(\frac{\partial w}{\partial y}\right) = 0. \end{aligned} \quad (2.2.12)$$

Differentiating equation (2.2.11) with respect to x and y , we obtain

$$\cos q \frac{\partial^2 w}{\partial x^2} - 2 \sin q \left(\frac{\partial w}{\partial x}\right) \left(\frac{\partial q}{\partial x}\right) - w \cos q \left(\frac{\partial q}{\partial x}\right)^2 - w \sin q \frac{\partial^2 q}{\partial x^2} + \sin q \frac{\partial^2 w}{\partial x\partial y}$$

$$\begin{aligned}
& + \cos q \left(\frac{\partial w}{\partial y} \right) \left(\frac{\partial q}{\partial x} \right) + \cos q \left(\frac{\partial w}{\partial x} \right) \left(\frac{\partial q}{\partial y} \right) - w \sin q \left(\frac{\partial q}{\partial y} \right) \left(\frac{\partial q}{\partial x} \right) + w \cos q \frac{\partial^2 q}{\partial x \partial y} = 0, \\
& \cos q \frac{\partial^2 w}{\partial x \partial y} - \sin q \left(\frac{\partial w}{\partial x} \right) \left(\frac{\partial q}{\partial y} \right) - \sin q \left(\frac{\partial w}{\partial y} \right) \left(\frac{\partial q}{\partial x} \right) - w \cos q \left(\frac{\partial q}{\partial y} \right) \left(\frac{\partial q}{\partial x} \right) \\
& - w \sin q \frac{\partial^2 q}{\partial x \partial y} + \sin q \frac{\partial^2 w}{\partial y^2} + 2 \cos q \left(\frac{\partial w}{\partial y} \right) \left(\frac{\partial q}{\partial y} \right) - w \sin q \left(\frac{\partial q}{\partial y} \right)^2 + w \cos q \frac{\partial^2 q}{\partial y^2} = 0.
\end{aligned}$$

Then, we use these two equations together to find $\frac{\partial^2 q}{\partial x \partial y}$ and $\frac{\partial^2 w}{\partial x \partial y}$. After that, substitute the value of mixed derivatives into equation (2.2.12), we get the following

$$\begin{aligned}
& -w^2 \frac{\partial^2 q}{\partial y^2} - \left(\frac{\partial w}{\partial x} \right) \left(\frac{\partial w}{\partial y} \right) - 3w \left(\frac{\partial w}{\partial y} \right) \left(\frac{\partial q}{\partial y} \right) - \underline{2w \cos q \sin q \left(\frac{\partial q}{\partial y} \right) \left(\frac{\partial w}{\partial x} \right)} \\
& - 2w^2 (\cos q)^2 \left(\frac{\partial q}{\partial x} \right) \left(\frac{\partial q}{\partial y} \right) - w \left(\frac{\partial q}{\partial x} \right) \left(\frac{\partial w}{\partial x} \right) + 2w (\cos q)^2 \left(\frac{\partial q}{\partial y} \right) \left(\frac{\partial w}{\partial y} \right) \\
& - w^2 \cos q \sin q \left(\frac{\partial q}{\partial y} \right)^2 - \underline{2w (\cos q)^2 \left(\frac{\partial w}{\partial x} \right) \left(\frac{\partial q}{\partial x} \right)} + w^2 \cos q \sin q \left(\frac{\partial q}{\partial x} \right)^2 \\
& - 2w \cos q \sin q \left(\frac{\partial w}{\partial y} \right) \left(\frac{\partial q}{\partial x} \right) + 2 (\cos q)^2 \left(\frac{\partial w}{\partial y} \right) \left(\frac{\partial w}{\partial x} \right) + \underline{\cos q \sin q \left(\frac{\partial w}{\partial y} \right)^2} \\
& \underline{- \cos q \sin q \left(\frac{\partial w}{\partial x} \right)^2} - w^2 \frac{\partial^2 q}{\partial x^2} + w^2 \left(\frac{\partial q}{\partial x} \right) \left(\frac{\partial q}{\partial y} \right) = 0.
\end{aligned} \tag{2.2.13}$$

To eliminate the terms underlined, it is convenient to use continuity equation (2.2.11). The multiplication of equation (2.2.11) by $\frac{\partial w}{\partial x} \sin q$ gives us the value of $\left(\frac{\partial w}{\partial x} \right)^2 \cos q \sin q$. The multiplication of equation (2.2.11) by $\frac{\partial w}{\partial y} \cos q$ gives us the value of $\left(\frac{\partial w}{\partial y} \right)^2 \cos q \sin q$. The multiplication of equation (2.2.11) by $w \cos q \frac{\partial q}{\partial x}$ gives us the value of $w (\cos q)^2 \left(\frac{\partial w}{\partial x} \right) \left(\frac{\partial q}{\partial x} \right)$. The multiplication of equation (2.2.11) by $w \sin q \frac{\partial q}{\partial y}$ gives us the value of $w \cos q \sin q \left(\frac{\partial w}{\partial x} \right) \left(\frac{\partial q}{\partial y} \right)$. Then the substituting these values, $\left(\frac{\partial w}{\partial x} \right)^2 \cos q \sin q$, $\left(\frac{\partial w}{\partial y} \right)^2 \cos q \sin q$, $w (\cos q)^2 \left(\frac{\partial w}{\partial x} \right) \left(\frac{\partial q}{\partial x} \right)$ and

$w \cos q \sin q \left(\frac{\partial w}{\partial x} \right) \left(\frac{\partial q}{\partial y} \right)$, into equation (2.2.13) instead of the terms underlined, after simplification, we obtain

$$\frac{\partial}{\partial x} \left(w^2 \frac{\partial q}{\partial x} \right) + \frac{\partial}{\partial y} \left(w^2 \frac{\partial q}{\partial y} \right) = 0. \quad (2.2.14)$$

All above algebraic manipulation are done by MAPLE program. The detailed MAPLE program can be found in Appendix A.

2.2.2 Transformation from Cartesian Coordinates (x, y) to Generalized Curvilinear Coordinates (φ, ψ)

The computation of flow fields in and around complex shapes such as ducts, engine, complete aircraft or automobiles, etc., involves computational boundaries that do not coincide with coordinate lines in a physical domain. For finite difference methods, the imposition of boundary conditions for such problems motivate the introduction of a mapping or transformation from a physical (x, y) domain to a generalized curvilinear coordinate space. The generalize coordinate domain is constructed so that a computational boundary in a physical domain coincides with a coordinate line in a generalized coordinate space.

The use of generalized coordinates implies that a distorted region in a physical domain is mapped into a rectangular region in the generalized coordinate space as shown in Figure 2.2.

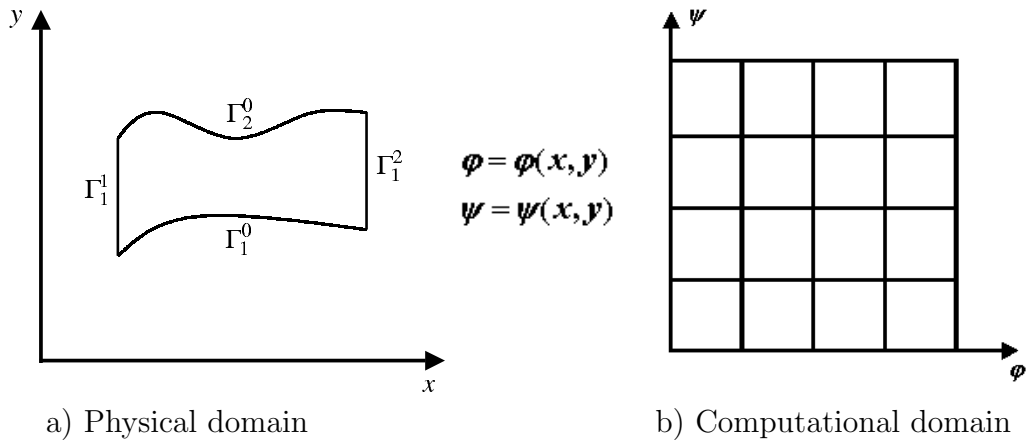


Figure 2.2: Physical and computational domain.

Next, we introduce new independent variables φ and ψ . We will choose ψ which is similar to a stream function and φ as an independent function which is similar to the potential. It is assumed that there is a unique, single-valued relationship between the generalized coordinates and the physical coordinates

which can be written as

$$\varphi = \varphi(x, y), \quad \psi = \psi(x, y) \quad (2.2.15)$$

and by implication

$$x = x(\varphi, \psi), \quad y = y(\varphi, \psi).$$

The specific relationship is given by the equations for total differentials of φ and ψ , respectively

$$d\varphi = \varphi_x dx + \varphi_y dy = \frac{\cos q}{\phi} dx + \frac{\sin q}{\phi} dy, \quad (2.2.16)$$

$$d\psi = \psi_x dx + \psi_y dy = -cw \sin q dx + cw \cos q dy. \quad (2.2.17)$$

In equations (2.2.16) and (2.2.17), c is a constant, and $\phi(x, y)$ is a new unknown function. These values are chosen such that the new variables (φ, ψ) are functionally independent, i.e. the Jacobian is not equal to zero

$$J(x, y) = \frac{\partial(\varphi, \psi)}{\partial(x, y)} = \frac{cw}{\phi} \neq 0.$$

Equation (2.2.16) has to determine unique function $\varphi(x, y)$. It means that the mixed derivatives are equal, i.e.

$$\frac{\partial^2 \varphi(x, y)}{\partial x \partial y} = \frac{\partial^2 \varphi(x, y)}{\partial y \partial x}. \quad (2.2.18)$$

Substitution of $\frac{\partial \varphi}{\partial y}$ and $\frac{\partial \varphi}{\partial x}$ from (2.2.16) into equation (2.2.18) gives the equation

$$\frac{\partial}{\partial x} \left(\frac{\sin q(x, y)}{\phi(x, y)} \right) = \frac{\partial}{\partial y} \left(\frac{\cos q(x, y)}{\phi(x, y)} \right). \quad (2.2.19)$$

Equation (2.2.19) may be used as an additional equation for the new unknown function $\phi(x, y)$. From equations (2.2.16) and (2.2.17), we have the value of partial derivatives

$$\begin{aligned} \frac{\partial \varphi}{\partial y} &= \frac{\sin q}{\phi(x, y)}; & \frac{\partial \varphi}{\partial x} &= \frac{\cos q}{\phi(x, y)}; \\ \frac{\partial \psi}{\partial x} &= -cw \sin q; & \frac{\partial \psi}{\partial y} &= cw \cos q. \end{aligned} \quad (2.2.20)$$

To transform the system of equations (2.2.11), (2.2.14) and (2.2.19) to new independent variables, we need to know the values of $\frac{\partial x}{\partial \varphi}$, $\frac{\partial x}{\partial \psi}$, $\frac{\partial y}{\partial \varphi}$ and $\frac{\partial y}{\partial \psi}$. It is easy to show that

$$\begin{bmatrix} \frac{\partial \varphi}{\partial x} & \frac{\partial \varphi}{\partial y} \\ \frac{\partial \psi}{\partial x} & \frac{\partial \psi}{\partial y} \end{bmatrix} \begin{bmatrix} \frac{\partial x}{\partial \varphi} & \frac{\partial x}{\partial \psi} \\ \frac{\partial y}{\partial \varphi} & \frac{\partial y}{\partial \psi} \end{bmatrix} = \begin{bmatrix} 1 & 0 \\ 0 & 1 \end{bmatrix}.$$

Really, we have

$$\begin{aligned} dx &= \frac{\partial x}{\partial \varphi} d\varphi + \frac{\partial x}{\partial \psi} d\psi, \\ dy &= \frac{\partial y}{\partial \varphi} d\varphi + \frac{\partial y}{\partial \psi} d\psi \end{aligned}$$

or in a matrix form

$$\begin{bmatrix} dx \\ dy \end{bmatrix} = \begin{bmatrix} \frac{\partial x}{\partial \varphi} & \frac{\partial x}{\partial \psi} \\ \frac{\partial y}{\partial \varphi} & \frac{\partial y}{\partial \psi} \end{bmatrix} \begin{bmatrix} d\varphi \\ d\psi \end{bmatrix}.$$

Solving this matrix equation, for the right-hand column matrix, we have

$$\begin{bmatrix} d\varphi \\ d\psi \end{bmatrix} = \begin{bmatrix} \frac{\partial x}{\partial \varphi} & \frac{\partial x}{\partial \psi} \\ \frac{\partial y}{\partial \varphi} & \frac{\partial y}{\partial \psi} \end{bmatrix}^{-1} \begin{bmatrix} dx \\ dy \end{bmatrix}.$$

This matrix form can be compared with the matrix form

$$\begin{bmatrix} d\varphi \\ d\psi \end{bmatrix} = \begin{bmatrix} \frac{\partial \varphi}{\partial x} & \frac{\partial \varphi}{\partial y} \\ \frac{\partial \psi}{\partial x} & \frac{\partial \psi}{\partial y} \end{bmatrix} \begin{bmatrix} dx \\ dy \end{bmatrix}.$$

Therefore

$$\begin{bmatrix} \frac{\partial \varphi}{\partial x} & \frac{\partial \varphi}{\partial y} \\ \frac{\partial \psi}{\partial x} & \frac{\partial \psi}{\partial y} \end{bmatrix} = \begin{bmatrix} \frac{\partial x}{\partial \varphi} & \frac{\partial x}{\partial \psi} \\ \frac{\partial y}{\partial \varphi} & \frac{\partial y}{\partial \psi} \end{bmatrix}^{-1}.$$

Following the standard rules for finding the inverse matrix, this equation is written as follows

$$\begin{bmatrix} \frac{\partial x}{\partial \varphi} & \frac{\partial x}{\partial \psi} \\ \frac{\partial y}{\partial \varphi} & \frac{\partial y}{\partial \psi} \end{bmatrix} = \frac{\begin{bmatrix} \frac{\partial \psi}{\partial y} & -\frac{\partial \varphi}{\partial y} \\ -\frac{\partial \psi}{\partial x} & \frac{\partial \varphi}{\partial x} \end{bmatrix}}{\begin{vmatrix} \frac{\partial \varphi}{\partial x} & \frac{\partial \varphi}{\partial y} \\ \frac{\partial \psi}{\partial x} & \frac{\partial \psi}{\partial y} \end{vmatrix}}$$

or

$$\begin{bmatrix} \frac{\partial x}{\partial \varphi} & \frac{\partial x}{\partial \psi} \\ \frac{\partial y}{\partial \varphi} & \frac{\partial y}{\partial \psi} \end{bmatrix} = \frac{1}{J} \begin{bmatrix} \frac{\partial \psi}{\partial y} & -\frac{\partial \varphi}{\partial y} \\ -\frac{\partial \psi}{\partial x} & \frac{\partial \varphi}{\partial x} \end{bmatrix} \quad (2.2.21)$$

where the Jacobian J is defined as

$$J = \frac{\partial(\varphi, \psi)}{\partial(x, y)} = \begin{vmatrix} \frac{\partial\varphi}{\partial x} & \frac{\partial\varphi}{\partial y} \\ \frac{\partial\psi}{\partial x} & \frac{\partial\psi}{\partial y} \end{vmatrix} = \frac{cw \cos^2 q}{\phi} + \frac{cw \sin^2 q}{\phi} = \frac{cw}{\phi} \neq 0.$$

Since the Jacobian $J \neq 0$, then ϕ and w are not equal to zero. Finally, we can rewrite (2.2.21) in the form

$$\begin{aligned} \frac{\partial x}{\partial\varphi} &= \frac{1}{J}\psi_y = \phi \cos q, & \frac{\partial x}{\partial\psi} &= -\frac{1}{J}\varphi_y = -\frac{\sin q}{cw}, \\ \frac{\partial y}{\partial\varphi} &= -\frac{1}{J}\psi_x = \phi \sin q, & \frac{\partial y}{\partial\psi} &= \frac{1}{J}\varphi_x = \frac{\cos q}{cw}. \end{aligned} \quad (2.2.22)$$

2.2.3 The Equations in New Generalized Curvilinear Coordinates (φ, ψ)

The first step: We transform the continuity equation (2.2.3). Substitution of $u = w \cos q$ and $v = w \sin q$ into this equation yields

$$\frac{\partial w \cos q}{\partial x} + \frac{\partial w \sin q}{\partial y} = 0$$

or

$$\cos q \frac{\partial w}{\partial x} - w \sin q \frac{\partial q}{\partial x} + \sin q \frac{\partial w}{\partial y} + w \cos q \frac{\partial q}{\partial y} = 0. \quad (2.2.23)$$

By using the chain rule, we have the formulas to change partial derivatives

$$\begin{aligned} \frac{\partial(\cdot)}{\partial x} &= \frac{\partial(\cdot)}{\partial\varphi} \frac{\partial\varphi}{\partial x} + \frac{\partial(\cdot)}{\partial\psi} \frac{\partial\psi}{\partial x} = \frac{\cos q}{\phi} \frac{\partial(\cdot)}{\partial\varphi} - cw \sin q \frac{\partial(\cdot)}{\partial\psi}, \\ \frac{\partial(\cdot)}{\partial y} &= \frac{\partial(\cdot)}{\partial\varphi} \frac{\partial\varphi}{\partial y} + \frac{\partial(\cdot)}{\partial\psi} \frac{\partial\psi}{\partial y} = \frac{\sin q}{\phi} \frac{\partial(\cdot)}{\partial\varphi} + cw \cos q \frac{\partial(\cdot)}{\partial\psi}. \end{aligned} \quad (2.2.24)$$

Substituting equations (2.2.24) into equation (2.2.23) and making simplifications, we get

$$\begin{aligned} &\frac{(\cos q)^2}{\phi} \frac{\partial w}{\partial\varphi} - cw \cos q \sin q \frac{\partial w}{\partial\psi} - w \frac{\cos q}{\phi} \sin q \frac{\partial q}{\partial\varphi} + cw^2 (\sin q)^2 \frac{\partial q}{\partial\psi} \\ &+ \frac{(\sin q)^2}{\phi} \frac{\partial w}{\partial\varphi} + cw \cos q \sin q \frac{\partial w}{\partial\psi} + w \frac{\sin q}{\phi} \cos q \frac{\partial q}{\partial\varphi} + cw^2 (\cos q)^2 \frac{\partial q}{\partial\psi} = 0 \end{aligned}$$

or

$$\frac{1}{\phi} [(\cos q)^2 + (\sin q)^2] \frac{\partial w}{\partial\varphi} + cw^2 [(\cos q)^2 + (\sin q)^2] \frac{\partial q}{\partial\psi} = 0$$

or

$$\frac{1}{\phi} \frac{\partial w}{\partial \varphi} + cw^2 \frac{\partial q}{\partial \psi} = 0,$$

which can be arranged into

$$\frac{\partial}{\partial \varphi} \left(\frac{1}{w} \right) = c\phi \frac{\partial q}{\partial \psi}. \quad (2.2.25)$$

The second step: We have to use the condition

$$\frac{\partial^2 \varphi}{\partial x \partial y} = \frac{\partial^2 \varphi}{\partial y \partial x}. \quad (2.2.26)$$

Substitution of $\frac{\partial \varphi}{\partial y}$ and $\frac{\partial \varphi}{\partial x}$ from equation (2.2.20) yields

$$\frac{\partial}{\partial y} \left(\frac{\cos q}{\phi} \right) = \frac{\partial}{\partial x} \left(\frac{\sin q}{\phi} \right) \quad (2.2.27)$$

or

$$-\phi \sin q \frac{\partial q}{\partial y} - \cos q \frac{\partial \phi}{\partial y} = \phi \cos q \frac{\partial q}{\partial x} - \sin q \frac{\partial \phi}{\partial x}.$$

Substituting equations (2.2.24) into equation (2.2.7) and making simplifications, we get the following equation in the term of new variables

$$\frac{\partial \phi}{\partial \psi} = -\frac{1}{cw} \frac{\partial q}{\partial \varphi}. \quad (2.2.28)$$

The third step: Substituting partial derivatives from equations (2.2.24) into equation

$$\frac{\partial}{\partial x} \left(w^2 \frac{\partial q}{\partial x} \right) + \frac{\partial}{\partial y} \left(w^2 \frac{\partial q}{\partial y} \right) = 0,$$

we obtain

$$\frac{\partial}{\partial x} \left(w^2 \frac{\cos q}{\phi} \frac{\partial q}{\partial \varphi} - cw^3 \sin q \frac{\partial q}{\partial \psi} \right) + \frac{\partial}{\partial y} \left(w^2 \frac{\sin q}{\phi} \frac{\partial q}{\partial \varphi} + cw^3 \cos q \frac{\partial q}{\partial \psi} \right) = 0.$$

By simplifying, we get then the equation in the terms of new variables as follows

$$\frac{\partial}{\partial \varphi} \left(\frac{w^2}{\phi} \frac{\partial q}{\partial \varphi} \right) + c^2 w \phi \frac{\partial}{\partial \psi} \left(w^3 \frac{\partial q}{\partial \psi} \right) = 0. \quad (2.2.29)$$

In order to transform equations (2.2.1), (2.2.3) and (2.2.26) to equations (2.2.25), (2.2.28) and (2.2.29), a program by MAPLE is developed the detailed description of this program can be found in Appendix A.

We have to find the image of fluid domain in the new variables (φ, ψ) . It is clear that impermeable boundaries Γ'_0 , Γ''_0 (AD and BC) are streamlines

and $\psi|_{AD}$ and $\psi|_{BC}$ are constants. The function $\psi(x, y)$ is determined up to an arbitrary constant, and without loss of generality, we can choose

$$\psi|_{BC} = 0.$$

Then we have

$$\psi|_{AD} = \psi(A) = \text{const.}$$

We can take the curvilinear integral of $d\psi$ along the boundary AB (see Figure 2.1) to estimate the value of $\psi(A)$ through the given values of w and q on the boundary AB

$$\int_A^B d\psi = \int_A^B [\psi_x dx + \psi_y dy] = \int_{AB} [-cw_1 \sin q_1 dx + cw_1 \cos q_1 dy]$$

where functions $w_1(x, y)$, $q_1(x, y)$ are given by boundary conditions (2.2.5). We can rewrite the previous equation in the form

$$\psi(B) - \psi(A) = c \left[\int_A^B [-w_1 \sin q_1 dx + w_1 \cos q_1 dy] \right].$$

If we choose the value of the constant c as

$$c = \frac{1}{\left[\int_A^B [-w_1 \sin q_1 dx + w_1 \cos q_1 dy] \right]},$$

and take into account that $\psi(B) = 0$, we obtain

$$\psi(A) = -1.$$

It means that the image of boundary AD is an interval of straight line

$$\psi|_{AD} = -1.$$

Now we have to find the image of AB and CD . Let us assume that equation of boundary AB is given in the explicit form

$$y = y_{AB}(x) \tag{2.2.30}$$

or in the differential form

$$dy = y'_{AB}(x) dx$$

then

$$dy - y'_{AB}(x) dx = 0. \tag{2.2.31}$$

Substitution of equalities

$$\begin{aligned} dy &= y_\varphi d\varphi + y_\psi d\psi, \\ dx &= x_\varphi d\varphi + x_\psi d\psi \end{aligned}$$

into equation (2.2.31) yields

$$(y_\varphi - y'_{AB}(x)x_\varphi) d\varphi + (y_\psi - y'_{AB}(x)x_\psi) d\psi = 0. \quad (2.2.32)$$

We assume that the image of AB is given by the equation

$$\varphi = \varphi_{A'B'}(\psi). \quad (2.2.33)$$

In (φ, ψ) -plane, equation (2.2.32) is ODE for unknown function $\varphi_{A'B'}(\psi)$

$$\frac{d\varphi_{A'B'}(\psi)}{d\psi} = -\frac{y_\psi - y'_{AB}(x)x_\psi}{y_\varphi - y'_{AB}(x)x_\varphi}. \quad (2.2.34)$$

Substitution of y_ψ , x_ψ , y_φ , x_φ from equations (2.2.22) gives

$$\varphi'_{A'B'}(\psi) = -\frac{\cos q_1 + y'_{AB}(x) \sin q_1}{c \phi w_1 (\sin q_1 - y'_{AB}(x) \cos q_1)}. \quad (2.2.35)$$

The function $\varphi_{A'B'}(\psi)$ is a new unknown and may be calculated from equation (2.2.35). In some particular practical cases, equation (2.2.35) has an analytical solution. These cases can be illustrated by the following examples:

Example 1: Let us assume that

$$y_{AB}(x) = \text{const and } q_1 = \pi/2.$$

It is clear that in this case

$$\frac{d\varphi_{A'B'}(\psi)}{d\psi} = 0,$$

therefore

$$\varphi_{A'B'}(\psi) = \text{const.}$$

Because $\varphi_{A'B'}(0) = 0$, we get

$$\varphi_{A'B'}(\psi) = 0.$$

Example 2: Let us assume that

$$y_{AB}(x) = lx + m$$

and fluid entering into domain by right angle, i.e.

$$\cos q_1 + y'_{AB}(x) \sin q_1 = 0.$$

In this case, again we have

$$\frac{d\varphi_{A'B'}(\psi)}{d\psi} = 0,$$

therefore

$$\varphi_{A'B'}(\psi) = 0.$$

Let us consider boundary CD . In the case of problem 3', we know the values of flow angle at the boundary CD

$$q(x, y) = q_2(x, y), \quad (x, y) \in \Gamma^2.$$

Let us assume that equation of boundary CD is given in the explicit form

$$x = x_{CD}(y),$$

or in the differential form

$$dx = x'_{CD}(y)dy,$$

then

$$dx - x'_{CD}(y)dy = 0. \quad (2.2.36)$$

Substitution of equalities

$$dy = y_\varphi d\varphi + y_\psi d\psi,$$

$$dx = x_\varphi d\varphi + x_\psi d\psi,$$

into equation (2.2.36) yields

$$(x_\varphi - x'_{CD}(y)y_\varphi)d\varphi + (x_\psi - x'_{CD}(y)y_\psi)d\psi = 0. \quad (2.2.37)$$

We assume that image of CD is given by the equation

$$\varphi = \varphi_{C'D'}(\psi).$$

In (φ, ψ) – plane equation (2.2.37) is ODE for unknown function $\varphi_{C'D'}(\psi)$

$$\frac{d\varphi_{C'D'}(\psi)}{d\psi} = -\frac{x_\psi - x'_{CD}(y)y_\psi}{x_\varphi - x'_{CD}(y)y_\varphi},$$

or

$$\varphi'_{C'D'}(\psi) = \frac{\sin q_2 + x'_{CD}(y) \cos q_2}{cw\phi(\cos q_2 - x'_{CD}(y) \sin q_2)}. \quad (2.2.38)$$

In some particular cases the function $\varphi_{C'D'}(\psi)$ has simple form. These cases can be illustrated by the following example:

Example 3: Let us assume that

$$x_{CD}(y) = \text{const}, \quad \text{and } q_2 = 0.$$

It is clear that in this case

$$\frac{d\varphi_{C'D'}(\psi)}{d\psi} = 0,$$

therefore

$$\varphi_{C'D'}(\psi) = \text{const},$$

and due to $\varphi_{C'D'}(0) = 1$, we get

$$\varphi_{C'D'}(\psi) = 1.$$

In the case of problem 2', we know the pressure at the boundary CD , $P(x, y) = P_2(x, y)$, $(x, y) \in \Gamma_2$. Here, the situation is slightly more complicated. Let us assume that equation of boundary $C'D'$ is given by the formula

$$\varphi = \varphi_{C'D'}(\psi)$$

and the equation of boundary CD is given by the formula

$$y = y_{CD}(x).$$

By analogy with two previous cases, we have

$$\varphi'_{C'D'}(\psi) = -\frac{\cos q + y'_{CD}(x) \sin q}{c \phi w_2 (\sin q - y'_{CD}(x) \cos q)}. \quad (2.2.39)$$

Main difference between formulas (2.2.38) and (2.2.39) is that values of q in (2.2.39) are still unknown on boundary CD . To get equation for q on CD , we have to use two equations (2.2.1) and (2.2.2). Let us consider a particular case when equation of boundary CD is $x = x_0 - \text{const}$ and $P = P_2(y) = \text{const}$, $y \in CD$. In this case we have

$$u \frac{\partial v}{\partial x} + v \frac{\partial v}{\partial y} = -\frac{\partial P}{\partial y} = 0. \quad (2.2.40)$$

Substitution of $u = w \cos q(x, y)$ and $v = w \sin q(x, y)$ into equation (2.2.40) and simplification with help of continuity equation (2.2.3) yield

$$\frac{\partial q}{\partial \varphi} = c \phi w \tan q \frac{\partial q}{\partial \psi}, \quad (\varphi, \psi) \in C'D'. \quad (2.2.41)$$

We must use equation (2.2.41) as the boundary condition for q on boundary $C'D'$.

Now we have to derive boundary condition for function $\phi = \phi(x, y)$. The new unknown function ϕ subject to the condition that the Jacobian $J(x, y) = \frac{cw}{\phi}$ is not equal to zero or infinity. This function also has to satisfy equation (2.2.27). The boundary conditions for $\phi(x, y)$ are arbitrary. We can put $\phi(x, y) = \phi_0 - \text{const}$ on the streamline BC. Then we can integrate equation (2.2.16)

$$d\varphi = \frac{1}{\phi}(\cos q dx + \sin q dy)$$

along the streamline BC

$$\int_{B'C'} d\varphi = \int_{B'}^{C'} \frac{1}{\phi}(\cos q dx + \sin q dy)$$

or

$$\varphi(C') - \varphi(B') = \frac{1}{\phi_0} L_{BC}$$

where L_{BC} is the length of boundary BC . If we choose $\phi_0 = L_{BC}$ and take into account that $\varphi(B') = 0$, we obtain

$$\varphi(C') = 1.$$

In order to summarize, we write the formulation of problem 3' and problem 2' in a compact form in terms of new unknown functions and new independent variables (φ, ψ) .

Problem 3':

We have to find the simultaneous solutions of the following set of partial differential equations

$$\frac{\partial}{\partial \varphi} \left(\frac{1}{w} \right) = c\phi \frac{\partial q}{\partial \psi} \quad (2.2.42)$$

$$\frac{\partial \phi}{\partial \psi} = -\frac{1}{cw} \frac{\partial q}{\partial \varphi} \quad (2.2.43)$$

$$\frac{\partial}{\partial \varphi} \left(\frac{w^2}{\phi} \frac{\partial q}{\partial \varphi} \right) + c^2 w \phi \frac{\partial}{\partial \psi} \left(w^3 \frac{\partial q}{\partial \psi} \right) = 0 \quad (2.2.44)$$

in the domain $A'B'C'D'$ depicted in Figure 2.3.

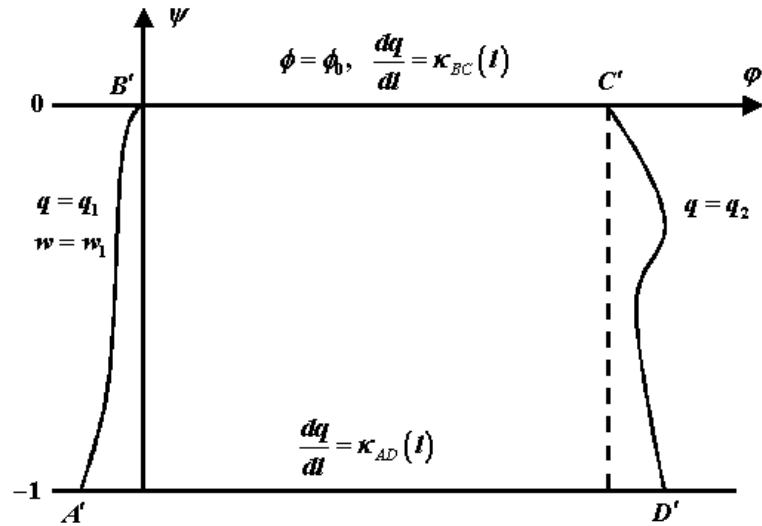


Figure 2.3: Domain $A'B'C'D'$ for problem 3'.

Equations (2.2.42)–(2.2.44) have to satisfy the following boundary conditions.

$$\begin{aligned}
A'B' : \quad \frac{d\varphi_{A'B'}}{d\psi} &= -\frac{\cos q_1 + y'_{AB}(x) \sin q_1}{c \phi w_1 (\sin q_1 - y'_{AB}(x) \cos q_1)}; \psi \in [0, -1] \\
\varphi_{A'B'}(0) &= 0, \\
q &= q_1(\varphi, \psi), \quad \varphi = \varphi_{A'B'}(\psi) \\
w &= w_1(\varphi, \psi), \quad \varphi = \varphi_{A'B'}(\psi)
\end{aligned} \tag{2.2.45}$$

$$\begin{aligned}
B'C' : \quad \phi(\varphi, 0) &= \phi_0, \quad \phi_0 \neq 0, \\
\frac{dq}{dl} &= k_{BC}(l),
\end{aligned} \tag{2.2.46}$$

$$\begin{aligned}
C'D' : \quad q &= q_2(\varphi, \psi), \quad \varphi = \varphi_{C'D'}(\psi) \\
\frac{d\varphi_{C'D'}}{d\psi} &= -\frac{\cos q_2 + y'_{CD}(x) \sin q_2}{c \phi w_2 (\sin q_2 - y'_{CD}(x) \cos q_2)}; \psi \in [0, -1] \\
\varphi_{C'D'}(0) &= 1
\end{aligned} \tag{2.2.47}$$

$$A'D' : \quad \frac{dq}{dl} = k_{AD}(l), \tag{2.2.48}$$

where $k_{AD}(l)$ and $k_{BC}(l)$, as functions of the length l along the curve are curvature of boundaries AD and BC .

Problem 2':

We have to find the simultaneous solutions of equations (2.2.42)–(2.2.44) in the domain $A'B'C'D'$ depicted in Figure 2.4 with boundary conditions

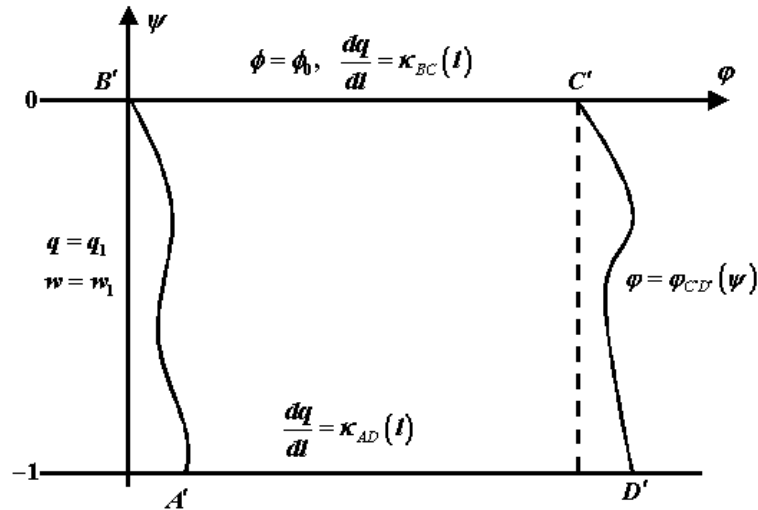


Figure 2.4: Domain $A'B'C'D'$ for problem 2'.

$$\begin{aligned}
A'B' : \quad \frac{d\varphi_{A'B'}}{d\psi} &= -\frac{\cos q_1 + y'_{AB}(x) \sin q_1}{c \phi w_1 (\sin q_1 - y'_{AB}(x) \cos q_1)}; \psi \in [0, -1] \\
\varphi_{A'B'}(0) &= 0 \\
q &= q_1(\varphi, \psi), \quad \varphi = \varphi_{A'B'}(\psi) \\
w &= w_1(\varphi, \psi), \quad \varphi = \varphi_{A'B'}(\psi)
\end{aligned} \tag{2.2.49}$$

$$\begin{aligned}
B'C' : \quad \phi(\varphi, 0) &= \phi_0, \quad \phi_0 \neq 0, \\
\frac{dq}{dl} &= k_{BC}(l),
\end{aligned} \tag{2.2.50}$$

$$\begin{aligned}
C'D' : \quad \frac{d\varphi_{C'D'}}{d\psi} &= -\frac{\cos q + y'_{CD}(x) \sin q}{c \phi w_2 (\sin q - y'_{CD}(x) \cos q)}; \psi \in [0, -1] \\
\varphi_{C'D'}(0) &= 1,
\end{aligned} \tag{2.2.51}$$

$$\frac{\partial q}{\partial \varphi} = c \phi w \tan q \frac{\partial q}{\partial \psi}, \quad (\varphi, \psi) \in C'D'$$

$$A'D' : \quad \frac{dq}{dl} = k_{AD}(l),$$

where $k_{AD}(l)$ and $k_{BC}(l)$, as functions of the length l along the curve are curvature of boundaries AD and BC .

2.3 Discretization of the Equations and the Solution Procedure

To explain the numerical procedure, we restrict ourself to the case of problem 3'. In this case, domain $A'B'C'D'$ is the uniform rectangular domain. In the case of the problem 2', we can use new variables

$$\begin{aligned}
\tilde{\psi} &= \psi, \\
\tilde{\varphi} &= \frac{\varphi - \varphi_{A'B'}(\psi)}{\varphi_{C'D'}(\psi) - \varphi_{A'B'}(\psi)}
\end{aligned}$$

to transform domain $A'B'C'D'$ into a rectangular domain. For a moment, we assume that the function q is given. Then equations (2.2.42) or (2.2.43) are the hyperbolic system of equations with respect to w and ϕ . We have the Goursat problem for the system of equations (2.2.42) and (2.2.43) with w is given on $A'B'$ and ϕ is known on $B'C'$. If we assume that w and ϕ are known then equation (2.2.44) is elliptic with respect to q . By virtue of this note, we will create an iterative process.

In domain $A'B'C'D'$, we construct a uniform rectangular finite difference grid $\Omega_h = \{(\psi_i, \varphi_j), \psi_i = -1 + (i-1)h_\psi, \varphi_j = (j-1)h_\varphi, i = 1, \dots, N_1;$

$j = 1, \dots, N_2\}$. All unknown functions are approximated at the nodes of grid. To calculate the solution of equations (2.2.42)-(2.2.44), we design the following iterative process:

- Suppose we know $q^{(n-1)}$, $w^{(n-1)}$ and $\phi^{(n-1)}$ from the previous iteration or from the initial guess.
- The solution of equations (2.2.42) and (2.2.43) with $q = q^{(n-1)}$ is evaluated by the method of characteristics.
- When the values $w^{(n)}$ and $\phi^{(n)}$ are found, we solve equation (2.2.44) by either the block SOR or the Stabilizing Correction method.

For finding the solution of equations (2.2.42) and (2.2.43) by the method of characteristic, the partial derivatives of $q(x, y)$ are taken from the $(n-1)$ -st iteration. On each line $\psi = \text{const}$ and $\varphi = \text{const}$ the Modified Euler Predictor-Corrector method (see J. D. Hoffman (1992)) is used. The derivatives $\frac{\partial q^{(n-1)}}{\partial \psi}$ and $\frac{\partial q^{(n-1)}}{\partial \varphi}$ are approximated by the central finite differences. At the boundary, these derivatives are approximated by one-sided finite differences of second order. The Predictor-Corrector method consists of the following two steps:

The first step (Predictor) is

$$\begin{aligned} \frac{\left(\frac{1}{w^*}\right)_{i,j} - \left(\frac{1}{w^{(n-1)}}\right)_{i,j-1}}{h_\varphi} &= c \phi_{i,j-1}^{(n-1)} \left(\delta_h q_\psi^{(n-1)}\right)_{i,j-1}, \\ &i = 1, \dots, N_1, j = 2, \dots, N_2 \\ \frac{\phi_{i+1,j}^{(n-1)} - \phi_{i,j}^*}{h_\psi} &= -\frac{1}{c w_{i+1,j}^{(n-1)}} \left(\delta_h q_\varphi^{(n-1)}\right)_{i+1,j}, \\ &i = N_1 - 1, \dots, 1, j = 1, \dots, N_2. \end{aligned}$$

The second step (Corrector) is

$$\begin{aligned} \frac{\left(\frac{1}{w^n}\right)_{i,j} - \left(\frac{1}{w^{(n-1)}}\right)_{i,j-1}}{h_\varphi} &= \frac{1}{2} \left[c \phi_{i,j}^* \left(\delta_h q_\psi^{(n-1)}\right)_{i,j} + c \phi_{i,j-1}^{(n-1)} \left(\delta_h q_\psi^{(n-1)}\right)_{i,j-1} \right], \\ &i = 1, \dots, N_1, j = 2, \dots, N_2 \\ \frac{\phi_{i+1,j}^{(n-1)} - \phi_{i,j}^{(n)}}{h_\psi} &= \frac{1}{2} \left[-\frac{1}{c w_{i,j}^*} \left(\delta_h q_\varphi^{(n-1)}\right)_{i,j} - \frac{1}{c w_{i+1,j}^{(n-1)}} \left(\delta_h q_\varphi^{(n-1)}\right)_{i+1,j} \right], \\ &i = N_1 - 1, \dots, 1, j = 1, \dots, N_2. \end{aligned}$$

Here the superscript (*) denotes the results of the predictor, and δ_h denotes the second order approximation of corresponding derivatives q_φ or q_ψ . Before to perform calculations in this stage, we have to calculate ϕ on line $A'B'$ and w on the boundary $B'C'$ by using the equation

$$\frac{\partial \phi}{\partial \psi} = -\frac{1}{c w_1} \frac{\partial q}{\partial \varphi}.$$

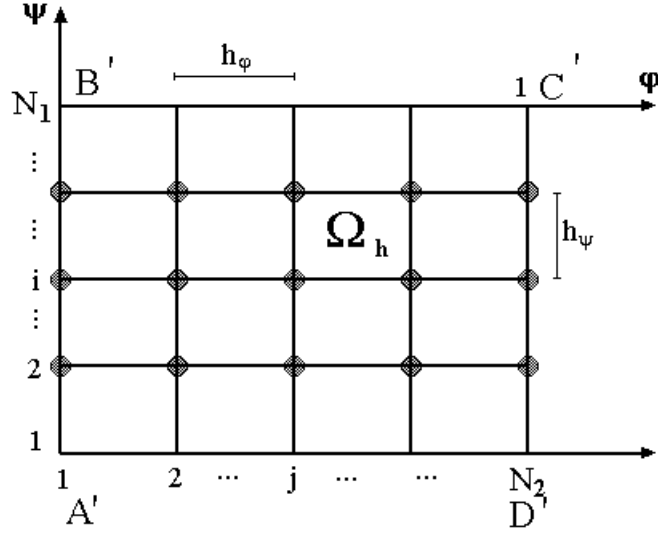


Figure 2.5: Sketch of finite difference grid.

$$\phi_{ij} = \phi(\varphi_j, \psi_i), \quad \psi_i = -1 + h_\psi(i - 1), \quad \varphi_j = (j - 1)h_\varphi.$$

Let us assume, for simplicity, that $w_1 = \text{const}$. Integrating this equation with respect to ψ from ψ_i to 0, we get

$$\begin{aligned} \int_{\psi_i}^0 \frac{\partial \phi}{\partial \psi} &= -\frac{1}{c w_1} \int_{\psi_i}^0 \frac{\partial q}{\partial \varphi}, \\ \phi(0, 0) - \phi(0, \psi_i) &= -\frac{1}{c w_1} \int_{\psi_i}^0 (q_\varphi) d\psi, \end{aligned}$$

or in the difference form

$$\phi_{i,1} = \phi_{N_1,1} + \frac{1}{c w_1} \int_{\psi_i}^0 q(\varphi) d\psi, \quad i = N_1 - 1, N_1 - 2, \dots, 1.$$

For $i = N_1 - 1$, we can approximate the last equation as follows

$$\phi_{N_1-1,1} \approx \phi_{N_1,1} + \frac{1}{2 c w_1} \left[(q_\varphi)_{N_1,1} + (q_\varphi)_{N_1-1,1} \right] h_1,$$

where $h_1 = \psi_{i+1} - \psi_i$. Here, to estimate $\int_{\psi_{N_1-1}}^0 (q_\varphi) d\psi$, we use the trapezoidal rule. For the case $i < N_1 - 1$ we use the Simpson formula of fourth order to

approximate the integral $\int_{\psi_i}^{\psi_{i+2}} (q_\varphi) d\psi$

$$\begin{aligned}\phi_{i,1} &= \phi_{N_1,1} + \frac{1}{c w_1} \left[\int_{\psi_i}^0 (q_\varphi) d\psi + \int_{\psi_i}^{\psi_{i+2}} (q_\varphi) d\psi \right] \\ &= \phi_{i+2,1} + \frac{1}{c w_1} \int_{\psi_i}^{\psi_{i+2}} (q_\varphi) d\psi \\ &\approx \phi_{i+2,1} + \frac{1}{6 c w_1} [(q_\varphi)_i + 4(q_\varphi)_{i+1} + (q_\varphi)_{i+2}] h_1, \\ & \quad i = N_1 - 2, \dots, 1.\end{aligned}$$

Equation (2.2.42) is used to find $w(x, y)$ along boundary BC . Integrating equation (2.2.42) with respect to φ from 0 to φ_j , we get

$$\begin{aligned}\int_0^{\varphi_j} \frac{\partial}{\partial \varphi} \left(\frac{1}{w} \right) d\varphi &= c \phi_0 \int_0^{\varphi_j} \frac{\partial q}{\partial \psi} d\varphi, \\ \frac{1}{w_{N_1,j}} - \frac{1}{w_{N_1,1}} &= c \phi_0 \int_0^{\varphi_j} \frac{\partial q}{\partial \psi} d\varphi, \quad j = 2, \dots, N_2\end{aligned}\quad (2.3.1)$$

For the case $j=2$, we approximate the right hand side of equation (2.3.1) by the trapezoidal rule

$$\frac{1}{w_{N_1,2}} \approx \frac{1}{w_{N_1,1}} + \frac{1}{2} c \phi_0 [(q_\psi)_{N_1,1} + (q_\psi)_{N_1,2}] h_2.$$

For the case $j > 2$, we use the Simpson formula of fourth order to approximate integral $\int_{\varphi_j}^{\varphi_{j+2}} (q_\psi) d\varphi$

$$\begin{aligned}\frac{1}{w_{N_1,j}} &= \frac{1}{w_{N_1,1}} + c \phi_0 \left[\int_0^{\varphi_{j-2}} (q_\psi) d\varphi + \int_{\varphi_{j-2}}^{\varphi_j} (q_\psi) d\varphi \right] \\ &= \frac{1}{w_{N_1,j-2}} + c \phi_0 \left[\int_{\varphi_{j-2}}^{\varphi_j} (q_\psi) d\varphi \right] \\ &\approx \frac{1}{w_{N_1,j-2}} + \frac{c \phi_0}{6} [(q_\psi)_j + 4(q_\psi)_{j-1} + (q_\psi)_{j-2}] h_2, \\ & \quad j = 3, \dots, N_2.\end{aligned}$$

where $h_2 = \varphi_{j+1} - \varphi_j$. The partial derivatives $\frac{\partial q}{\partial \psi}$ and $\frac{\partial q}{\partial \varphi}$ are approximated by the second order central difference and by one side second order difference near edge points A', C', B'

$$\left(\frac{\partial q}{\partial \psi} \right)_{i,j_0} = \begin{cases} \frac{1}{2} \frac{q_{i+1,j_0} - q_{i-1,j_0}}{h_1}; & i \neq 1 \text{ and } i \neq N_1, \\ \frac{1}{2} \frac{3q_{N_1,j_0} - 4q_{N_1-1,j_0} + q_{N_1-2,j_0}}{h_1}; & i = N_1, \\ \frac{1}{2} \frac{-3q_{1,j_0} + 4q_{2,j_0} - q_{3,j_0}}{h_1}; & i = 1, \end{cases}$$

$$\left(\frac{\partial q}{\partial \varphi}\right)_{i_0,j} = \begin{cases} \frac{1}{2} \frac{q_{i_0,j+1} - q_{i_0,j-1}}{h_2}; & j \neq 1 \text{ and } j \neq N_2, \\ \frac{1}{2} \frac{3q_{i_0,N_2} - 4q_{i_0,N_2-1} + q_{i_0,N_2-2}}{h_2}; & j = N_2, \\ \frac{1}{2} \frac{-3q_{i_0,1} + 4q_{i_0,2} - q_{i_0,3}}{h_2}; & j = 1. \end{cases}$$

When the values $w^{(n)}$ and $\phi^{(n)}$ are found for all grid points, we can solve equation (2.2.44). Before to perform calculations in this stage, we have to find $q^{(n)}$ on the boundaries $B'C'$ and $A'D'$. Due to the boundary condition imposed on $\phi(x, y)$ at the boundary BC , we have

$$d\varphi = \frac{1}{\phi_0}(\cos q dx + \sin q dy) = \frac{1}{\phi_0} dl \quad (2.3.2)$$

where ϕ_0 is nonzero constant and l is the natural parameter of curve AD . Let us integrate (2.3.2) from 0 to $\varphi_j = (j-1)h_\varphi$

$$\int_0^{\varphi_j} d\varphi = \frac{1}{\phi_0} \int_0^{\varphi_j} dl$$

or

$$\varphi_j = \frac{1}{\phi_0} l_j$$

where l_j is length of curve BC from the point which corresponds to $\varphi_1 = 0$ to the point which corresponds to $\varphi = \varphi_j$. To find q_j we can use natural equation of curve BC (see E. V. Shikin(1995))

$$\frac{dq}{dl} = k_{BC}(l),$$

where $k_{BC}(l)$ is equation of curve BC in natural form. Integrating this equations with respect to l from 0 to l_j we get

$$q_{1,j} - q_{N_1,0} = \int_0^{l_j} k_{BC}(l) dl.$$

It is important to remark that the boundary condition for q at boundary BC has to be estimated only once before starting the iterative process. On the boundary AD we do not know the exact values of $\phi(\varphi, \psi)$. The boundary condition for q on the boundary AD has to be involved into the outer iterative process. In this case we have

$$\phi(\psi, \varphi) d\varphi = dl,$$

or after integration

$$l_j = \int_0^{\varphi_j} \phi^{(n)}(\psi, \varphi) d\varphi, \quad \psi = -1.$$

Utilizing the natural equation of boundary AD , we obtain

$$\frac{d\tilde{q}^{(n)}}{dl} = k_{AD}(l),$$

or after integration

$$\tilde{q}_{1,j}^{(n)} - \tilde{q}_{1,0}^{(n)} = \int_0^{l_j} k_{AD}(l) dl$$

where $\tilde{q}^{(n)}$, $\phi^{(n)}$ denote the values on $n - th$ iteration.

For the sake of simplicity, either the block SOR or the Stabilizing Corrections method (see N. N. Yanenko(1971)) is used to find the approximate solution $\tilde{q}^{(n)}$ of equation (2.2.44). We utilize the second order central differences to approximate the partial derivatives. The system of tridiagonal linear algebraic equations is solved by the “sweep method” (see for example N. N. Yanenko(1971)). Relaxation is needed to achieve the convergence

$$q_{ij}^{(n)} = q_{ij}^{(n-1)} + \omega(\tilde{q}_{ij}^{(n)} - q_{ij}^{(n-1)}). \quad (2.3.3)$$

The relaxation factor ω is chosen by trial and error method. The iterative process is terminated when the convergence criterion is achieved

$$\begin{aligned} \max_{i,j \in \Omega h} \left| \frac{q_{ij}^{(n)} - q_{ij}^{(n-1)}}{q_{ij}^{(n)}} \right| &< \epsilon_q, \\ \max_{i,j \in \Omega h} \left| \frac{\phi_{ij}^{(n)} - \phi_{ij}^{(n-1)}}{\phi_{ij}^{(n)}} \right| &< \epsilon_\phi, \\ \max_{i,j \in \Omega h} \left| \frac{w_{ij}^{(n)} - w_{ij}^{(n-1)}}{w_{ij}^{(n)}} \right| &< \epsilon_w \end{aligned} \quad (2.3.4)$$

where ϵ_q , ϵ_ϕ and ϵ_w are the convergence tolerances. A flowchart of the iterative process is presented in Figure 2.6. It is needed to point that there are also efficient numerical methods to solve equation (2.2.44) such as some direct method, preconditioning techniques, etc.. However, these methods require more storage than the relaxation methods or fractional step methods and also they are more complicated to develop a computing programme. For convenience, we write the formulas of the block SOR method as well as formulas of the Stabilizing Correction method.

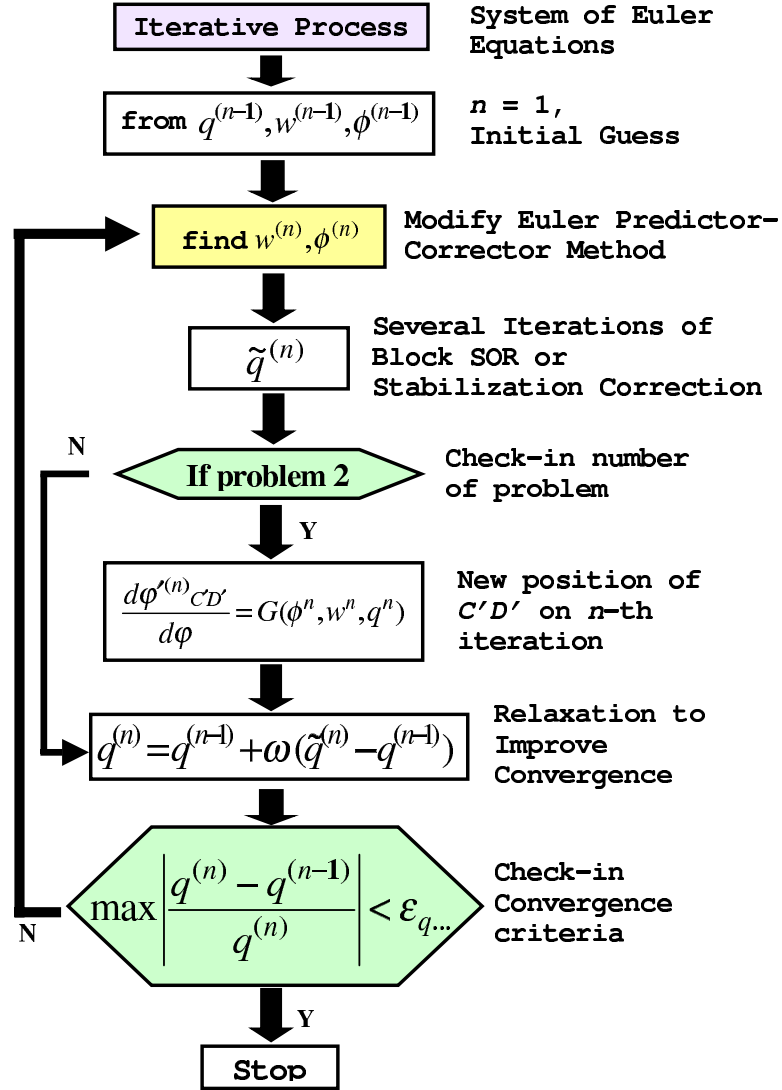


Figure 2.6: Flowchart of the iterative process.

2.3.1 The Method of Block SOR

The solution of equation (2.2.29) is sought in the domain shown in Figure 2.7. A three-point finite difference discretization of equation (2.2.29) is

$$\begin{aligned}
 & \frac{(w^2/\phi)_{i,j+1/2} \left(q_{i,j+1}^{(n-1)} - \tilde{q}_{i,j} \right) - (w^2/\phi)_{i,j-1/2} \left(\tilde{q}_{i,j} - q_{i,j-1}^{(n-1)} \right)}{h_\phi^2} + \\
 & \frac{c^2 w_{ij} \phi_{ij} \left(w_{i+1/2,j}^3 \left(\tilde{q}_{i+1,j} - \tilde{q}_{i,j} \right) - w_{i-1/2,j}^3 \left(\tilde{q}_{i,j} - \tilde{q}_{i-1,j} \right) \right)}{h_\psi^2} = 0, \quad (2.3.5) \\
 & i = 2, \dots, N_1 - 1, \quad j = 2, \dots, N_2 - 1,
 \end{aligned}$$

where $w_{i,j\pm 1/2} = \frac{1}{2}(w_{i,j\pm 1} + w_{i,j})$, $w_{i\pm 1/2,j} = \frac{1}{2}(w_{i\pm 1,j} + w_{i,j})$ and $\tilde{q}_{i,j}$ is the intermediate values of the unknown vector q .

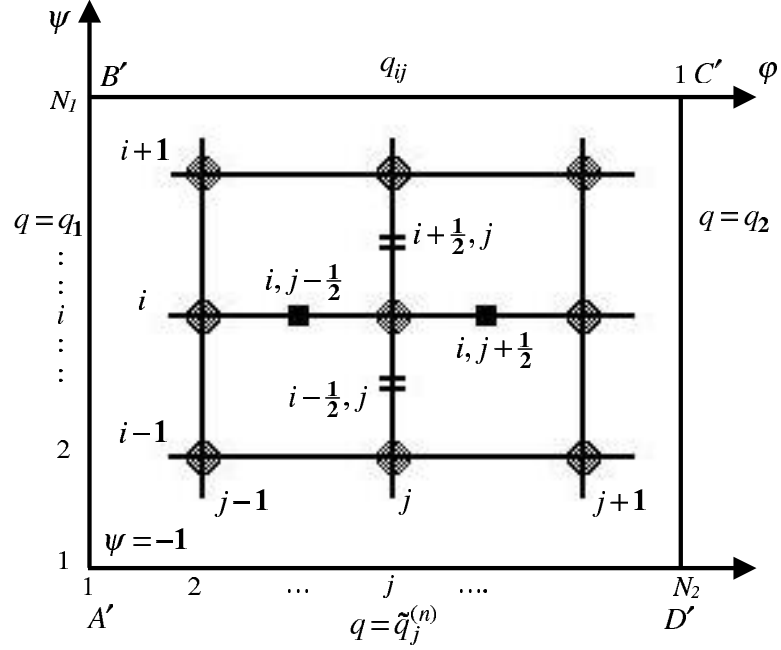


Figure 2.7: Computational stencil for finite difference equation (2.3.5).

We can rewrite equation (2.3.5) in the form of a linear system of algebraic equations with a tridiagonal matrix

$$-A_i \tilde{q}_{i-1,j} + C_i \tilde{q}_{i,j} - B_i \tilde{q}_{i+1,j} = f_{ij}, \quad (2.3.6)$$

$$i = 2, \dots, N_1 - 1, \quad j = 2, \dots, N_2 - 1,$$

where

$$A_i = c^2 w_{ij} \phi_{ij} w_{i-1/2,j}^3 \frac{1}{h_\psi^2},$$

$$B_i = c^2 w_{ij} \phi_{ij} w_{i+1/2,j}^3 \frac{1}{h_\psi^2},$$

$$C_i = \left[\left(\frac{w^2}{\phi} \right)_{i,j+1/2} + \left(\frac{w^2}{\phi} \right)_{i,j-1/2} \right] \frac{1}{h_\phi^2} + A_i + B_i,$$

$$f_{ij} = \frac{1}{h_\phi^2} \left[\left(\frac{w^2}{\phi} \right)_{i,j+1/2} q_{i,j+1}^{(n-1)} + \left(\frac{w^2}{\phi} \right)_{i,j-1/2} q_{i,j-1}^{(n-1)} \right],$$

The sweep method for the solution of (2.3.6) is given by the following formulas

$$\begin{aligned}
\tilde{q}_{i,j} &= \alpha_{i+1}\tilde{q}_{i+1,j} + \beta_{i+1}, \\
i &= 1, \dots, N_1 - 1, \\
j &= 2, \dots, N_2 - 1, \\
\alpha_{i+1} &= \frac{\beta_i}{C_i - A_i\alpha_i}; \quad i = 2, \dots, N_1 - 1, \\
\beta_{i+1} &= \frac{f_{ij} + A_i\beta_i}{C_i - A_i\alpha_i}; \quad i = 2, \dots, N_1 - 1, \\
\tilde{q}_{N_1,j} &= \tilde{q}_{BC}(j), \\
\tilde{q}_{1,j} &= \tilde{q}_{AD}(j).
\end{aligned}$$

In the SOR scheme, the solution of (2.3.6) is combined with the solution in the previous iteration $q_{ij}^{(n-1)}$

$$q_{ij}^{(n)} = \lambda\tilde{q}_{ij} + (1 - \lambda)q_{ij}^{(n-1)}, \quad i = 1, \dots, N_1, \quad j = 1, \dots, N_2, \quad (2.3.7)$$

where λ is the relaxation factor. The SOR method in the range $0 < \lambda < 2$ produces a sequence of convergent solutions.

2.3.2 The Method of Stabilizing Corrections

The method of Stabilizing Corrections which was introduced by J. Douglas and H. H. Rachford (1956) and formulated into a general form by J. Douglas and J. E. Gunn (1964) is a very effective method for the construction of scheme with fractional step. It consists of two fractional steps

$$\begin{aligned}
\frac{q_{ij}^* - q_{ij}^{(n-1)}}{\tau} &= \frac{(w^2/\phi)_{i,j+1/2}(q_{i,j+1}^* - q_{ij}^*) - (w^2/\phi)_{i,j-1/2}(q_{ij}^* - q_{i,j-1}^*)}{h_\phi^2} \\
&+ c^2 w_{ij} \phi_{ij} \frac{w_{i+1/2,j}^3 (q_{i+1,j}^{(n-1)} - q_{ij}^{(n-1)}) - w_{i-1/2,j}^3 (q_{ij}^{(n-1)} - q_{i-1,j}^{(n-1)})}{h_\psi^2}, \quad (2.3.8)
\end{aligned}$$

$$\begin{aligned}
i &= 2, \dots, N_1 - 1, \quad j = 2, \dots, N_2 - 1, \\
\frac{q_{ij}^{(n)} - q_{ij}^*}{\tau} &= c^2 w_{ij} \phi_{ij} \left[\frac{w_{i+1/2,j}^3 (q_{i+1,j}^{(n)} - q_{ij}^{(n)}) - w_{i-1/2,j}^3 (q_{ij}^{(n)} - q_{i-1,j}^{(n)})}{h_\psi^2} \right. \\
&+ \left. \frac{w_{i+1/2,j}^3 (q_{i+1,j}^{(n-1)} - q_{ij}^{(n-1)}) - w_{i-1/2,j}^3 (q_{ij}^{(n-1)} - q_{i-1,j}^{(n-1)})}{h_\psi^2} \right], \quad (2.3.9) \\
i &= 2, \dots, N_1 - 1, \quad j = 2, \dots, N_2 - 1.
\end{aligned}$$

To find solution of equations (2.3.8) and (2.3.9), we have to solve a linear system of an algebraic equations with the tridiagonal matrix.

2.3.3 Interpretation and Presentation of Results of Numerical Calculations

In this section, we discuss how to display the results of numerical calculations. We will use various generally accepted graphical techniques for the

presentation of data. Presentations of results in the physical domain are more desirable. When the iterative process is completed, we have to transform back to the variables x, y to find distribution of all unknown functions in the physical domain.

Let us consider the line $\psi = \psi_i - \text{const}$ (streamline). Along this line we have

$$\frac{dx(\varphi, \psi_i)}{d\varphi} = \phi(\varphi, \psi_i) \cos q(\varphi, \psi_i).$$

Integrating this equation with respect to φ from $\varphi = 0$ to $\varphi = \varphi_j$, we obtain

$$\int_0^{\varphi_j} dx(\varphi, \psi_i) = \int_0^{\varphi_j} \phi(\varphi, \psi_i) \cos q(\varphi, \psi_i) d\varphi,$$

or

$$\begin{aligned} x_{i,j} - x_{1,j} &= x(\varphi_j, \psi_i) - x(0, \psi_i) \\ &= \int_0^{\varphi_j} \phi(\varphi, \psi_i) \cos q(\varphi, \psi_i) d\varphi, \end{aligned}$$

where $x_{1,j} = x(0, \psi_i)$ is x coordinate of the point $(0, \psi_i)$ in the physical domain. To find $x_{1,j}$, consider the image of Γ_1 boundary in a particular case where

$$AB : y = y_0 - \text{const}, x_0 \leq x \leq x_1. \quad (2.3.10)$$

In this case, we have (see equation (2.2.17))

$$\frac{d\psi}{dx} = -c w(0, \psi) \sin q(0, \psi).$$

Integrating this equation with respect from 0 to ψ_i , we get

$$- \int_0^{\psi_i} \frac{d\psi}{c w(0, \psi) \sin q(0, \psi)} = x_{1,i} - x_{1,1},$$

or

$$x_{1,i} = x_{1,1} - \int_0^{\psi_i} \frac{d\psi}{c w(0, \psi) \sin q(0, \psi)},$$

where the functions $w(0, \psi)$ and $\sin q(0, \psi)$ are given by the boundary conditions $q = q_1(x, y)$ and $w = w_1(x, y)$. By analogy with the previous case, we can find y - coordinates $y_{i,j}$ of the streamline $\psi = \psi_{i,j}$; $j = 1, \dots, N_2$,

$$\frac{dy(\varphi, \psi_i)}{d\varphi} = \phi(\varphi, \psi_i) \sin q(\varphi, \psi_i).$$

Integration yields

$$y(\varphi_j, \psi_i) = y(0, \psi_i) + \int_0^{\varphi_j} \phi(\varphi, \psi_i) \sin q(\varphi, \psi_i) d\varphi.$$

In particular case of boundary condition (2.3.10), it is easy to see that

$$y(0, \psi_i) = y_0.$$

Once the unknown functions q , w , ϕ are determined, it is possible to find distribution of the pressure in the physical and computational domain. To find the pressure, we use equations (2.2.1) and (2.2.2)

$$\begin{aligned} u \frac{\partial u}{\partial x} + v \frac{\partial u}{\partial y} &= -\frac{\partial P}{\partial x}, \\ u \frac{\partial v}{\partial x} + v \frac{\partial v}{\partial y} &= -\frac{\partial P}{\partial y}. \end{aligned} \quad (2.3.11)$$

Utilizing the chain rule, we receive formulas to change the partial derivatives

$$\begin{aligned} \frac{\partial P}{\partial x} &= -cw \frac{\partial P}{\partial \psi} \sin q + \frac{\partial P}{\partial \varphi} \frac{\cos q}{\phi}, \\ \frac{\partial P}{\partial y} &= cw \frac{\partial P}{\partial \psi} \cos q + \frac{\partial P}{\partial \varphi} \frac{\sin q}{\phi}. \end{aligned}$$

Multiplying the first equation by $\sin q$ and the second equation by $\cos q$, then by subtraction, we get

$$-cw \frac{\partial P}{\partial \psi} = \frac{\partial P}{\partial x} \sin q - \frac{\partial P}{\partial y} \cos q. \quad (2.3.12)$$

Multiplying the first equation by $\cos q$ and the second equation by $\sin q$, then by addition, we get

$$\frac{1}{\phi} \frac{\partial P}{\partial \varphi} = \frac{\partial P}{\partial x} \cos q + \frac{\partial P}{\partial y} \sin q. \quad (2.3.13)$$

Substituting $\frac{\partial P}{\partial x}$ and $\frac{\partial P}{\partial y}$ into equations (2.3.12) and (2.3.13), we get

$$-cw \frac{\partial P}{\partial \psi} = -(u \frac{\partial u}{\partial x} + v \frac{\partial u}{\partial y}) \sin q + (u \frac{\partial v}{\partial x} + v \frac{\partial v}{\partial y}) \cos q \quad (2.3.14)$$

$$\frac{1}{\phi} \frac{\partial P}{\partial \varphi} = -(u \frac{\partial u}{\partial x} + v \frac{\partial u}{\partial y}) \cos q - (u \frac{\partial v}{\partial x} + v \frac{\partial v}{\partial y}) \sin q. \quad (2.3.15)$$

Substituting $u = w \cos q$ and $v = w \sin q$ into equations (2.3.14) and (2.3.15) and simplifying, we obtain

$$\begin{aligned} \frac{\partial P}{\partial \psi} &= -\frac{w}{c\phi} \frac{\partial q}{\partial \varphi}, \\ \frac{\partial P}{\partial \varphi} &= -w \frac{\partial w}{\partial \varphi} \text{ (or } w^3 c\phi \frac{\partial q}{\partial \psi} \text{)}. \end{aligned} \quad (2.3.16)$$

In order to transform equations (2.2.1) and (2.2.2) to equations (2.3.16), a program by MAPLE is developed. The detailed description of this program can be found in Appendix A.

Assume that the value of the pressure is given at some point of domain Ω . The pressure determine up to an arbitrary constant. We can use equations (2.3.16) to find the values of the pressure in the physical domain.

Let $P(A) = P_0$ be a given value of the pressure at the point A of boundary AB (see Figure 2.1). To find the pressure distribution along AB , we have

$$\begin{aligned} \frac{\partial P}{\partial \psi} &= -\frac{w}{c\phi} \frac{\partial q}{\partial \varphi}, \\ \frac{\partial P(\psi, 0)}{\partial \psi} &= -\frac{w}{c\phi(\psi, 0)} \left(\frac{\partial q}{\partial \varphi} \right)_{\varphi=0}, \\ \int_A^{\psi_i} \frac{\partial P(\psi, 0)}{\partial \psi} d\psi &= -\frac{1}{c} \int_A^{\psi_i} \frac{w}{\phi(\psi, 0)} \left(\frac{\partial q}{\partial \varphi} \right)_{\varphi=0} d\psi, \\ P(\psi_i, 0) - P(A) &= -\frac{1}{c} \int_{-1}^{\psi_i} \frac{w}{\phi(\psi, 0)} \left(\frac{\partial q}{\partial \varphi} \right)_{\varphi=0} d\psi; \quad P(A) = P_0, \\ P_{i,1} &= P_0 - \frac{1}{c} \left[\int_{-1}^{\psi_{i-1}} \frac{w}{\phi(\psi, -1)} \left(\frac{\partial q}{\partial \varphi} \right)_{\varphi=-1} d\psi \right. \\ &\quad \left. - \int_{\psi_{i-1}}^{\psi_i} \frac{w}{\phi(\psi, 0)} \left(\frac{\partial q}{\partial \varphi} \right)_{\varphi=0} d\psi \right] \\ &= P_{i-1,1} - \frac{1}{c} \int_{\psi_{i-1}}^{\psi_i} \frac{w}{\phi(\psi, 0)} \left(\frac{\partial q}{\partial \varphi} \right)_{\varphi=0} d\psi, \end{aligned}$$

where $\left(\frac{\partial q}{\partial \varphi} \right)_{\varphi=0} = \frac{-3q_{i,1} + 4q_{i,2} - q_{i,3}}{2h_2}$.

We use equation

$$\frac{\partial P}{\partial \varphi} = -w \frac{\partial w}{\partial \varphi} \quad (\text{or} \quad \frac{\partial P}{\partial \varphi} = w^3 c \phi \frac{\partial q}{\partial \psi}).$$

to find the pressure distribution everywhere in the computational domain. Integrating this equation, we have

$$\begin{aligned} \int_0^{\varphi_j} \frac{\partial P}{\partial \varphi} d\varphi &= - \int_0^{\varphi_j} w \frac{\partial w}{\partial \varphi} d\varphi, \\ P(\psi_i, \varphi_j) - P(\psi_i, 0) &= - \int_0^{\varphi_j} w \frac{\partial w}{\partial \varphi} d\varphi, \\ P_{i,j} &= P_{i,1} - \int_0^{\varphi_{j-1}} w \frac{\partial w}{\partial \varphi} d\varphi - \int_{\varphi_{j-1}}^{\varphi_j} w \frac{\partial w}{\partial \varphi} \Big|_{\psi=\psi_i} d\varphi \\ &= P_{i,j-1} - \int_{\varphi_{j-1}}^{\varphi_j} w \frac{\partial w}{\partial \varphi} \Big|_{\psi=\psi_i} d\varphi, \\ &\quad i = 1, \dots, N_1, \\ &\quad j = 2, \dots, N_2, \end{aligned}$$

where

$$\left(\frac{\partial w}{\partial \varphi}\right)_{i,j} = \begin{cases} \frac{w_{i,j+1} - w_{i,j-1}}{2h_2} & ; j \neq N_2, \\ \frac{3w_{i,N_2} - 4w_{i,N_2-1} + w_{i,N_2-2}}{2h_2} & ; j = N_2, \end{cases}$$

$$\left(\frac{\partial w}{\partial \varphi}\right)_{i,j-1} = \begin{cases} \frac{w_{i,j} - w_{i,j-2}}{2h_2} & ; j \neq N_2, \\ \frac{-3w_{i,1} + 4w_{i,2} - w_{i,3}}{2h_2} & ; j = 2. \end{cases}$$

2.4 Results and Discussions

In this section, the numerical method developed in section 2.3 will be implemented to study an internal flow of an ideal incompressible fluid in an α degree elbow channel and two-dimensional channel with curve walls.

2.4.1 90 Degree Elbow with Contraction

The channel geometry is shown in Figure 2.8. Parts of solid impermeable boundary FL and KE are circular arcs with centers at the points O and F , respectively. In Figure 2.8, we also show the flow domain in new variables in the case of problem 2' and problem 3'. In the case of problem 2', the image of CD boundary is not vertical. We will present this boundary $C'D'$ by the equation

$$\varphi = 1 + \varphi_{C'D'}(\psi).$$

Taking into account the natural parameterization of circle we can write out the natural equations of boundaries AD and BC . In the case of boundary BC we can write

$$x(l) = \begin{cases} -R_1, & 0 \leq l \leq y_0, \\ -R_1 + R_1 \cos\left(\frac{l-y_0}{R_1}\right), & y_0 < l < y_0 + \frac{\pi}{2}R_1, \\ l - (y_0 + \frac{\pi}{2}R_1), & y_0 + \frac{\pi}{2}R_1 \leq l \leq L_{BC}, \end{cases} \quad (2.4.1)$$

$$y(l) = \begin{cases} y_0 - l, & 0 \leq l \leq y_0, \\ -R_1 \sin\left(\frac{l-y_0}{R_1}\right), & y_0 < l < y_0 + \frac{\pi}{2}R_1, \\ -R_1, & y_0 + \frac{\pi}{2}R_1 \leq l \leq L_{BC}, \end{cases} \quad (2.4.2)$$

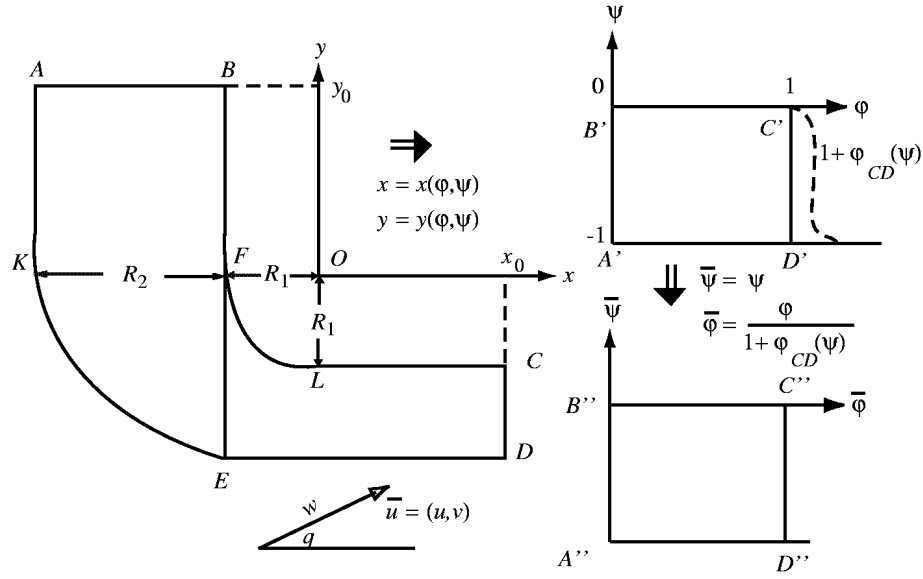


Figure 2.8: Sketch of an elbow-shaped domain and coordinates.

where l is a natural parameter of curve BC , L_{BC} is the length of curve BC . The similar description is also valid for the boundary AD

$$x(l) = \begin{cases} -(R_1 + R_2), & 0 \leq l \leq y_0, \\ -(R_1 + R_2) + R_2 \cos\left(\frac{l-y_0}{R_2}\right), & y_0 < l < y_0 + \frac{\pi}{2}R_1, \\ l - (y_0 + \frac{\pi}{2}R_1), & y_0 + \frac{\pi}{2}R_1 \leq l \leq L_{AD}, \end{cases} \quad (2.4.3)$$

$$y(l) = \begin{cases} y_0 - l, & 0 \leq l \leq y_0, \\ -R_2 \sin\left(\frac{l-y_0}{R_2}\right), & y_0 < l < y_0 + \frac{\pi}{2}R_1, \\ -R_2, & y_0 + \frac{\pi}{2}R_1 \leq l \leq L_{AD}. \end{cases} \quad (2.4.4)$$

2.4.2 Convergence of Numerical Algorithm

To prove that the solution of the numerical method converges to the solution of the partial differential equations is generally very difficult. For the equations governing fluid flow, convergence is usually impossible to demonstrate theoretically. The convergence can be demonstrated numerically by obtaining solutions on a sequence of refined grids. Convergence implies that the solution error should decrease as the grid spacing is reduced. It is clear, that in the case of 90 degree elbow with contraction, we do not know an exact solution of the Euler equations. Our algorithm developed by such way that some *priori* known quantities have to be estimated during the iterative process. For example, in the case of problem 3', we know the exact location of point D , and the exact value of length of channel's boundary AD but while the numerical process is carried out, we have to compute the quantities of these data. The corresponding rela-

tive errors between exact values of these quantities and their numerical approach are shown in Table 2.1 for the following set of parameters $R_1 = 1.0$, $R_2 = 2.0$, $x_0 = 2.0$, $y_0 = 2.0$, $w = w_1(x) = 2.0$, $q_1 = q(x, y_0) = -\pi/2$, and $q_2 = q(x_d, y) = 0$. In the first and the second columns, we present the number of grid points in the computational domain. The third and the fifth columns of Table 2.1 present the (x, y) - coordinates of point D found by numerical algorithm. The seventh column presents the length of curve AD which is found by the numerical algorithm. In the fourth, sixth and eighth columns, we demonstrate relative difference between exact and approximate values

$$\text{error} = \frac{(\cdot)\text{exact} - (\cdot)\text{ approximate}}{(\cdot)\text{ exact}} \times 100\% .$$

It is clear to see from results in Table 2.1 that the relative errors decrease as the grid size tends to zero. The last column demonstrates the optimal value of the relaxation parameter. The optimal values of relaxation factor are chosen by method of trail and error.

Using results of Table 2.1, we can find rate of convergence of our numerical algorithm

$$m = \frac{1}{\ln(2)} \frac{\ln(\text{err1})}{\ln(\text{err2})},$$

where err1 and err2 are relative error between the exact and approximate values which were obtained on grids $N_1 \times N_1$ and $N_2 \times N_2$. Rate of convergence is shown in Table 2.2.

Table 2.1: Convergence to exact solution. The results of numerical simulations for different grids for 90 degree elbow.

| N_1 | N_2 | x_D | relative error in x_D | y_D | relative error in y_D | L_{AD}^h | relative error in L_{AD} | ω optimal |
|-------|-------|----------|-------------------------|-----------|-------------------------|------------|----------------------------|------------------|
| 11 | 11 | 2.045695 | -2.28475 | -2.031267 | -1.56335 | 8.1925 | -0.6252 | 0.8 |
| 21 | 21 | 2.025775 | -1.28875 | -2.007746 | -0.38730 | 8.1659 | -0.2985 | 0.8 |
| 41 | 41 | 2.017319 | -0.86595 | -2.001790 | -0.08950 | 8.1566 | -0.1842 | 0.93 |
| 81 | 81 | 2.009273 | -0.46365 | -2.000499 | -0.02495 | 8.1509 | -0.1142 | 0.93 |
| 11 | 21 | 2.033372 | -1.66860 | -2.008183 | -0.40915 | 8.1729 | -0.3844 | 0.8 |
| 11 | 41 | 2.026327 | -1.31635 | -2.001492 | -0.07460 | 8.1654 | -0.2923 | 1.2 |
| 21 | 41 | 2.020008 | -1.00040 | -2.001718 | -0.08590 | 8.1593 | -0.2174 | 1.2 |
| 21 | 11 | 2.035630 | -1.78150 | -2.031677 | -1.58385 | 8.1824 | -0.5011 | 0.8 |
| 41 | 11 | 2.030568 | -1.52840 | -2.031859 | -1.59295 | 8.1774 | -0.4391 | 0.6 |
| 11 | 81 | 2.018081 | -0.90405 | -2.000682 | -0.03410 | 8.1590 | -0.2137 | 1.4 |

The results of numerical calculations to estimate the optimal values of the relaxation parameter are shown in the Table 2.3. The first and the second columns show the number of grid points in the computational domain. The third

Table 2.2: Rate of convergence of numerical algorithm.

| Notes about grids | x_D | y_D | L_D |
|---------------------|-------|-------|-------|
| (11 × 11)/(21 × 21) | 0.83 | 2.01 | 1.06 |
| (21 × 21)/(41 × 41) | 0.57 | 2.11 | 0.69 |
| (41 × 41)/(81 × 81) | 0.90 | 1.83 | 0.69 |

column shows the tolerances used for convergence of the outer iterative process. The fourth and the fifth columns show the number of inner and outer iterations, respectively. The last column shows the value of the relaxation parameter used in the iterative process. It can be seen that optimal values of relaxation parameter vary in the interval $0.6 < \omega < 1.4$. It is needed to point out that in each inner iterative process, it is enough to execute only few iterations by the block SOR or the Stabilizing Correction methods to achieve the convergence of the outer iterative process.

In Table 2.4, we show the detailed description of the results of numerical simulations for 90 degree elbow with contraction. The first and the second columns show the number of grid points in the computational domain. The third column shows the values of relaxation parameter which are used in numerical experiment. The fourth column gives us information about the number of outer iterations to achieve convergence with tolerances $\varepsilon_\phi = 10^{-4}$, $\varepsilon_w = 10^{-4}$, $\varepsilon_q = 10^{-4}$. The fifth to the eleventh columns show the values of geometrical parameters in equations (2.4.5) - (2.4.8). The last column shows the corresponding Figure numbers in which computational results are illustrated by graphics.

Table 2.3: The choice of the relaxation parameter. The results of numerical calculations for the case of 90 degree elbow with $x_0 = 2.0$, $y_0 = 2.0$, $R_1 = 1.0$, $R_2 = 2.0$, $\frac{R_2 - R_1}{R_2} = \frac{1}{2}$.

| N_1 | N_2 | Tolerances of convergence (ϕ , w , q) | Number of inner iterations | Number of outer iterations | Parameter of relaxation ω |
|-------|-------|---|----------------------------|----------------------------|----------------------------------|
| 21 | 21 | $10^{-4}, 10^{-4}, 10^{-4}$ | 1 | 85 | 0.3 |
| 21 | 21 | $10^{-4}, 10^{-4}, 10^{-4}$ | 1 | 53 | 0.5 |
| 21 | 21 | $10^{-4}, 10^{-4}, 10^{-4}$ | 1 | 35 | 0.8 |
| 21 | 21 | $10^{-4}, 10^{-4}, 10^{-4}$ | 1 | 31 | 0.9 |
| 21 | 21 | $10^{-4}, 10^{-4}, 10^{-4}$ | 1 | 31 | 1.0 |
| 21 | 21 | $10^{-4}, 10^{-4}, 10^{-4}$ | 1 | 26 | 1.1 |
| 21 | 21 | $10^{-4}, 10^{-4}, 10^{-4}$ | 1 | 62 | 1.2 |
| 41 | 41 | $10^{-4}, 10^{-5}, 10^{-5}$ | 1 | 190 | 0.2 |
| 41 | 41 | $10^{-4}, 10^{-5}, 10^{-5}$ | 1 | 187 | 0.5 |
| 41 | 41 | $10^{-4}, 10^{-5}, 10^{-5}$ | 1 | 142 | 0.8 |
| 41 | 41 | $10^{-4}, 10^{-5}, 10^{-5}$ | 1 | 133 | 0.9 |
| 41 | 41 | $10^{-4}, 10^{-5}, 10^{-5}$ | 1 | 218 | 0.946 |
| 41 | 41 | $10^{-4}, 10^{-4}, 10^{-4}$ | 1 | 106 | 0.7 |
| 41 | 41 | $10^{-4}, 10^{-4}, 10^{-4}$ | 1 | 87 | 0.9 |
| 41 | 41 | $10^{-4}, 10^{-4}, 10^{-4}$ | 1 | 95 | 0.946 |
| 41 | 41 | $10^{-4}, 10^{-4}, 10^{-4}$ | 2 | 53 | 0.8 |
| 41 | 41 | $10^{-4}, 10^{-4}, 10^{-4}$ | 5 | 41 | 0.8 |
| 41 | 41 | $10^{-4}, 10^{-4}, 10^{-4}$ | 100 | 36 | 0.8 |
| 81 | 81 | $10^{-4}, 10^{-4}, 10^{-4}$ | 1 | 519 | 0.2 |
| 81 | 81 | $10^{-4}, 10^{-4}, 10^{-4}$ | 1 | 341 | 0.5 |
| 81 | 81 | $10^{-4}, 10^{-4}, 10^{-4}$ | 1 | 386 | 0.6 |
| 81 | 81 | $10^{-4}, 10^{-4}, 10^{-4}$ | 1 | 276 | 0.7 |
| 81 | 81 | $10^{-4}, 10^{-4}, 10^{-4}$ | 1 | 318 | 0.8 |
| 81 | 81 | $10^{-4}, 10^{-4}, 10^{-4}$ | 1 | 84 | 0.91 |
| 81 | 81 | $10^{-4}, 10^{-4}, 10^{-4}$ | 1 | 83 | 0.93 |
| 81 | 81 | $10^{-4}, 10^{-4}, 10^{-4}$ | 1 | 86 | 0.945 |
| 81 | 81 | $10^{-4}, 10^{-4}, 10^{-4}$ | 2 | 219 | 0.6 |
| 81 | 81 | $10^{-4}, 10^{-4}, 10^{-4}$ | 2 | 188 | 0.7 |
| 21 | 41 | $10^{-4}, 10^{-4}, 10^{-4}$ | 1 | 143 | 0.5 |
| 21 | 41 | $10^{-4}, 10^{-4}, 10^{-4}$ | 1 | 94 | 0.8 |
| 21 | 41 | $10^{-4}, 10^{-4}, 10^{-4}$ | 1 | 82 | 1.1 |
| 21 | 41 | $10^{-4}, 10^{-4}, 10^{-4}$ | 1 | 65 | 1.2 |
| 21 | 41 | $10^{-4}, 10^{-4}, 10^{-4}$ | 1 | 291 | 1.4 |
| 21 | 41 | $10^{-4}, 10^{-4}, 10^{-4}$ | 2 | 43 | 1.1 |
| 11 | 81 | $10^{-4}, 10^{-4}, 10^{-4}$ | 1 | 338 | 0.7 |
| 11 | 81 | $10^{-4}, 10^{-4}, 10^{-4}$ | 1 | 187 | 1.4 |
| 11 | 81 | $10^{-4}, 10^{-4}, 10^{-4}$ | 1 | 189 | 1.5 |
| 11 | 81 | $10^{-4}, 10^{-4}, 10^{-4}$ | 1 | 309 | 1.51 |
| 11 | 81 | $10^{-4}, 10^{-4}, 10^{-4}$ | 2 | 192 | 0.7 |

Table 2.4: Detailed description of data of numerical simulations for 90 degree elbow with contraction. Tolerance criteria $\epsilon_\phi = 10^{-4}$, $\epsilon_w = 10^{-4}$, $\epsilon_q = 10^{-4}$.

| N_1 | N_2 | Num. of inner iters. | Num. of outer iters. | Para. of relax. ω | x_0 | y_0 | R_1 | R_2 | $\frac{R_2-R_1}{R_2}$ | Fig. num. |
|-------|-------|----------------------|----------------------|--------------------------|-------|-------|-------|-------|-----------------------|------------|
| 21 | 21 | 1 | 39 | 0.7 | 2 | 2 | 1 | 2 | 0.5 | – |
| 41 | 41 | 2 | 61 | 0.7 | 2 | 2 | 1 | 2 | 0.5 | 2.10, 2.13 |
| 81 | 81 | 1 | 106 | 0.7 | 2 | 2 | 1 | 2 | 0.5 | – |
| 21 | 81 | 2 | 218 | 0.6 | 2 | 2 | 1 | 2 | 0.5 | – |
| 41 | 41 | 1 | 106 | 0.7 | 2 | 2 | 1 | 1.5 | 0.3 | 2.11, 2.15 |
| 41 | 41 | 1 | 104 | 0.5 | 2 | 2 | 1 | 1.5 | 0.3 | – |
| 41 | 41 | 2 | 74 | 0.7 | 3 | 3 | 1 | 3 | 0.6 | 2.9, 2.14 |
| 81 | 81 | 2 | 753 | 0.8 | 5 | 5 | 4 | 5 | 0.2 | – |
| 81 | 81 | 2 | 263 | 0.2 | 5 | 5 | 1 | 1.5 | 0.3 | 2.12, 2.16 |
| 41 | 41 | 2 | 280 | 0.8 | 2 | 2 | 1 | 1.5 | 0.3 | – |

2.4.3 Numerical Results for 90 Degree Elbow with Contraction

In next, we present the results of numerical simulation of an ideal incompressible fluid flow through 90 degree elbow. We vary the relative size of entrance and output parts of the channel. The length of straight part of entrance and the length of straight part of exit are fixed at $x_0 = 2.0$ and $y_0 = 2.0$, respectively. Serial calculations demonstrated that distribution of the pressure field does not change when the length of exit and entrance increase. Figures 2.9-2.11 show the computed results of the pressure contours for problem 3' with $w = w_1 = 2.0$, $q_1 = -\pi/2$, $q_2 = 0$, $N_1 = 41$, $N_2 = 41$, and different values of parameters: $x_0 = 3.0$, $y_0 = 3.0$, $\frac{R_2-R_1}{R_2} = \frac{2}{3}$; $x_0 = 2.0$, $y_0 = 2.0$, $\frac{R_2-R_1}{R_2} = \frac{1}{2}$; $x_0 = 2.0$, $y_0 = 2.0$, $\frac{R_2-R_1}{R_2} = \frac{1}{3}$.

Figures 2.12 illustrates the computational results that are obtained by using the grid with 81×81 nodes and $x_0 = 5.0$, $y_0 = 5.0$, and $\frac{R_2-R_1}{R_2} = \frac{1}{3}$.

Figures 2.13-2.16 show the pressure distribution by colored graphics. For all of these four cases, we put the pressure equal to two at point A . Oscillations of pressure contours on Figures 2.9-2.11 occur due to the interpolation program in MATLAB.

The distribution of the velocity vectors and the streamlines for an ideal incompressible fluid flow mainly determined by channel geometry. Figures 2.17 and 2.18 show the computed results of the velocity vectors and the streamlines distribution for the case $R_1 = 1$, $R_2 = 3$ and $\frac{R_2-R_1}{R_2} = \frac{2}{3}$.

Let us present some results of numerical simulation for problem 2, in which only the value of pressure $P = P_2$, on the exit boundary CD , $x \in \Gamma^2$ are known. Assume that the boundary $C'D'$ in computation domain is given by the following

equation

$$\varphi = 1 + \varphi_{C'D'}(\psi).$$

In this case, we can perform the transformation

$$\psi' = \psi, \quad \varphi' = \frac{\varphi}{1 + \varphi_{C'D'}(\psi)},$$

to transform domain $A'B'C'D'$ into rectangle $A''B''C''D''$ in new computational domain (see Figure 2.8).

Let us consider the problem 2' for the 90 degree elbow with geometry given by the following parameters: $x_0 = 1.0$, $y_0 = 2.0$, $R_1 = 1.0$ and $R_2 = 2.0$. Numerical calculations show that the main parameters of flow are very close to those parameters in the problem 3' for sufficiently large x_0 . This relates to the obvious fact that if length of the exit part is sufficiently large, then we will observe almost one-dimensional flow. One more evidence of this is clear by the observation of the results presented in Table 2.5. Table 2.5 shows the maximum difference of the values of the two functions, $\varphi = 1$, $\varphi = 1 + \varphi_{C'D'}(\psi)$, $\psi \in [0, 1]$ for different length of the exit part of channel x_0 . It is clear that when x_0 increases, the $\max_{\psi} |\varphi_{C'D'}(\psi)|$ decreases.

Results for different geometries and flow conditions with $R_1 = 1.0$, $R_2 = 2.0$, $x_0 = 2.0$, $y_0 = 2.0$, $P = P_{CD} = \text{constant}$, and $w_k = 2.0$ are illustrated in Figures 2.19, 2.20 and 2.21. Figure 2.19 shows the pressure depending on φ along streamlines $\psi = -1, -0.5, 0$. Figure 2.20 shows the modulus of the velocity vector w as a function of φ along streamlines $\psi = -1, -0.5, 0$. The graph of $\varphi = \varphi_{C'D'}(\psi)$, $\psi \in [-1, 0]$ is shown in Figure 2.21 for the case $x_0 = 2.0$ and $P_{CD} = 2.0$.

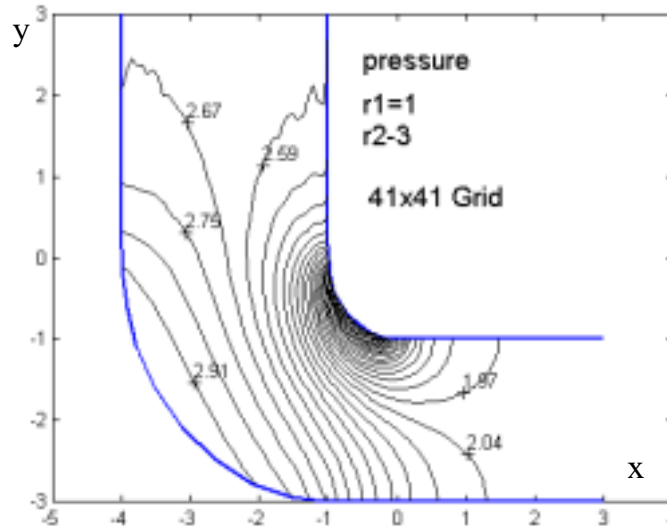


Figure 2.9: Pressure contours for 90 degree elbow with contraction, $\frac{R_2-R_1}{R_2} = \frac{2}{3}$.

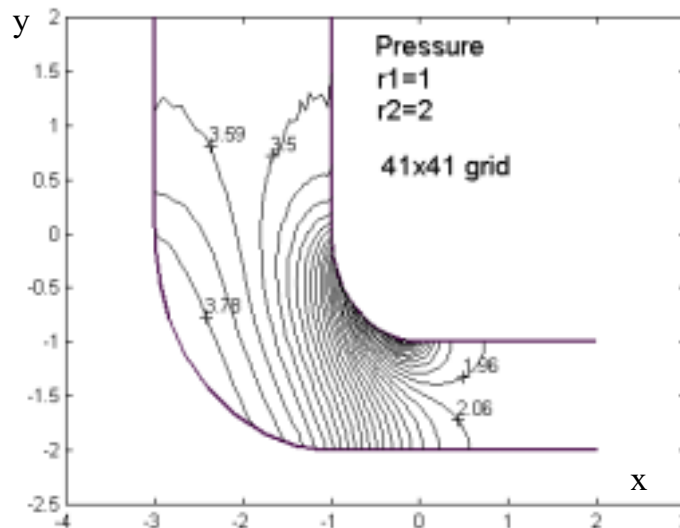


Figure 2.10: Pressure contours for 90 degree elbow with contraction, $\frac{R_2-R_1}{R_2} = \frac{1}{2}$.

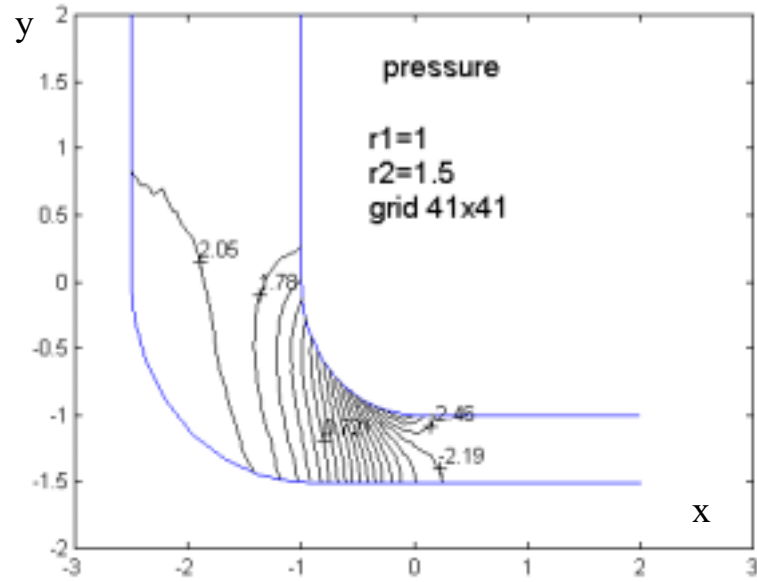


Figure 2.11: Pressure contours for 90 degree elbow with contraction, $\frac{R_2-R_1}{R_2} = \frac{1}{3}$.

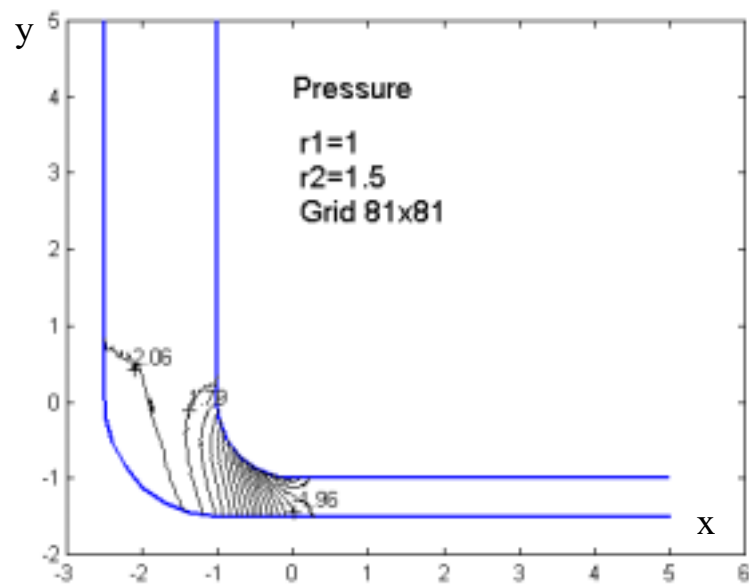


Figure 2.12: Pressure contours for 90 degree elbow with contraction, $\frac{R_2-R_1}{R_2} = \frac{1}{3}$.

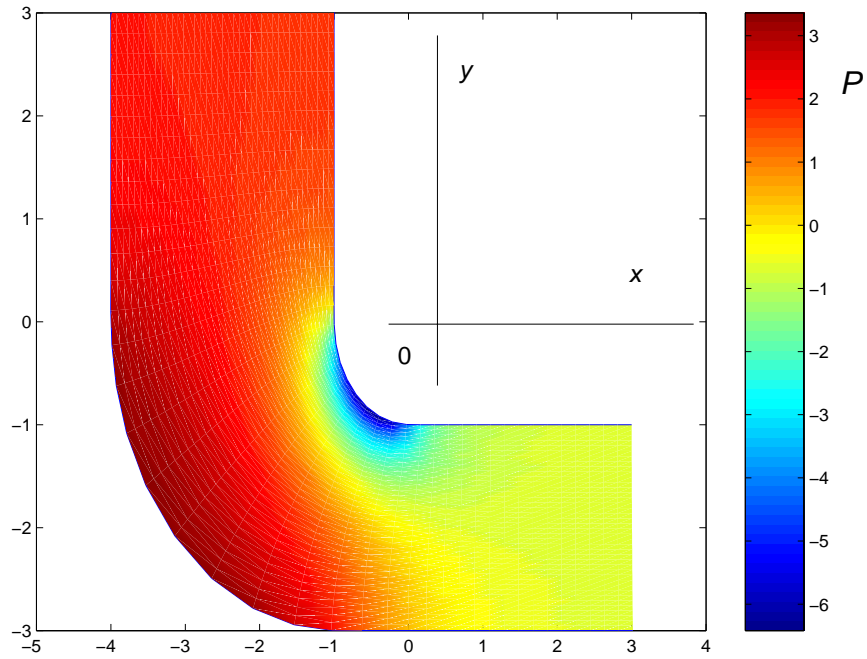


Figure 2.13: Colored graphics of pressure contours for 90 degree elbow with contraction, $\frac{R_2 - R_1}{R_2} = \frac{2}{3}$.

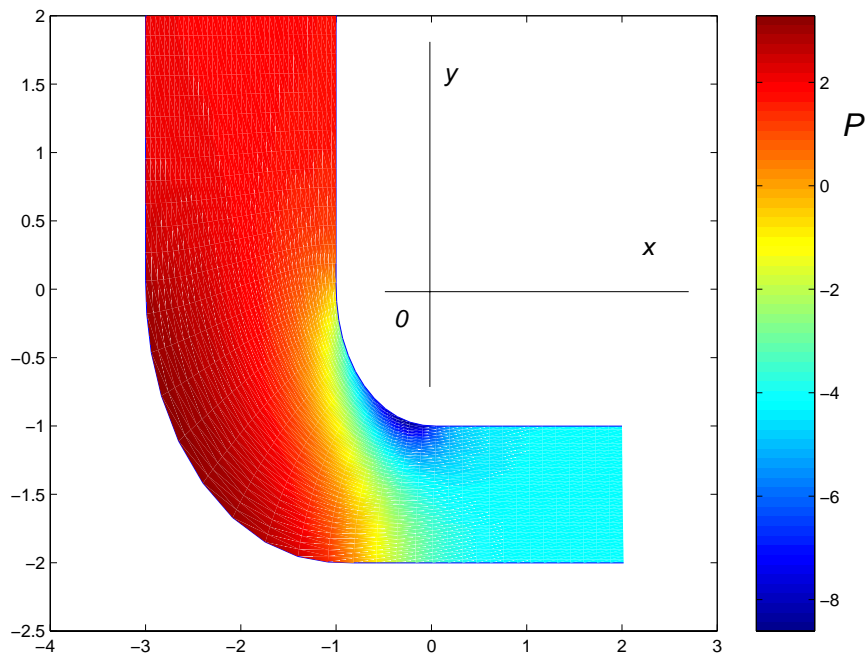


Figure 2.14: Colored graphics of pressure contours for 90 degree elbow with contraction, $\frac{R_2 - R_1}{R_2} = \frac{1}{2}$.

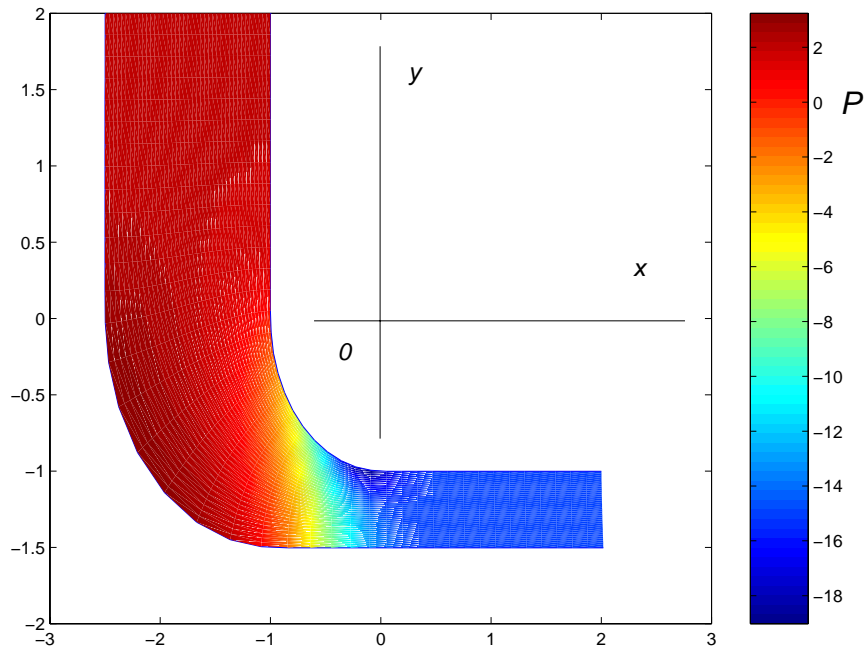


Figure 2.15: Colored graphics of pressure contours for 90 degree elbow with contraction, $\frac{R_2 - R_1}{R_2} = \frac{1}{3}$.

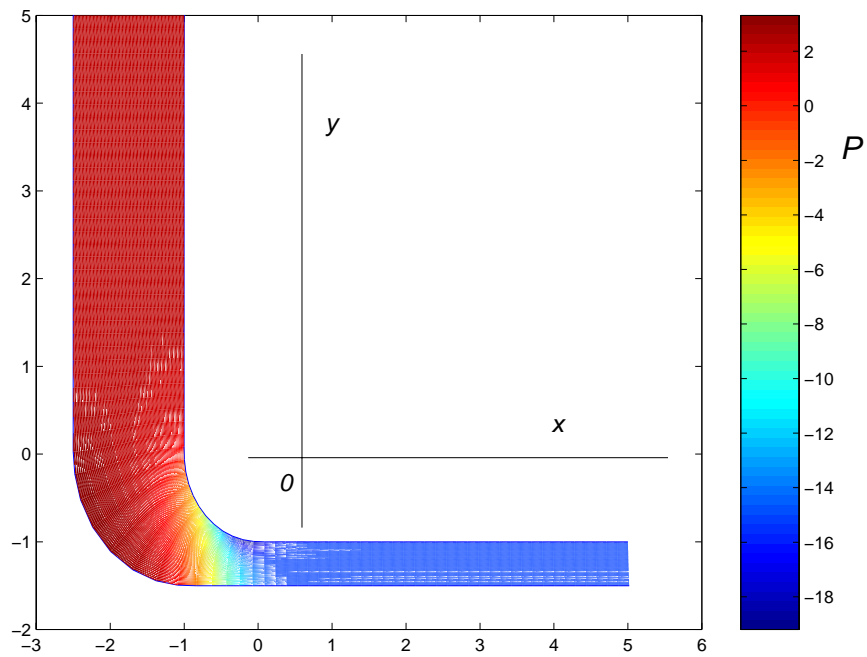


Figure 2.16: Colored graphics of pressure contours for 90 degree elbow with contraction, $\frac{R_2 - R_1}{R_2} = \frac{1}{3}$.

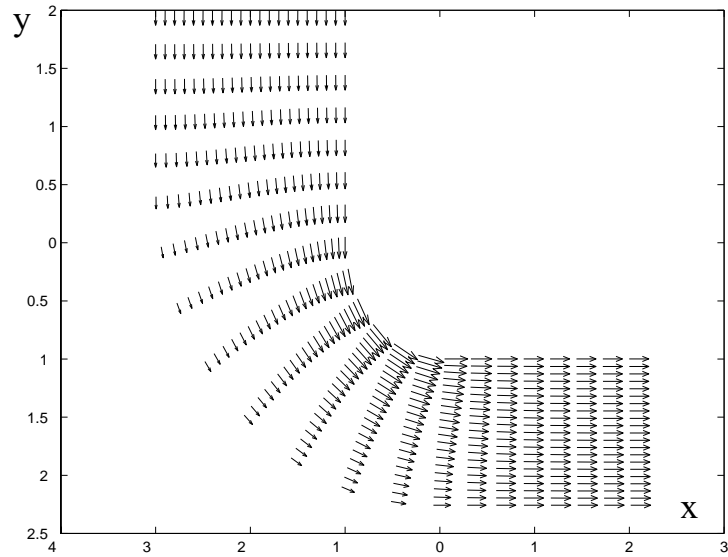


Figure 2.17: Velocity vectors for 90 degree elbow with contraction, $\frac{R_2 - R_1}{R_2} = \frac{2}{3}$.

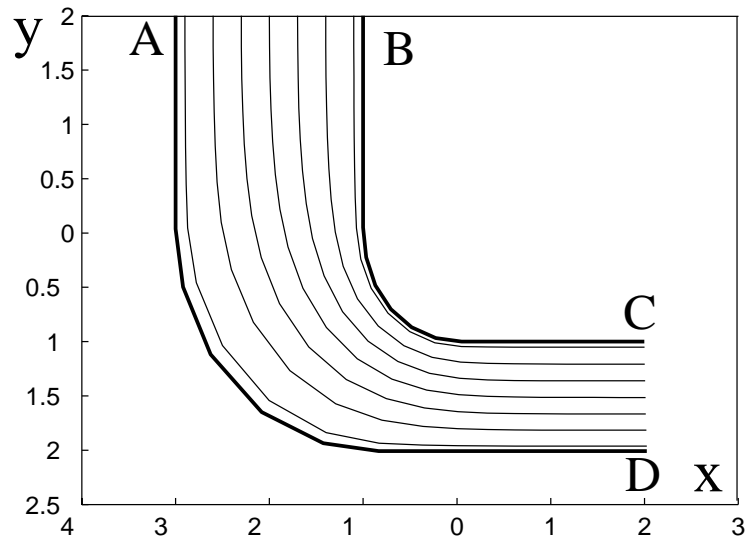


Figure 2.18: Streamlines for 90 degree elbow with contraction, $\frac{R_2 - R_1}{R_2} = \frac{2}{3}$.

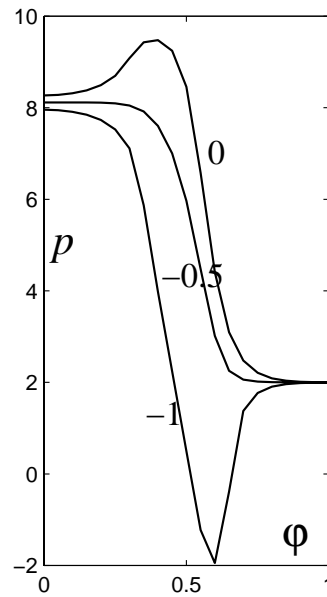


Figure 2.19: Pressure as a function of φ along streamlines $\psi = -1, -0.5, 0$ for 90 degree elbow with contraction, $\frac{R_2-R_1}{R_2} = \frac{2}{3}$, $R_1 = 1$, $R_2 = 3$, $x_0 = 2$, $y_0 = 2$, $P_{CD} = 2$.

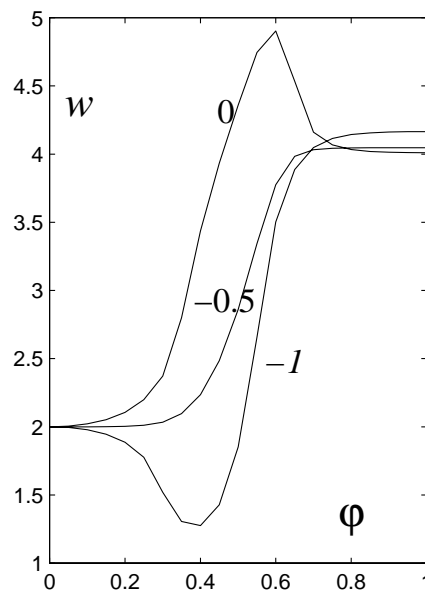


Figure 2.20: Modulus of the velocity vector as a function of φ along streamline $\psi = -1, -0.5, 0$ for 90 degree elbow with contraction, $\frac{R_2-R_1}{R_2} = \frac{2}{3}$, $R_1 = 1$, $R_2 = 3$, $x_0 = 2$, $y_0 = 2$, $P_{CD} = 2$.

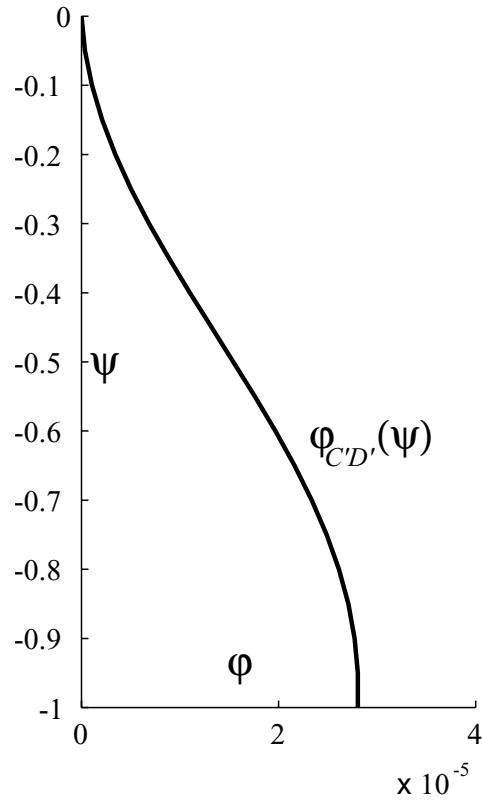


Figure 2.21: Graph of $C'D'$ boundary for 90 degree elbow with contraction, $\frac{R_2-R_1}{R_2} = \frac{2}{3}$, $R_1 = 1$, $R_2 = 3$, $x_0 = 2$, $y_0 = 2$, $P_{CD} = 2$.

Table 2.5: The maximum of $|\varphi_{C'D'}(\psi)|$ for different length of exit for 90 degree elbow with contraction, $y_0 = 2$, $R_1 = 1$, $R_2 = 2$.

| x_0 | 1.0 | 1.5 | 2.0 | 3.0 |
|--------------------------------------|-------------------------|-------------------------|-------------------------|-------------------------|
| $\max_{\psi} \varphi_{C'D'}(\psi) $ | 9.3408×10^{-4} | 1.7559×10^{-4} | 3.2658×10^{-5} | 1.1008×10^{-6} |

2.4.4 Numerical Results for Two-Dimensional Channel with Curved Walls

To demonstrate the efficiency of numerical code, we give here some more examples. Let us consider the channel shown in Figure 2.22. We assume that the

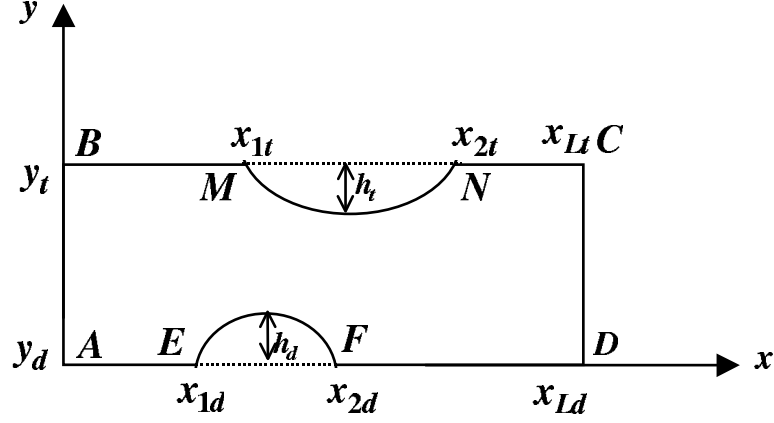


Figure 2.22: Physical domain.

arcs MN and EF are arcs of circle

$$\begin{aligned} r_t^2 &= (x - x_0)^2 + (y - y_0)^2, \\ r_d^2 &= (x - \bar{x})^2 + (y - \bar{y})^2, \end{aligned}$$

with radius

$$\begin{aligned} r_t &= \sqrt{(x_{1t} - x_0)^2 + (y_t - y_0)^2}, \\ r_d &= \sqrt{(x_{1d} - \bar{x})^2 + (y_t - \bar{y})^2}, \end{aligned}$$

and coordinates of circles centers

$$\begin{aligned} x_0 &= \frac{x_{1t} + x_{2t}}{2}, & y_0 &= \frac{1}{8|h_t|} [(x_{1t} - x_{2t})^2 - 4|h_t|^2] + y_t, \\ \bar{x} &= \frac{x_{1d} + x_{2d}}{2}, & \bar{y} &= \frac{1}{8|h_d|} [(x_{1d} - x_{2d})^2 - 4|h_d|^2] + y_d. \end{aligned}$$

We can write the natural equations of boundaries AD and BC . In the case of boundary BC , we obtain

$$x(l) = \begin{cases} l, & 0 \leq l \leq x_{1t}, \\ x_{1t} + x_0 - r_t \sin\left(q - \frac{l - x_{1t}}{r_t}\right), & x_{1t} < l < x_{1t} + L_{MN}, \\ l + x_{2t} - (x_{1t} + L_{MN}), & x_{1t} + L_{MN} \leq l \leq L_{BC}, \end{cases} \quad (2.4.5)$$

$$y(l) = \begin{cases} y_t, & 0 \leq l \leq x_{1t}, \\ y_t + \frac{h_t}{|h_t|} \sqrt{r_t^2 - (x(l) - x_0)^2}, & x_{1t} < l < x_{1t} + L_{MN}, \\ y_t, & x_{1t} + L_{MN} \leq l \leq L_{BC}, \end{cases} \quad (2.4.6)$$

where $q = \sin^{-1} \left(\frac{x_0 - x_{1t}}{r_t} \right)$, l is a natural parameter of curve BC , $L_{MN} = 2r_t \sin^{-1} \left(\frac{x_0 - x_{1t}}{r_t} \right)$ is the length of the curve MN and $L_{BC} = x_{1t} + L_{MN} + (x_{L_t} - x_{2t})$ is the length of the curve BC .

The similar representation of the curve AD is

$$x(l) = \begin{cases} l, & 0 \leq l \leq x_{1d}, \\ x_{1d} + x_0 - r_d \sin \left(q - \frac{l - x_{1d}}{r_d} \right), & x_{1d} < l < x_{1d} + L_{EF}, \\ l + x_{2d} - (x_{1d} + L_{EF}), & x_{1d} + L_{EF} \leq l \leq L_{AD}, \end{cases} \quad (2.4.7)$$

$$y(l) = \begin{cases} y_d, & 0 \leq l \leq x_{1d}, \\ y_d + \frac{h_d}{|h_d|} \sqrt{r_d^2 - (x(l) - \bar{x})^2}, & x_{1d} < l < x_{1d} + L_{EF}, \\ y_d, & x_{1d} + L_{EF} \leq l \leq L_{AD}, \end{cases} \quad (2.4.8)$$

where $q = \sin^{-1} \left(\frac{x_0 - x_{1d}}{r_d} \right)$, l is a natural parameter of the curve AD , $L_{EF} = 2r_d \sin^{-1} \left(\frac{x_0 - x_{1d}}{r_d} \right)$ is the length of the curve EF and $L_{AD} = x_{1d} + L_{EF} + (x_{1d} - x_{2d})$ is the length of the curve AD .

Solution of the flowing-through problems 2' and 3' in a channel with curved walls are obtained with developed solvers. Table 2.6 designs for the following set of parameters: $x_{1t} = 1.0$, $x_{2t} = 2.0$, $x_{1d} = 2.0$, $x_{2d} = 3.0$, $h_t = -0.1$, $h_d = 0.1$, $x_{L_t} = 5.0$, $x_{L_d} = 5.0$, $y_t = 1.0$, $y_d = 0.0$. This table shows the results of numerical simulation for different grids. The first and the second columns present the number of grid points in a computational domain. The third column shows the tolerances for convergence of outer iterative process. The fourth column shows the number of outer iterations. The fifth column shows the values of relaxation parameter used in the iterative process. The sixth and the seventh columns show the length of boundary AD which is obtained as a result of numerical simulation and the relative error which is measured with the exact value of $L_{AD} = 5.026457$. The computations show that the relative error is reduced when the grid becomes finer.

Table 2.6: Results of numerical simulations for different grids.

| N_1 | N_2 | Convergence tolerances (ϕ, w, q) | Num. of outer iters. | ω relaxation | L_{AD}^h | $\frac{L_{AD}^h - L_{AD}}{L_{AD}}$ |
|-------|-------|---|----------------------|---------------------|------------|------------------------------------|
| 21 | 21 | $10^{-4} 10^{-4} 10^{-5}$ | 13 | 1.1 | 5.015554 | 0.002169 |
| 41 | 41 | $10^{-4} 10^{-4} 10^{-5}$ | 24 | 1.3 | 5.016303 | 0.002020 |
| 21 | 41 | $10^{-4} 10^{-5} 10^{-5}$ | 23 | 1.2 | 5.017374 | 0.001807 |
| 21 | 81 | $10^{-4} 10^{-4} 10^{-5}$ | 86 | 1.0 | 5.026363 | 0.000019 |

Table 2.7 shows the choice of the optimal values of the relaxation parameter for different grids in a computational domain. The first and the second columns

show the number of grid points in the computational domain. The third column shows the tolerances for convergence of the outer iterative process. The fourth column shows the number of outer iterations. The last column shows the values of relaxation parameter used in the iterative process. In each particular case, it is necessary to make several numerical experiments to find a range of optimal values of the relaxation parameter. The optimal values of relaxation parameter vary in the range $0.7 \leq \omega \leq 1.2$.

Table 2.7: Choices of the relaxation parameter for channel with curved walls
 $x_{1t} = 1.0$, $x_{2t} = 2.0$, $x_{Lt} = 5.0$, $h_t = 0.0$, $x_{1d} = 2.0$, $x_{2d} = 3.0$, $x_{Ld} = 5.0$, $h_d = 0.05$.

| N_1 | N_2 | Convergence tolerances (ϕ , w , q) | Number of outer iterations | ω relaxation |
|-------|-------|---|----------------------------|---------------------|
| 11 | 11 | 10^{-4} , 10^{-4} , 10^{-5} | 20 | 0.5 |
| 11 | 11 | 10^{-4} , 10^{-4} , 10^{-5} | 17 | 0.6 |
| 11 | 11 | 10^{-4} , 10^{-4} , 10^{-5} | 14 | 0.8 |
| 11 | 11 | 10^{-4} , 10^{-4} , 10^{-5} | 62 | 1.4 |
| 21 | 21 | 10^{-4} , 10^{-4} , 10^{-5} | 23 | 0.5 |
| 21 | 21 | 10^{-4} , 10^{-4} , 10^{-5} | 16 | 0.8 |
| 21 | 21 | 10^{-4} , 10^{-4} , 10^{-5} | 13 | 1.1 |
| 21 | 21 | 10^{-4} , 10^{-4} , 10^{-5} | 13 | 1.2 |
| 21 | 21 | 10^{-4} , 10^{-4} , 10^{-5} | 17 | 1.3 |
| 41 | 41 | 10^{-4} , 10^{-4} , 10^{-5} | 47 | 0.5 |
| 41 | 41 | 10^{-4} , 10^{-4} , 10^{-5} | 37 | 0.7 |
| 41 | 41 | 10^{-4} , 10^{-4} , 10^{-5} | 24 | 1.3 |
| 41 | 41 | 10^{-4} , 10^{-4} , 10^{-5} | 39 | 1.4 |
| 41 | 41 | 10^{-4} , 10^{-4} , 10^{-5} | 83 | 1.5 |
| 21 | 41 | 10^{-4} , 10^{-4} , 10^{-5} | 47 | 0.5 |
| 21 | 41 | 10^{-4} , 10^{-4} , 10^{-5} | 41 | 0.6 |
| 21 | 41 | 10^{-4} , 10^{-4} , 10^{-5} | 37 | 0.7 |
| 21 | 41 | 10^{-4} , 10^{-4} , 10^{-5} | 77 | 1.5 |
| 21 | 81 | 10^{-4} , 10^{-4} , 10^{-5} | 96 | 0.7 |
| 21 | 81 | 10^{-4} , 10^{-4} , 10^{-5} | 86 | 1.0 |
| 21 | 81 | 10^{-4} , 10^{-4} , 10^{-5} | 69 | 1.3 |
| 21 | 81 | 10^{-4} , 10^{-4} , 10^{-5} | 151 | 1.5 |

Table 2.8 shows the detailed description of results of numerical simulations for the channel with curved walls. The first and the second columns show the number of grid points in the computational domain. The third column shows the values of relaxation parameter which is used in the numerical calculations. The fourth column gives us the information about the number of outer iterations to achieve convergence with tolerances $\varepsilon_\phi = 10^{-4}$, $\varepsilon_w = 10^{-4}$, $\varepsilon_q = 10^{-4}$. The fifth to the eleventh columns show the values of geometrical parameters used in equations (2.4.5)-(2.4.8). The last column shows the corresponding Figure numbers in which computational results are illustrated by graphics.

Table 2.8: Detailed description of results of numerical simulations with tolerances criteria $\varepsilon_\phi = 10^{-4}$, $\varepsilon_w = 10^{-4}$, $\varepsilon_q = 10^{-4}$. Channel with curve walls.

| N_1 | N_2 | ω relax. | Num. of outer iters. | x_{1t} | x_{2t} | $x_{Lt},$ x_{Ld} | h_t | x_{1d} | x_{2d} | h_d | Figure number |
|-------|-------|--------------------|-------------------------|----------|----------|-----------------------|-------|----------|----------|-------|------------------|
| 11 | 11 | 0.8 | 14 | 1 | 2 | 5 | 0 | 2 | 3 | 0.05 | – |
| 21 | 21 | 1.1 | 13 | 1 | 2 | 5 | 0 | 2 | 3 | 0.05 | – |
| 21 | 21 | 1.1 | 13 | 1 | 2 | 5 | -0.1 | 2 | 3 | 0.1 | 2.39, 2.41 |
| 21 | 21 | 1.3 | 24 | 2 | 3 | 5 | 0.2 | 2 | 3 | -0.2 | 2.40, 2.42 |
| 41 | 41 | 1.3 | 24 | 1 | 2 | 5 | 0 | 2 | 3 | 0.05 | – |
| 41 | 41 | 1.3 | 25 | 0 | 0 | 3 | 0 | 1 | 2 | 0.04 | 2.35 |
| 41 | 41 | 1.3 | 28 | 0 | 0 | 3 | 0 | 1 | 2 | 0.1 | 2.26 |
| 41 | 41 | 1.3 | 33 | 0 | 0 | 3 | 0 | 1 | 2 | -0.07 | 2.27 |
| 41 | 41 | 1.3 | 26 | 0 | 0 | 3 | 0 | 1 | 2 | -0.03 | 2.28 |
| 41 | 41 | 1.1 | 12 | 2 | 3 | 5 | -0.1 | 2 | 3 | 0.1 | 2.29 |
| 41 | 41 | 1.2 | 24 | 2 | 3 | 5 | -0.1 | 2.5 | 3.5 | 0.2 | 2.30 |
| 41 | 41 | 1.3 | 24 | 1 | 2 | 5 | -0.1 | 3 | 4 | 0.1 | 2.33 |
| 41 | 41 | 1.3 | 17 | 2 | 3 | 5 | 0.1 | 2 | 3 | -0.1 | 2.34 |
| 41 | 41 | 1.1 | 11 | 2 | 3 | 5 | 0.05 | 3 | 4 | -0.05 | 2.36 |
| 41 | 41 | 0.9 | 35 | 2 | 3 | 5 | -0.1 | 2 | 3 | -0.1 | 2.37 |
| 41 | 41 | 1.3 | 30 | 2 | 3 | 5 | -0.1 | 2.5 | 3.5 | -0.1 | 2.38 |
| 61 | 61 | 1.4 | 71 | 2 | 3 | 5 | 0.2 | 2 | 3 | -0.2 | 2.33 |
| 21 | 41 | 0.7 | 37 | 1 | 2 | 5 | 0 | 2 | 3 | 0.05 | – |
| 21 | 81 | 1.3 | 69 | 1 | 2 | 5 | 0 | 2 | 3 | 0.05 | – |

In Figures 2.23 and 2.24 the pressure contours for flow through a curved channel obtained by using the developed numerical algorithm (section 2.3) is compared to the solution obtained by T. W. Roberts et al. (1999). Solution for incompressible, inviscid fluid flow through a curved channel have been obtained by T. W. Roberts et al. using a multigrid method with unstructured grid and structured grid. The shape of the lower wall between $1 \leq x \leq 2$ was $y(x) = \tau \sin^2 \pi(x)$. For the computations shown in Figure 2.23 the thickness ratio τ is 0.05. T. W. Roberts et al. used the following boundary conditions:

- a) The flow angle and total pressure was specified at the inflow parts and the pressure was specified at the outflow parts of domain boundary.
- b) The flow tangency condition $\mathbf{u} \cdot \mathbf{n} = 0$ was enforced at the upper and lower walls of channel.

Figure 2.24 shows the pressure contours for flow through the channel with curved walls obtained by using the developed numerical method (section 2.3). The shape of the lower wall between $1 \leq x \leq 2$ was given by equations (2.4.7) and (2.4.8). The value of thickness ratio h_d is 0.05. In our case, the boundary conditions were imposed at the inflow parts for flow angle and modulus of velocity vector. The pressure is known at the outflow parts of domain boundary. In spite of the fact that different boundary conditions at the inflow parts, we can compare distribution of the pressure field. Really, for sufficiently long entrance and exit parts of channel the pressure at the cross section near the entrance will be close to constant due the fact that almost one-dimensional flow observed

in this case. Using the property that pressure field are determined up to an arbitrary constant, we can transform the values of total pressure to the values of the modulus of velocity vector. It needed to point out that, we can make only qualitative comparison of our results with results of T. W. Roberts et al. Comparison of pressure contours in Figures 2.23 and 2.24 show that distribution of pressure gradient within flow domain are essentially identical.

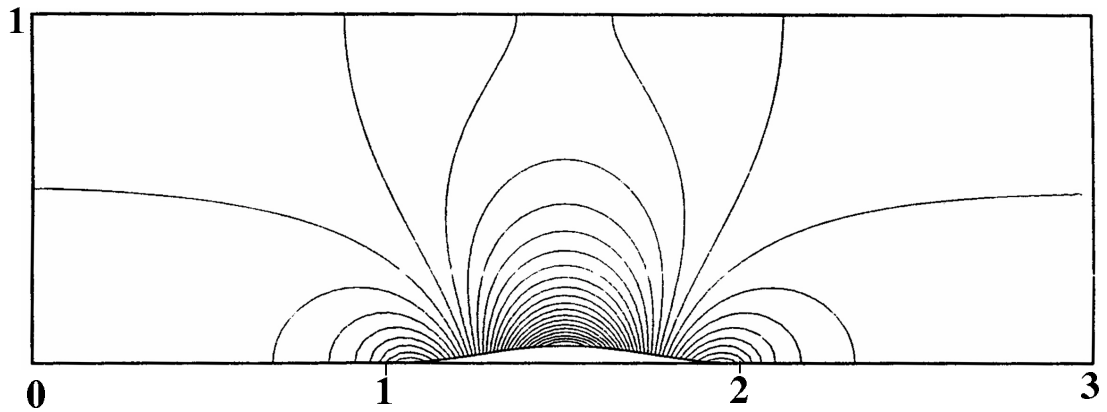


Figure 2.23: Pressure contours by T. W. Roberts et al. Contour increment $\Delta P = 0.01$.

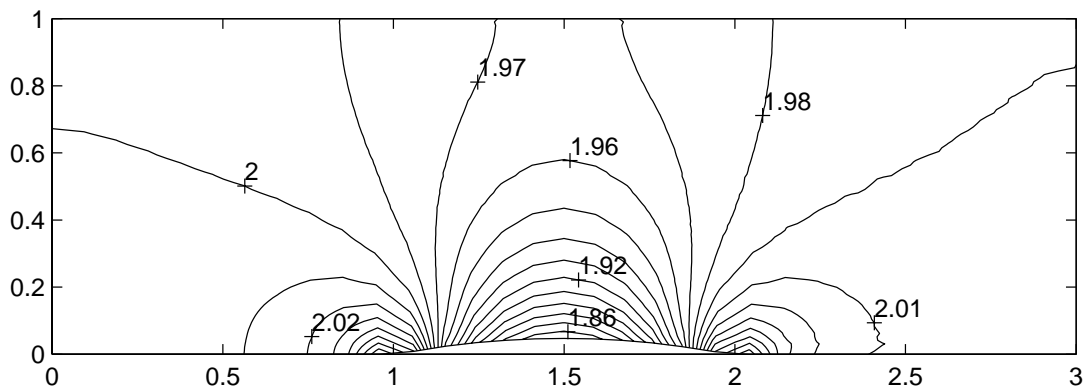


Figure 2.24: Pressure contours for channel with curved walls. Results of numerical simulations for $x_{1d} = 1$, $x_{2d} = 2$, $x_{Ld} = 3$, $h_d = 0.05$, $N1 = 97$, $N2 = 33$. Contour increment $\Delta P = 0.01$.

Figures 2.25-2.38 show the distribution of pressure for varied geometry of channel. For the computational results shown in Figures 2.25-2.28 the upper wall is straight and the lower wall between $x_{1d} \leq x \leq x_{2d}$ is given by equations (2.4.7) and (2.4.8). In these Figures we vary the thickness (or extension) ratio h_d . The positive values of h_d correspond to the thickness of channel width and negative values of h_d correspond to the extension of channel width. For the pressure

distribution in Figures 2.29 to 2.38 both upper and lower walls of channel is given by equations (2.4.5) and (2.4.8). We vary the thickness and extension ratio h_d and h_t . Also, at the same time, we considered different location of thickness or extensions of walls. Figures 2.39 and 2.40 present the streamlines for two particular case of channel geometry. The velocity field illustrated in Figures 2.41 and 2.42 . Figures 2.43 and 2.44 demonstrate the pressure distribution by colored graphics.

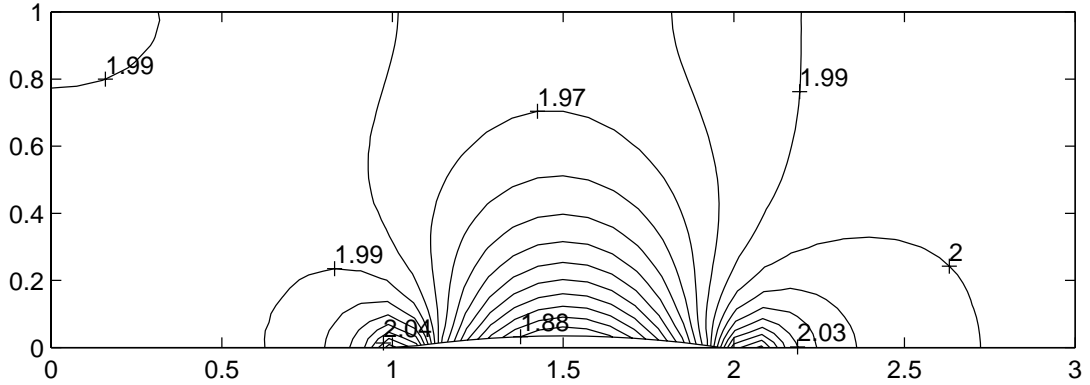


Figure 2.25: Pressure contours for channel with curved walls. Results of numerical simulations for $x_{1t} = 0$, $x_{2t} = 0$, $x_{Lt} = 3$, $h_t = 0$, $x_{1d} = 1$, $x_{2d} = 2$, $x_{Ld} = 3$, $h_d = 0.04$, $N1 = 41$, $N2 = 41$.

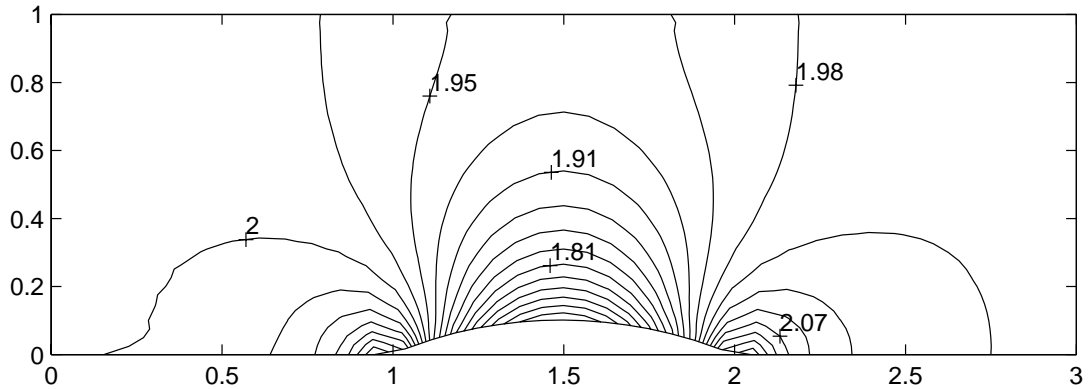


Figure 2.26: Pressure contours for channel with curved walls. Results of numerical simulations for $x_{1t} = 0$, $x_{2t} = 0$, $x_{Lt} = 3$, $h_t = 0$, $x_{1d} = 1$, $x_{2d} = 2$, $x_{Ld} = 3$, $h_d = 0.1$, $N1 = 41$, $N2 = 41$.

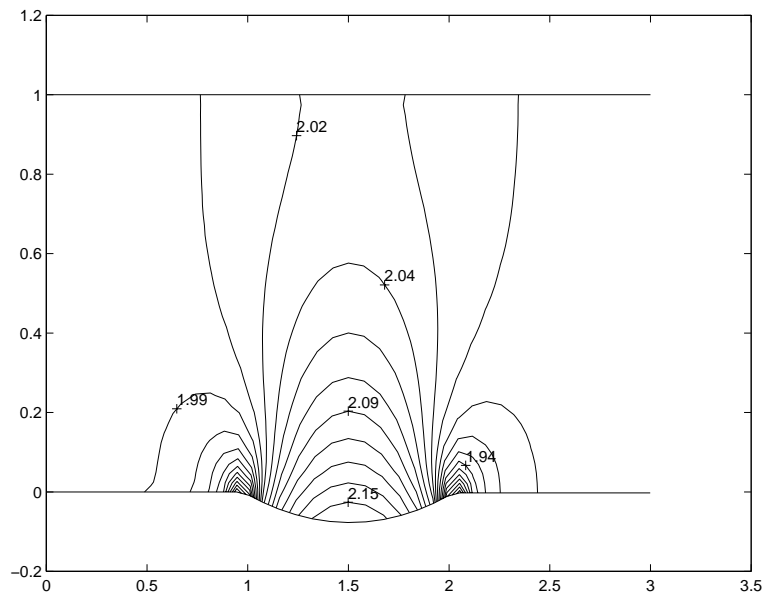


Figure 2.27: Pressure contours for channel with curved walls. Results of numerical simulations for $x_{1t} = 0$, $x_{2t} = 0$, $x_{Lt} = 3$, $h_t = 0$, $x_{1d} = 1$, $x_{2d} = 2$, $x_{Ld} = 3$, $h_d = -0.07$, $N1 = 41$, $N2 = 41$.

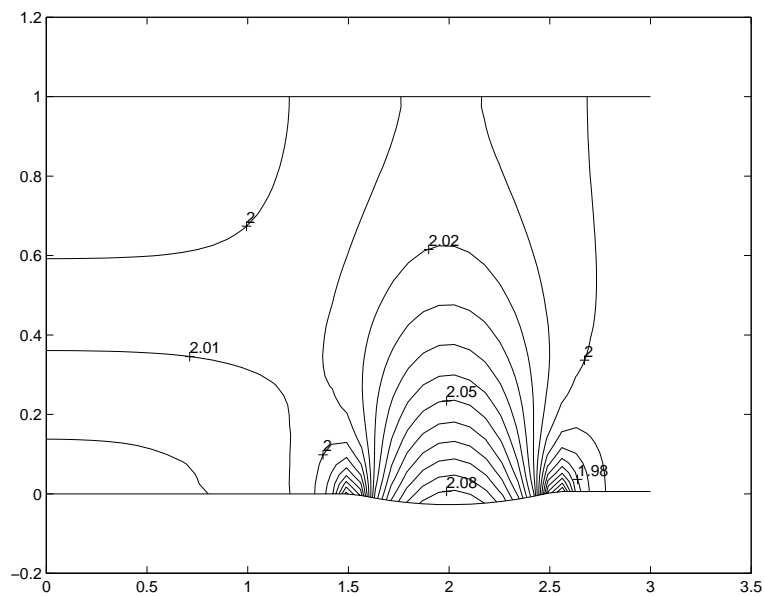


Figure 2.28: Pressure contours for channel with curved walls. Results of numerical simulations for $x_{1t} = 0$, $x_{2t} = 0$, $x_{Lt} = 3$, $h_t = 0$, $x_{1d} = 1.5$, $x_{2d} = 2.5$, $x_{Ld} = 3$, $h_d = -0.03$, $N1 = 41$, $N2 = 41$.

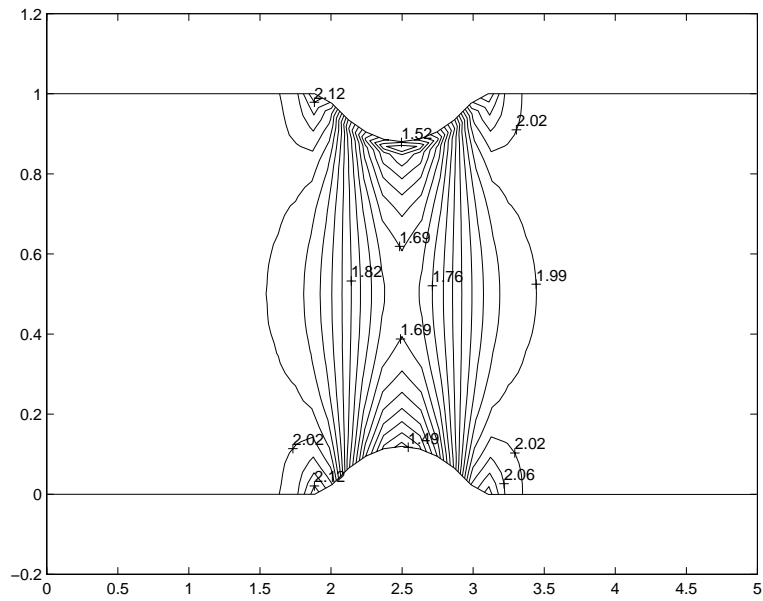


Figure 2.29: Pressure contours for channel with curved walls. Results of numerical simulations for $x_{1t} = 2$, $x_{2t} = 3$, $x_{Lt} = 5$, $h_t = -0.1$, $x_{1d} = 2$, $x_{2d} = 3$, $x_{1d} = 5$, $h_d = 0.1$, $N1 = 41$, $N2 = 41$.

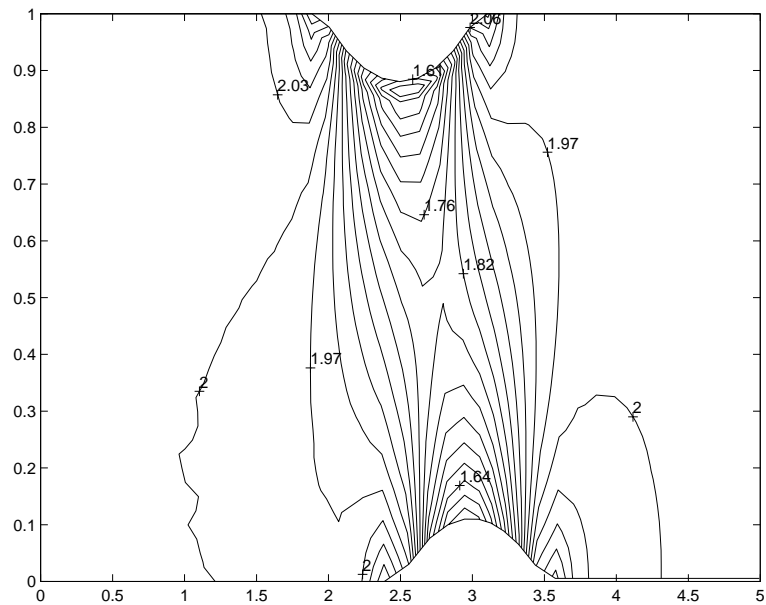


Figure 2.30: Pressure contours for channel with curved walls. Results of numerical simulations for $x_{1t} = 2$, $x_{2t} = 3$, $x_{Lt} = 5$, $h_t = -0.1$, $x_{1d} = 2.5$, $x_{2d} = 3.5$, $x_{Ld} = 5$, $h_d = 0.1$, $N1 = 41$, $N2 = 41$.

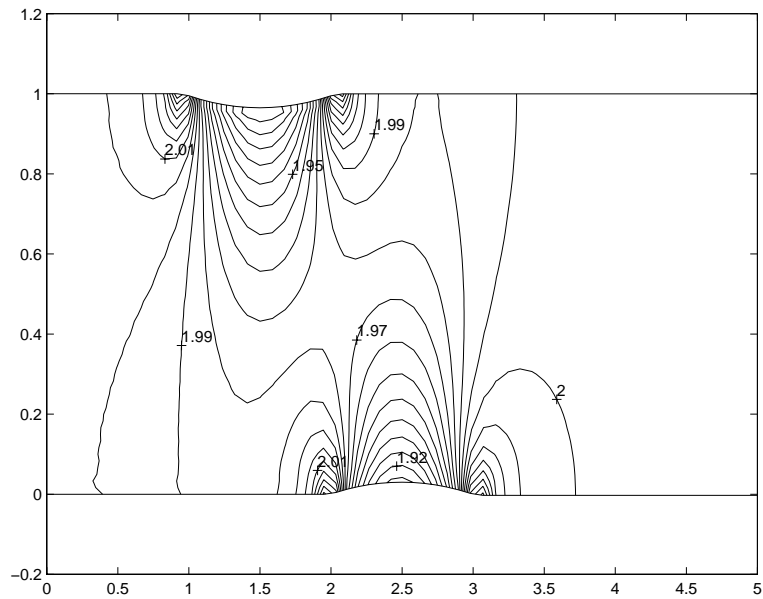


Figure 2.31: Pressure contours for channel with curved walls. Results of numerical simulations for $x_{1t} = 1$, $x_{2t} = 2$, $x_{Lt} = 5$, $h_t = -0.03$, $x_{1d} = 2$, $x_{2d} = 3$, $x_{Ld} = 5$, $h_d = 0.03$, $N1 = 61$, $N2 = 61$.

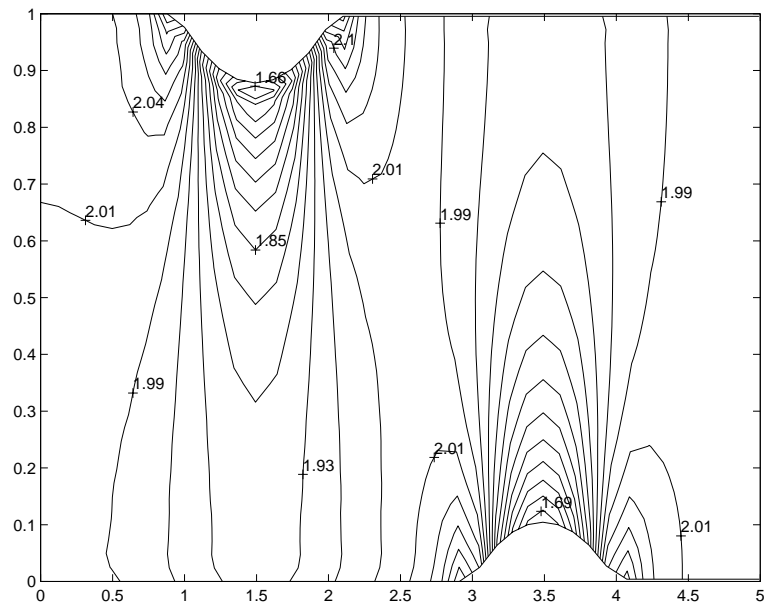


Figure 2.32: Pressure contours for channel with curved walls. Results of numerical simulations for $x_{1t} = 1$, $x_{2t} = 2$, $x_{Lt} = 5$, $h_t = -0.1$, $x_{1d} = 3$, $x_{2d} = 4$, $x_{Ld} = 5$, $h_d = 0.1$, $N1 = 41$, $N2 = 41$.

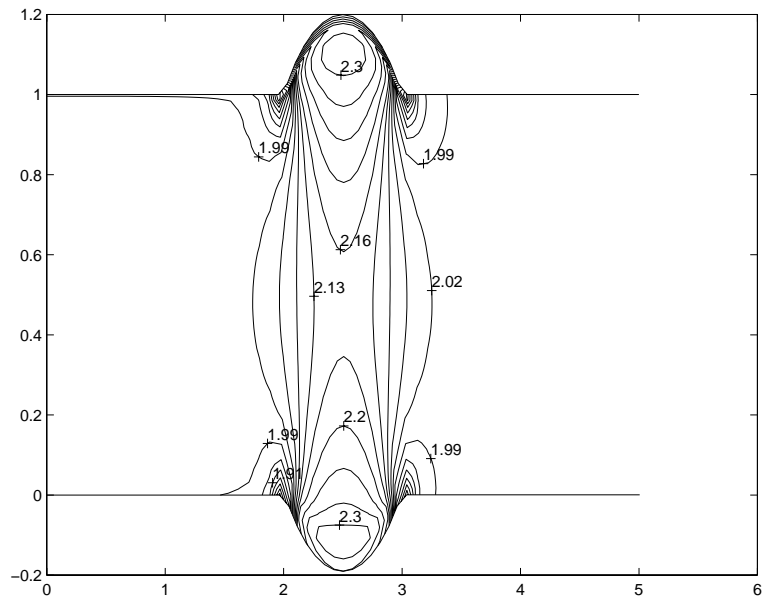


Figure 2.33: Pressure contours for channel with curved walls. Results of numerical simulations for $x_{1t} = 2$, $x_{2t} = 3$, $x_{Lt} = 5$, $h_t = 0.2$, $x_{1d} = 2$, $x_{2d} = 3$, $x_{Ld} = 5$, $h_d = -0.2$, $N1 = 61$, $N2 = 61$.

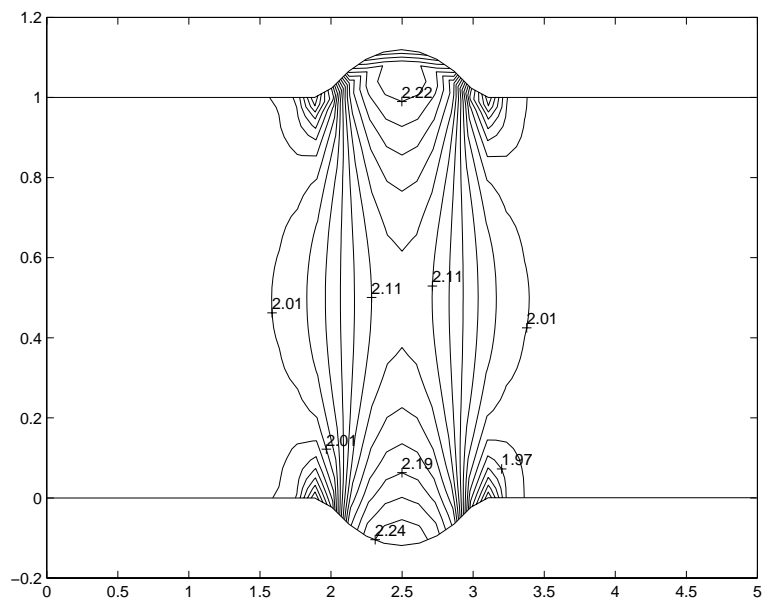


Figure 2.34: Pressure contours for channel with curved walls. Results of numerical simulations for $x_{1t} = 2$, $x_{2t} = 3$, $x_{Lt} = 5$, $h_t = 0.1$, $x_{1d} = 2$, $x_{2d} = 3$, $x_{Ld} = 5$, $h_d = -0.1$, $N1 = 41$, $N2 = 41$.

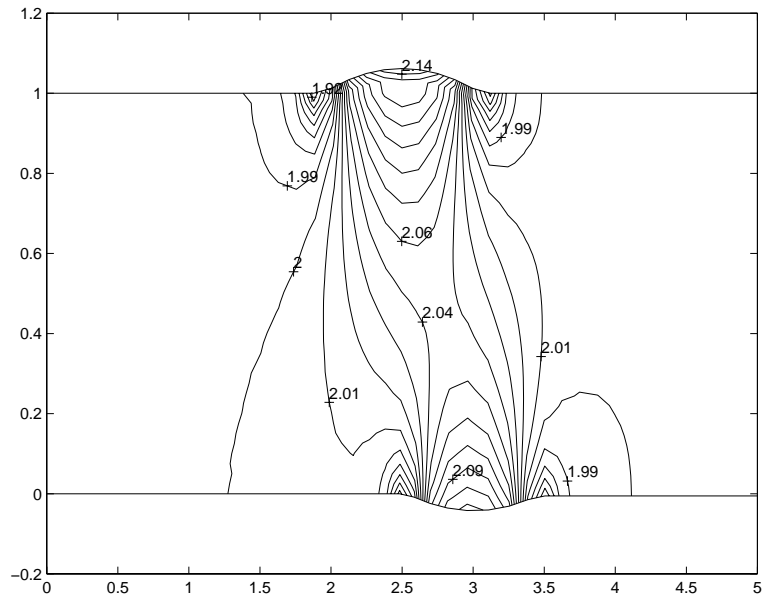


Figure 2.35: Pressure contours for channel with curved walls. Results of numerical simulations for $x_{1t} = 2$, $x_{2t} = 3$, $x_{Lt} = 5$, $h_t = 0.05$, $x_{1d} = 2.5$, $x_{2d} = 3.5$, $x_{Ld} = 5$, $h_d = -0.05$, $N1 = 41$, $N2 = 41$.

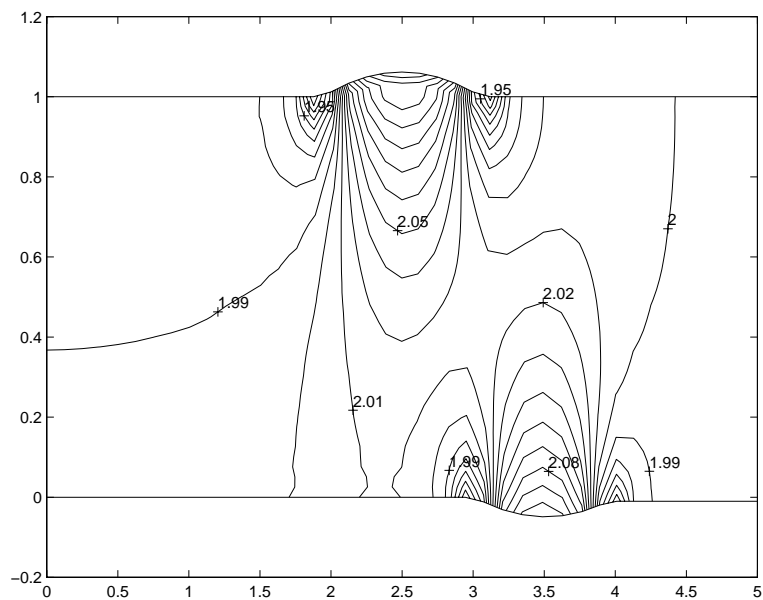


Figure 2.36: Pressure contours for channel with curved walls. Results of numerical simulations for $x_{1t} = 2$, $x_{2t} = 3$, $x_{Lt} = 5$, $h_t = 0.05$, $x_{1d} = 3$, $x_{2d} = 4$, $x_{Ld} = 5$, $h_d = -0.05$, $N1 = 41$, $N2 = 41$.

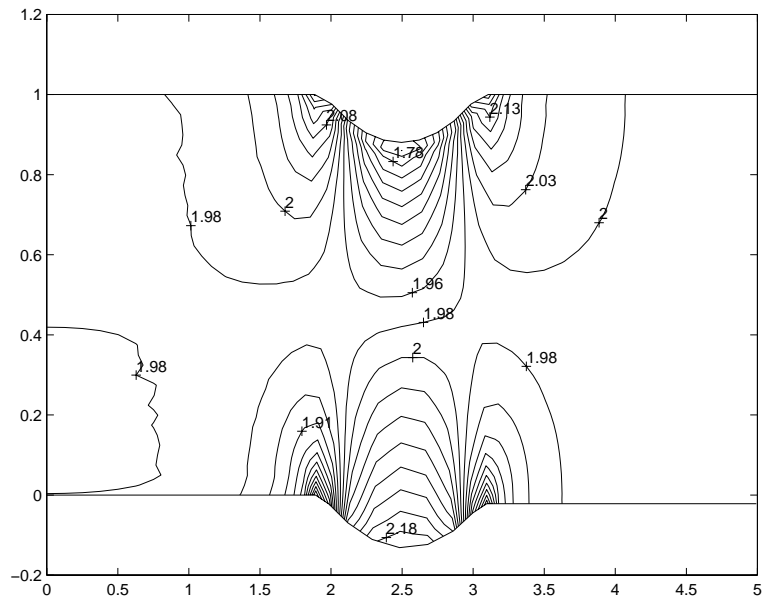


Figure 2.37: Pressure contours for channel with curved walls. Results of numerical simulations for $x_{1t} = 2$, $x_{2t} = 3$, $x_{Lt} = 5$, $h_t = -0.1$, $x_{1d} = 2$, $x_{2d} = 3$, $x_{Ld} = 5$, $h_d = -0.1$, $N1 = 41$, $N2 = 41$.

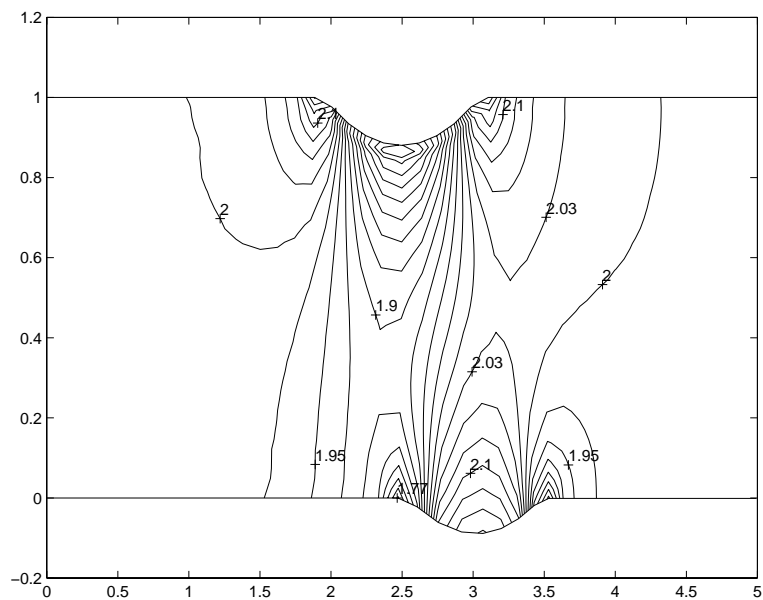


Figure 2.38: Pressure contours for channel with curved walls. Results of numerical simulations for $x_{1t} = 2$, $x_{2t} = 3$, $x_{Lt} = 5$, $h_t = -0.1$, $x_{1d} = 2.5$, $x_{2d} = 3.5$, $x_{Ld} = 5$, $h_d = -0.1$, $N1 = 41$, $N2 = 41$.

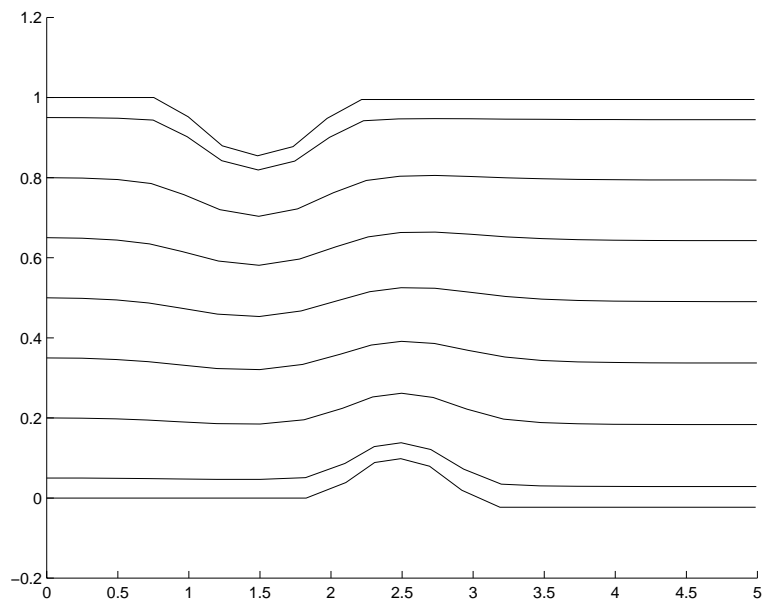


Figure 2.39: Streamlines for channel with curved walls. Results of numerical simulations for $x_{1t} = 1$, $x_{2t} = 2$, $x_{Lt} = 5$, $h_t = -0.1$, $x_{1d} = 2$, $x_{2d} = 3$, $x_{Ld} = 5$, $h_d = 0.1$, $N1 = 21$, $N2 = 21$.

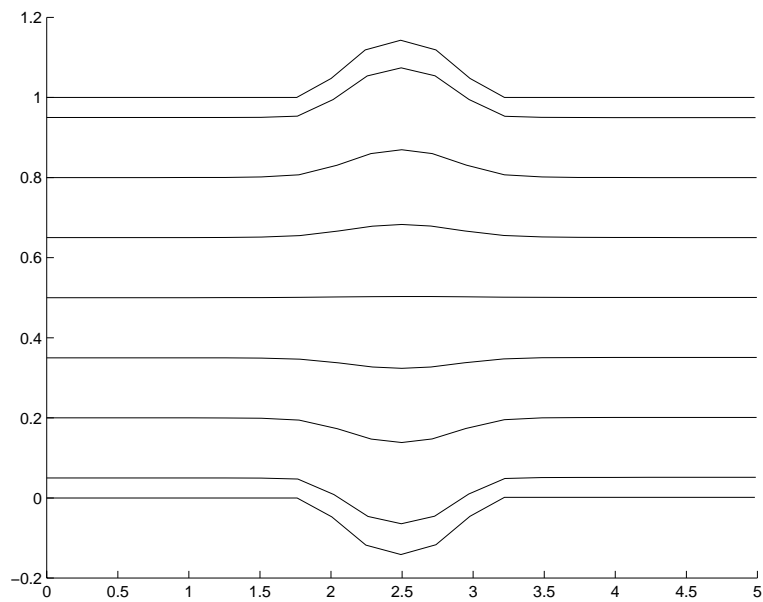


Figure 2.40: Streamlines for channel with curved walls. Results of numerical simulations for $x_{1t} = 2$, $x_{2t} = 3$, $x_{Lt} = 5$, $h_t = 0.2$, $x_{1d} = 2$, $x_{2d} = 3$, $x_{Ld} = 5$, $h_d = -0.2$, $N1 = 21$, $N2 = 21$.

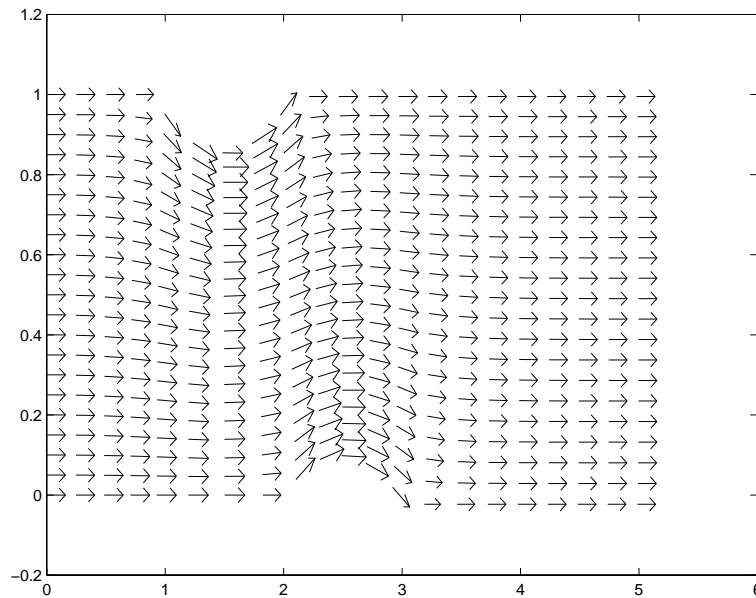


Figure 2.41: Velocity vectors for channel with curved walls. Results of numerical simulations for $x_{1t} = 1$, $x_{2t} = 2$, $x_{Lt} = 5$, $h_t = -0.1$, $x_{1d} = 2$, $x_{2d} = 3$, $x_{Ld} = 5$, $h_d = 0.1$, $N1 = 21$, $N2 = 21$.

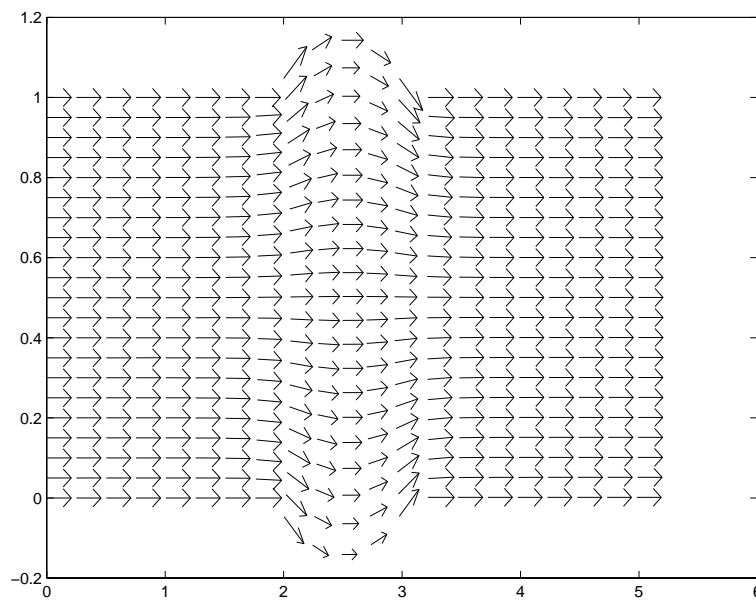


Figure 2.42: Velocity vectors for channel with curved walls. Results of numerical simulations for $x_{1t} = 2$, $x_{2t} = 3$, $x_{Lt} = 5$, $h_t = 0.2$, $x_{1d} = 2$, $x_{2d} = 3$, $x_{Ld} = 5$, $h_d = -0.2$, $N1 = 21$, $N2 = 21$.

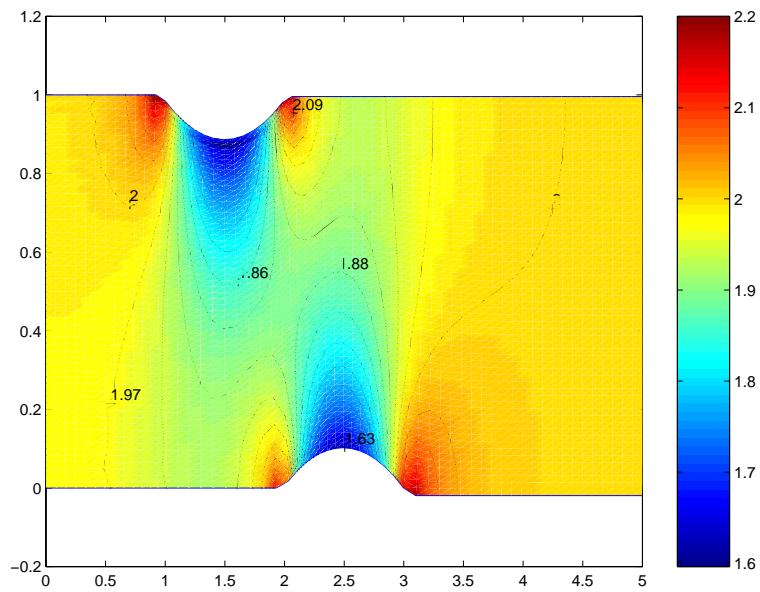


Figure 2.43: Colored graphics of pressure contours for channel with curved walls. Results of numerical simulations for $x_{1t} = 1$, $x_{2t} = 2$, $x_{Lt} = 5$, $h_t = -0.1$, $x_{1d} = 2$, $x_{2d} = 3$, $x_{Ld} = 5$, $h_d = 0.1$, $N1 = 61$, $N2 = 61$.

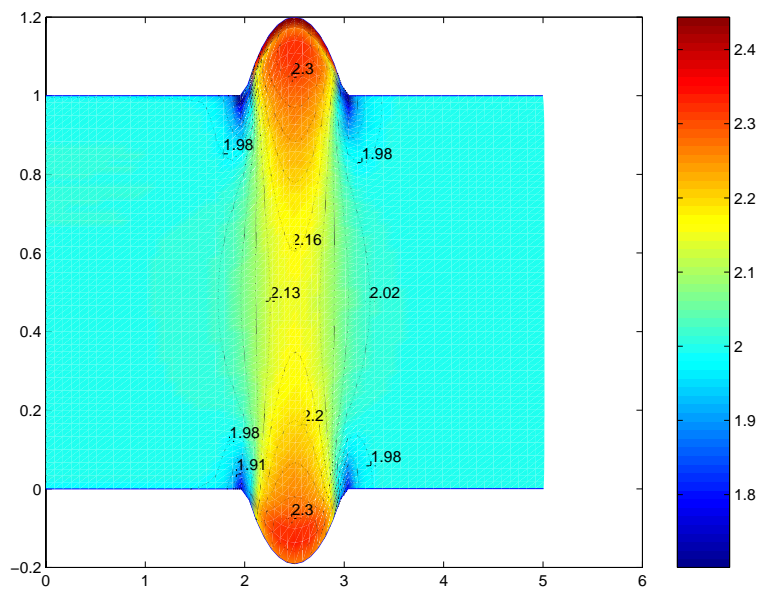


Figure 2.44: Colored graphics of pressure contours for channel with curved walls. Results of numerical simulations for $x_{1t} = 2$, $x_{2t} = 3$, $x_{Lt} = 5$, $h_t = 0.2$, $x_{1d} = 2$, $x_{2d} = 3$, $x_{Ld} = 5$, $h_d = -0.2$, $N1 = 61$, $N2 = 61$.

2.4.5 Numerical Results for α Degree Elbow

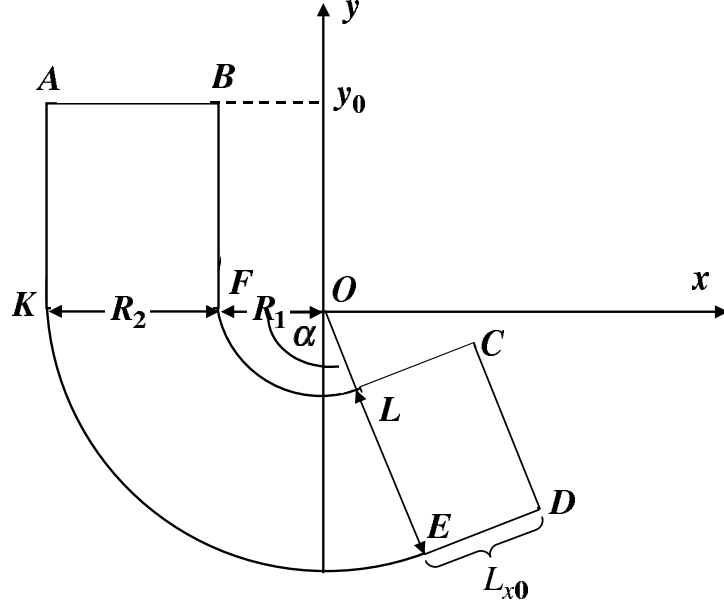


Figure 2.45: Geometry of α° elbow channel.

In this section, the numerical code will be implemented to study the flow through α degree elbow channel without contraction or extension. Figure 2.45 provides a typical example of geometry configuration. The parts of solid impermeable boundary FL and KE are α degree arcs of circles with center at the point O . Taking into account the natural parameterization of a circle, we can write the natural equations of boundaries AD and BC . In the case of boundary BC , we obtain

$$x(l) = \begin{cases} -R_1, & 0 \leq l \leq y_0, \\ -R_1 + R_1 \cos\left(\frac{l-y_0}{R_1}\right), & y_0 \leq l \leq y_0 + \alpha R_1, \\ l - (y_0 + \alpha R_1), & y_0 + \alpha R_1 \leq l \leq L_{BC}, \end{cases}$$

$$y(l) = \begin{cases} y_0 - l, & 0 \leq l \leq y_0, \\ -R_1 \sin\left(\frac{l-y_0}{R_1}\right), & y_0 \leq l \leq y_0 + \alpha R_1, \\ -R_1, & y_0 + \alpha R_1 \leq l \leq L_{BC}, \end{cases}$$

where l is a natural parameter of the curve BC , L_{BC} is the length of the curve

BC. The similar representation of boundary *AD* is

$$x(l) = \begin{cases} -(R_1 + R_2), & 0 \leq l \leq y_0, \\ -(R_1 + R_2) + R_2 \cos\left(\frac{l-y_0}{R_2}\right), & y_0 \leq l \leq y_0 + \alpha R_1, \\ l - (y_0 + \alpha R_1), & y_0 + \alpha R_1 \leq l \leq L_{AD}, \end{cases}$$

$$y(l) = \begin{cases} y_0 - l, & 0 \leq l \leq y_0, \\ -R_2 \sin\left(\frac{l-y_0}{R_2}\right), & y_0 \leq l \leq y_0 + \alpha R_1, \\ -R_2, & y_0 + \alpha R_1 \leq l \leq L_{AD}. \end{cases}$$

Table 2.9 shows the results of numerical experiments for flow through α degree elbow channel. The first and the second columns show the number of grid points in computational domain. The third column shows the quantity of span angle in radians. The fourth column shows the values of relaxation parameter used in the iterative process. The fifth column shows the number of outer iterations. The sixth column shows the length of boundary *AD* which is obtained in numerical simulation. The exact values of length of *AD* are shown in the seventh column. The last column shows the relative difference between exact and approximate values of length of boundary *AD*. It is apparent from the analysis of results of Table 2.9 that the relative error decreases when grid refine and consequently numerical algorithm converges to the exact value.

Figures 2.46 - 2.49 show the pressure contour in α degree elbow channel for span angles $\alpha = \pi/2, \alpha = 3\pi/4, \alpha = \pi,$ and $\alpha = 5\pi/4,$ respectively. Figures 2.50 - 2.53 show the pressure contour by colored graphics.

Table 2.9: Detailed descriptions of numerical experiments on different grids for α degree elbow with $L_{x0} = 2.0, y_0 = 2.0, R_1 = 1.0, R_2 = 2.0.$

| N_1 | N_2 | α | ω relaxation | Number of outer iterations | L_{AD}^h | L_{AD} | $\frac{ L_{AD}^h - L_{AD} }{L_{AD}}$ |
|-------|-------|----------|------------------------|-------------------------------|------------|----------|--------------------------------------|
| 11 | 11 | $\pi/4$ | 1.2 | 17 | 8.801972 | 8.83322 | 0.003537 |
| 21 | 21 | $\pi/4$ | 1.1 | 18 | 8.829091 | 8.83322 | 0.000467 |
| 41 | 41 | $\pi/4$ | 1.0 | 31 | 8.832898 | 8.83322 | 0.000036 |
| 21 | 41 | $\pi/4$ | 1.0 | 35 | 8.833157 | 8.83322 | 0.000007 |
| 11 | 11 | $\pi/2$ | 1.1 | 18 | 10.260600 | 10.28319 | 0.002196 |
| 21 | 21 | $\pi/2$ | 1.0 | 19 | 10.281880 | 10.28319 | 0.000127 |
| 41 | 41 | $\pi/2$ | 1.0 | 38 | 10.283200 | 10.28319 | 0.000001 |
| 21 | 41 | $\pi/2$ | 0.9 | 38 | 10.283530 | 10.28319 | 0.000033 |
| 11 | 11 | $5\pi/4$ | 1.0 | 18 | 11.877130 | 11.85398 | 0.001952 |
| 21 | 21 | $5\pi/4$ | 1.1 | 22 | 11.874780 | 11.85398 | 0.001755 |
| 41 | 41 | $5\pi/4$ | 0.7 | 60 | 11.859910 | 11.85398 | 0.000499 |
| 21 | 41 | $5\pi/4$ | 0.8 | 42 | 11.860220 | 11.85398 | 0.000526 |

2.5 Conclusions

All the algorithms described in this Chapter have been developed by finite difference discretization. The numerical algorithms are appropriate for a two-dimensional incompressible inviscid fluid flow through domain with an inflow and outflow parts of the domain boundary. The boundary conditions on the inflow parts are imposed for all components of the velocity vector, whereas, the values of the pressure or normal component of the velocity vector are given on the outflow parts.

The coordinate transformation (see section 2.2.2) maps the physical domain into the canonical domain in a computational space. This allows accurate solutions to be obtained within a relatively complicated geometry of the domain. Computer codes have been developed for a relatively simple physical domain. We assume that impermeable boundaries can be described by the equation in a natural form (curvature versus length). The suggested finite difference method has some constraints due to the coordinate transformation. There is a requirement that the modulus of the velocity vector cannot be vanished within the flow domain including boundaries.

Since the algebraic equations produced by discretising the Euler equations are nonlinear, the iterative procedure is suggested (see section 2.3). An outer iterations are designed to cope with the nonlinear nature of the discretized equations. At each step of the outer iterations, a linear system of equations is solved. This system is solved by either the iterative method of SOR or the Stabilizing Correction. However, the system of linear equations may be solved by a direct or more sophisticated iterative method as well.

The convergence of iterative procedure is shown by comparison of numerical solutions on a sequence of grids. We have shown that the norm of error (difference between exact and approximated values) tends to zero as the grid size decreases.

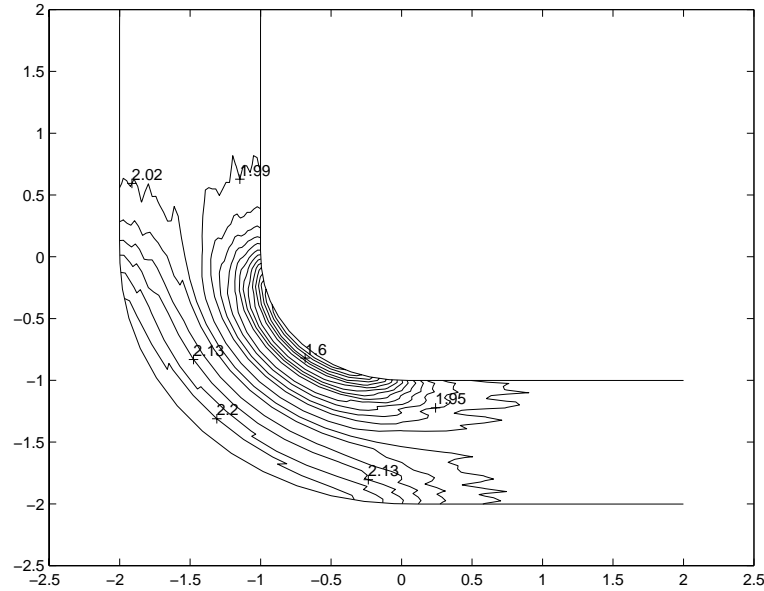


Figure 2.46: Pressure contours for channel with curved walls. Results of numerical simulations for $R_1 = 1$, $R_2 = 2$, $L_{x0} = 2$, $y_0 = 2$, $\alpha = \pi/2$, $N_1 = 41$, $N_2 = 41$.

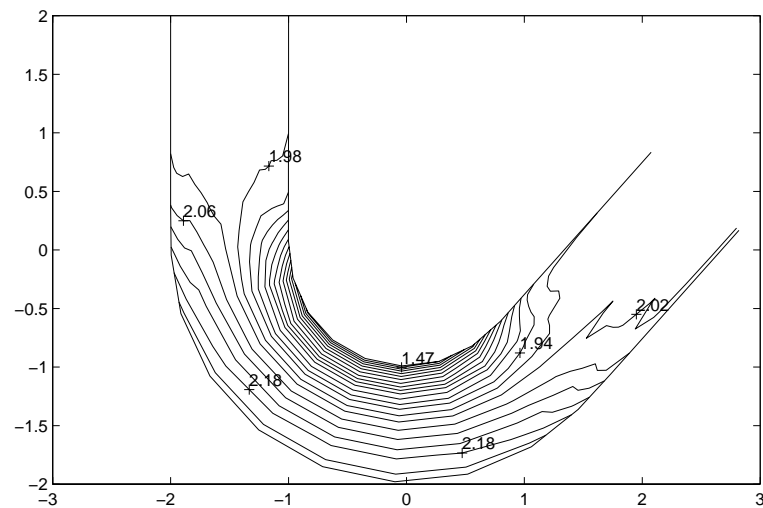


Figure 2.47: Pressure contours for channel with curved walls. Results of numerical simulations for $R_1 = 1$, $R_2 = 2$, $L_{x0} = 2$, $y_0 = 2$, $\alpha = 3\pi/4$, $N_1 = 21$, $N_2 = 21$.

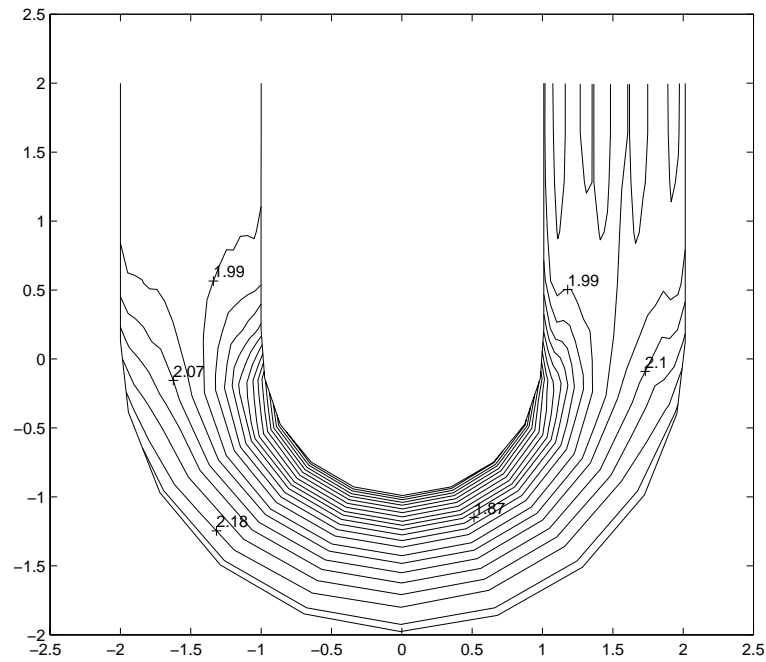


Figure 2.48: Pressure contours for channel with curved walls. Results of numerical simulations for $R_1 = 1$, $R_2 = 2$, $L_{x0} = 2$, $y_0 = 2$, $\alpha = \pi$, $N_1 = 21$, $N_2 = 21$.

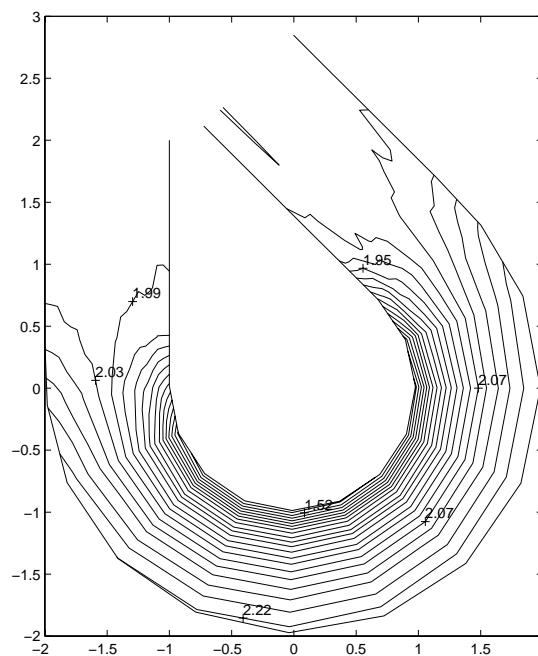


Figure 2.49: Pressure contours for channel with curved walls. Results of numerical simulations for $R_1 = 1$, $R_2 = 2$, $L_{x0} = 2$, $y_0 = 2$, $\alpha = 5\pi/4$, $N_1 = 21$, $N_2 = 21$.

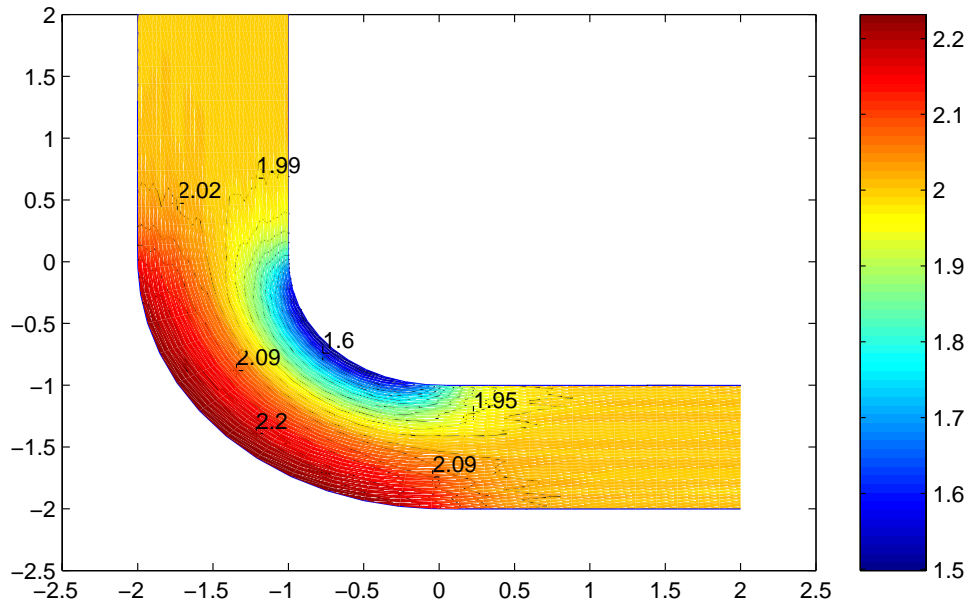


Figure 2.50: Colored graphics of pressure contours for channel with curved walls. Results of numerical simulations for $R_1 = 1$, $R_2 = 2$, $L_{x0} = 2$, $y_0 = 2$, $\alpha = \pi/2$, $N_1 = 41$, $N_2 = 41$.

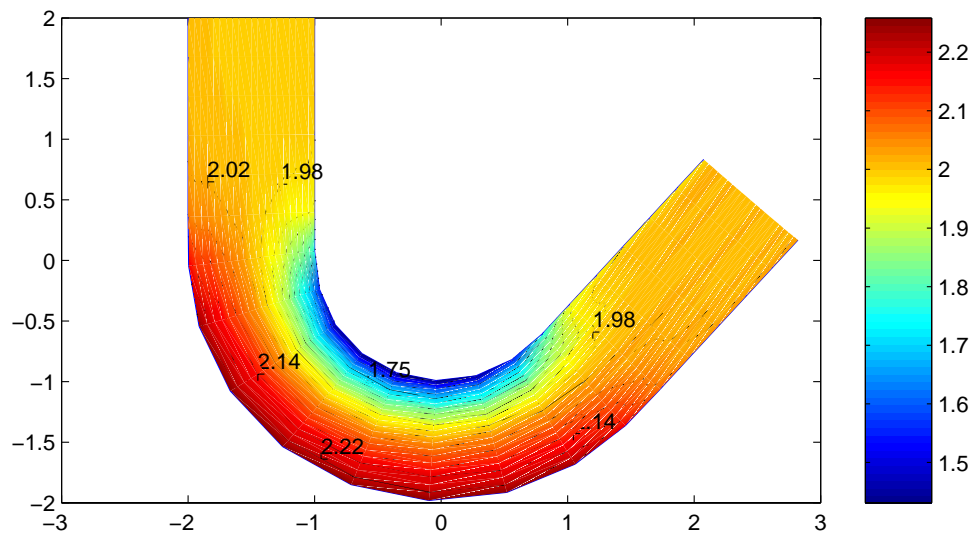


Figure 2.51: Colored graphics of pressure contours for channel with curved walls. Results of numerical simulations for $R_1 = 1$, $R_2 = 2$, $L_{x0} = 2$, $y_0 = 2$, $\alpha = 3\pi/4$, $N_1 = 21$, $N_2 = 21$.

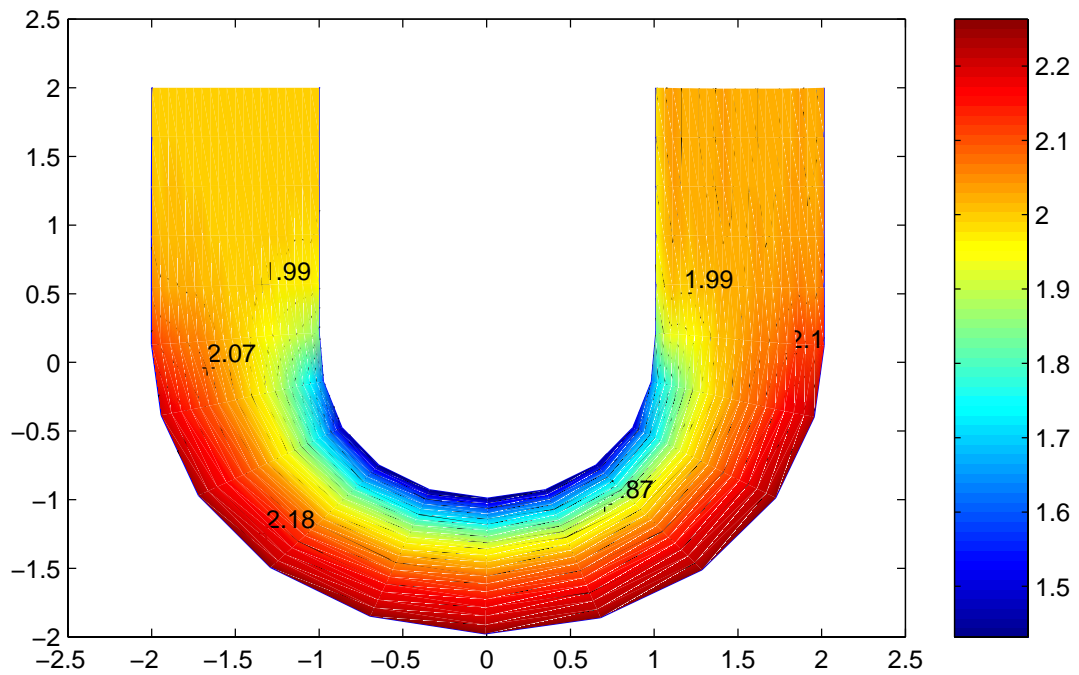


Figure 2.52: Colored graphics of pressure contours for channel with curved walls. Results of numerical simulations for $R_1 = 1$, $R_2 = 2$, $L_{x0} = 2$, $y_0 = 2$, $\alpha = \pi$, $N_1 = 21$, $N_2 = 21$.

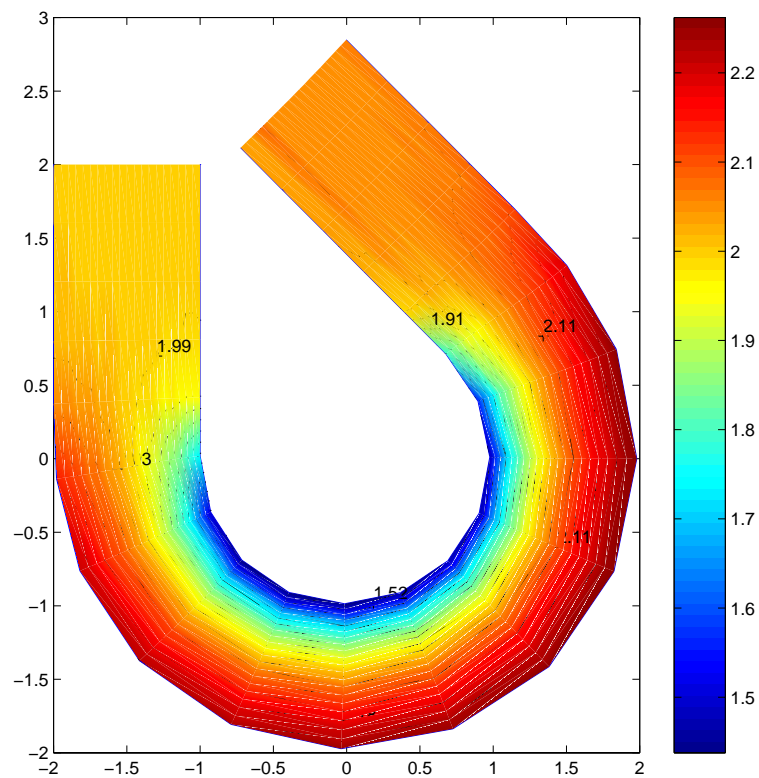


Figure 2.53: Colored graphics of pressure contours for channel with curved walls. Results of numerical simulations for $R_1 = 1$, $R_2 = 2$, $L_{x0} = 2$, $y_0 = 2$, $\alpha = 5\pi/4$, $N_1 = 21$, $N_2 = 21$.

Chapter III

Numerical Methods for Steady Flowing-Through Problem: Problem 1

3.1 Introduction

In this Chapter, we develop the numerical algorithm to study the boundary value problem in which the governing equations are the steady Euler equations and the vorticity is given on the inflow parts of the boundary. We rewrite the Euler equations in terms of the stream function and vorticity. To illustrate a numerical algorithm, we consider the fluid flow through a two-dimensional channel with curved walls. We transform irregular physical domain into a rectangle in the computational domain and rewrite the Euler equations with respect to an arbitrary curvilinear coordinate system. The convergence of the finite difference equation is shown experimentally by comparing the computational results on the sequence of grids. To find the pressure, we utilize the Euler equations in the Gromeka-Lamb form. The analysis of calculation shows strong dependence of a pressure field on the vorticity given at the inflow parts of the boundary. The plotting of the flow structure and isobars, for different geometries of channel and for different values of vorticity on entrance, are also presented.

3.2 Mathematical Statement of the Problem

The steady incompressible Euler equations in primitive variables are

$$\begin{aligned}(\bar{u} \cdot \nabla) \bar{u} + \nabla P &= 0, & \bar{x} \in \Omega, \\ \nabla \cdot \bar{u} &= 0,\end{aligned}\tag{3.2.1}$$

where Ω is a simply connected domain. In two-dimensional case, $\nabla = (\frac{\partial}{\partial x_1}, \frac{\partial}{\partial x_2})$ is the gradient operator, $\bar{u} = (u_1, u_2) = (u, v)$ is the velocity vector with components u_1, u_2 along the coordinate axes x_1, x_2 (or x, y) and P is the pressure. Without loss of generality, the density is taken to be one. The “flowing-through” problem with vorticity given on the inflow parts of boundary is formulated as follows: Find the solution of equations (3.2.1) in Ω with boundary conditions

$$\Gamma_0 : \bar{u} \cdot \bar{n} = 0, \quad \bar{x} \in \Gamma_0, \quad (3.2.2)$$

$$\Gamma_1 : \omega = g(\bar{x}), \quad \bar{u} \cdot \bar{n} = v_1(\bar{x}), \quad \bar{x} \in \Gamma_1, \quad (3.2.3)$$

$$\begin{aligned} \Gamma_2 : \bar{u} \cdot \bar{n} &= v_2(\bar{x}), \quad \bar{x} \in \Gamma_2, \\ P(M_0) &= P_0 = \text{const}, \end{aligned} \quad (3.2.4)$$

where ω is a vorticity, \bar{n} is the vector of outward normal to the boundary of Ω , $g(x)$, $v_1(\bar{x})$, $v_2(\bar{x})$, are given functions, Γ_0 is the impermeable part of the domain boundary, Γ_1 is the inflow part of the domain boundary and Γ_2 is outflow part of the domain boundary, M_0 is an arbitrary point within domain Ω . To eliminate the pressure, we introduce the stream function and the vorticity by the formulas

$$u_1 = \frac{\partial \psi}{\partial x_2}; \quad u_2 = -\frac{\partial \psi}{\partial x_1}; \quad \omega = -\frac{\partial u_1}{\partial x_2} + \frac{\partial u_2}{\partial x_1}. \quad (3.2.5)$$

In terms of ψ and ω , the boundary value problem (3.2.1)–(3.2.4) become

$$(\bar{u} \cdot \nabla) \omega = 0, \quad (3.2.6)$$

$$\Delta \psi = -\omega. \quad (3.2.7)$$

$$\Gamma_1 : \omega = g(\bar{x}), \quad \psi(\bar{x}) = \psi(\bar{x}_0) + \int_{\bar{x}_0}^{\bar{x}} v_1(\bar{x}) d\gamma, \quad \bar{x}, \bar{x}_0 \in \Gamma_1, \quad (3.2.8)$$

$$\Gamma_2 : \psi(\bar{x}) = \psi(\bar{x}_0) + \int_{\bar{x}_0}^{\bar{x}} v_2(\bar{x}) d\gamma, \quad \bar{x}, \bar{x}_0 \in \Gamma_2, \quad (3.2.9)$$

$$\Gamma_0 : \psi(\bar{x}) = \text{const}, \quad \bar{x} \in \Gamma_0, \quad (3.2.10)$$

where the integrals are calculated along the boundaries Γ_1 and Γ_2 .

3.3 Problem in Two-Dimensional Generalized Curvilinear Coordinates

The computation of flow fields in the domain of complex shapes, such as shown in Figure 3.1 a), involves computational boundaries that do not coincide with coordinate lines in physical domain. For finite difference methods, the formulation of boundary conditions for such problem requires interpolation of the data, a local loss of accuracy in the computational solution will occur. These difficulties motivate the introduction of a mapping from a physical domain in the (x, y) -plane to a generalized curvilinear coordinate domain in the (q_1, q_2) -plane. The generalized coordinate domain is constructed so that a computational boundary in a physical domain coincides with a coordinate line in a generalized coordinate domain. Let

$$x = x(q_1, q_2), \quad y = y(q_1, q_2), \quad (3.3.1)$$

be a one to one nonsingular transformation of curvilinear domain $ABCD$ into a rectangular domain $A'B'C'D'$. We assume that the inflow, the outflow and the impermeable parts Γ_i ; $i = 0, 1, 2$ of domain boundary are transformed into γ_i ; $i = 0, 1, 2$, respectively. The boundaries γ_1 , γ_2 , γ'_0 and γ''_0 are the inflow, the outflow and the impermeable parts of the boundary in the computational domain (see Figure 3.1).

$$\begin{aligned}\Gamma_1 &\rightarrow \gamma_1, & \Gamma_2 &\rightarrow \gamma_2, \\ \Gamma'_0 &\rightarrow \gamma'_0, & \Gamma''_0 &\rightarrow \gamma''_0.\end{aligned}$$

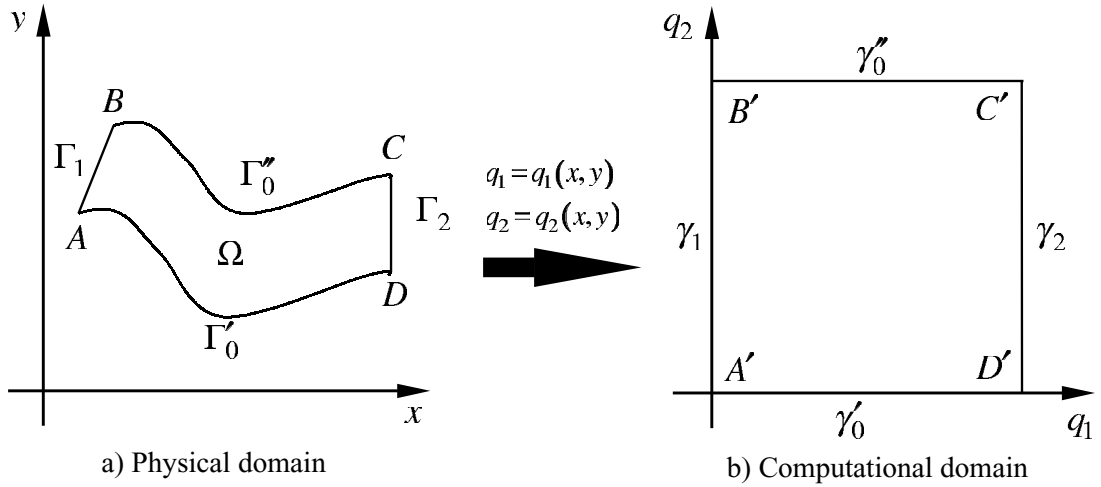


Figure 3.1: Physical and computational domain.

3.4 Relations between Metric and Differential Equations

Next, we will denote generalized curvilinear coordinates for (q_1, q_2) as (ξ_1, ξ_2) or (ξ, η) . The metric relations between $\frac{\partial x}{\partial \xi}$, $\frac{\partial x}{\partial \eta}$, $\frac{\partial y}{\partial \xi}$, $\frac{\partial y}{\partial \eta}$, and $\frac{\partial \xi}{\partial x}$, $\frac{\partial \xi}{\partial y}$, $\frac{\partial \eta}{\partial x}$, $\frac{\partial \eta}{\partial y}$ for transformation (3.3.1) are

$$\begin{bmatrix} \frac{\partial x}{\partial \xi} & \frac{\partial x}{\partial \eta} \\ \frac{\partial y}{\partial \xi} & \frac{\partial y}{\partial \eta} \end{bmatrix} \begin{bmatrix} \frac{\partial \xi}{\partial x} & \frac{\partial \xi}{\partial y} \\ \frac{\partial \eta}{\partial x} & \frac{\partial \eta}{\partial y} \end{bmatrix} = \begin{bmatrix} 1 & 0 \\ 0 & 1 \end{bmatrix},$$

or

$$\begin{aligned}\frac{\partial \xi}{\partial x} &= \frac{1}{J} y_\eta, & \frac{\partial \xi}{\partial y} &= -\frac{1}{J} x_\eta, \\ \frac{\partial \eta}{\partial x} &= -\frac{1}{J} y_\xi, & \frac{\partial \eta}{\partial y} &= \frac{1}{J} x_\xi,\end{aligned}\tag{3.4.1}$$

where the Jacobian J is

$$J = \frac{\partial(x, y)}{\partial(\xi, \eta)} = \begin{vmatrix} \frac{\partial x}{\partial \xi} & \frac{\partial x}{\partial \eta} \\ \frac{\partial y}{\partial \xi} & \frac{\partial y}{\partial \eta} \end{vmatrix}.$$

The metric tensor components are

$$\begin{aligned}g_{ij} &= \nabla \xi_i \cdot \nabla \xi_j \\ &= \nabla q_i \cdot \nabla q_j, \quad i, j = 1, 2,\end{aligned}$$

where

$$\nabla q_i = \left\{ \frac{\partial q_i}{\partial x_1}, \frac{\partial q_i}{\partial x_2} \right\}, \quad i = 1, 2.$$

The partial differential operators in (x, y) space can be rewritten to those in (ξ, η) space as follows

$$\begin{aligned}\frac{\partial(\cdot)}{\partial x_i} &= \frac{\partial q_j}{\partial x_i} \frac{\partial(\cdot)}{\partial q_j}, \quad i, j = 1, 2, \\ \nabla &= (\nabla \xi_j) \frac{\partial}{\partial \xi_j}.\end{aligned}$$

Here, we use Einstein's summation convention.

$$\begin{aligned}g_{11} &= \nabla q_1 \cdot \nabla q_1 = \left\{ \frac{\partial q_1}{\partial x_1} \right\}^2 + \left\{ \frac{\partial q_1}{\partial x_2} \right\}^2 \\ &= \frac{1}{J^2} \left[\left\{ \frac{\partial x_2}{\partial q_2} \right\}^2 + \left\{ \frac{\partial x_1}{\partial q_2} \right\}^2 \right], \\ g_{22} &= \nabla q_2 \cdot \nabla q_2 = \left\{ \frac{\partial q_2}{\partial x_1} \right\}^2 + \left\{ \frac{\partial q_2}{\partial x_2} \right\}^2 \\ &= \frac{1}{J^2} \left[\left\{ \frac{\partial x_1}{\partial q_1} \right\}^2 + \left\{ \frac{\partial x_2}{\partial q_1} \right\}^2 \right],\end{aligned}$$

$$\begin{aligned}
g_{12} &= \nabla_{q_1} \cdot \nabla_{q_2} = \left\{ \frac{\partial q_1}{\partial x_1}, \frac{\partial q_1}{\partial x_2} \right\} \cdot \left\{ \frac{\partial q_2}{\partial x_1}, \frac{\partial q_2}{\partial x_2} \right\} \\
&= \frac{\partial q_1}{\partial x_1} \frac{\partial q_2}{\partial x_1} + \frac{\partial q_1}{\partial x_2} \frac{\partial q_2}{\partial x_2} \\
&= -\frac{1}{J^2} \left[\frac{\partial x_2}{\partial q_2} \frac{\partial x_2}{\partial q_1} + \frac{\partial x_1}{\partial q_1} \frac{\partial x_1}{\partial q_2} \right].
\end{aligned}$$

The Poisson equation (3.2.7) can be rewritten into the generalized curvilinear coordinates as follows

$$\frac{\partial}{\partial q_1} \left(Jg_{11} \frac{\partial \psi}{\partial q_1} + Jg_{12} \frac{\partial \psi}{\partial q_2} \right) + \frac{\partial}{\partial q_2} \left(Jg_{21} \frac{\partial \psi}{\partial q_1} + Jg_{22} \frac{\partial \psi}{\partial q_2} \right) = -J\omega. \quad (3.4.2)$$

Using the notations $K_{11} = Jg_{11}$, $K_{12} = K_{21} = Jg_{12}$, $K_{22} = Jg_{22}$, we can rewrite equation (3.4.2) in the form

$$\frac{\partial}{\partial q_1} \left(K_{11} \frac{\partial \psi}{\partial q_1} + K_{12} \frac{\partial \psi}{\partial q_2} \right) + \frac{\partial}{\partial q_2} \left(K_{21} \frac{\partial \psi}{\partial q_1} + K_{22} \frac{\partial \psi}{\partial q_2} \right) = -J\omega. \quad (3.4.3)$$

Equation (3.2.6) in generalized curvilinear coordinates (ξ_1, ξ_2) takes the form

$$U_j \frac{\partial \omega}{\partial \xi_j} = 0; \quad j = 1, 2. \quad (3.4.4)$$

The contravariant velocity components U_j in equation (3.4.4) can be regarded as ξ_j - velocity components in (ξ, η) - space. They are

$$U_j = (\nabla \xi_j) \cdot \bar{u}, \quad \left(u_i = \left(\frac{\partial x_i}{\partial \xi_j} \right) U_j \right). \quad (3.4.5)$$

Utilizing the continuity equation

$$\frac{\partial}{\partial q_1} (J U_1) + \frac{\partial}{\partial q_2} (J U_2) = 0,$$

we can present equation (3.4.4) in the form

$$\frac{\partial}{\partial q_1} (J U_1 \omega) + \frac{\partial}{\partial q_2} (J U_2 \omega) = 0. \quad (3.4.6)$$

The contravariant velocity components U_j can be expressed in terms of derivatives of the stream function:

$$U_1 = \frac{1}{J} \frac{\partial \psi}{\partial q_2}, \quad U_2 = -\frac{1}{J} \frac{\partial \psi}{\partial q_1}. \quad (3.4.7)$$

To calculate the pressure, we use the Euler equations in the Gromeka–Lamb form. In generalized curvilinear coordinates, they are

$$J[g_{11} U_2 \omega - g_{12} U_1 \omega] = -g_{11} \frac{\partial H}{\partial q_1} - g_{12} \frac{\partial H}{\partial q_2},$$

$$J[g_{21}U_2\omega - g_{22}U_1\omega] = -g_{21}\frac{\partial H}{\partial q_1} - g_{22}\frac{\partial H}{\partial q_2}.$$

Solving these equations with respect to $\frac{\partial H}{\partial q_1}$ and $\frac{\partial H}{\partial q_2}$ as a linear algebraic system of equations, we get

$$\begin{aligned}\frac{\partial H}{\partial q_1} &= -J \omega U_2, \\ \frac{\partial H}{\partial q_2} &= J \omega U_1,\end{aligned}\tag{3.4.8}$$

where $H = p + |\bar{u}|^2/2$ is the total pressure and $|\bar{u}|^2 = (\bar{u} \cdot \bar{u})$ is square of the modulus of the velocity vector.

3.5 Discretization of the Equations and the Solution Procedure

We reformulate the boundary value problem (3.2.6)-(3.2.10) in terms of the generalized curvilinear coordinates (q_1, q_2) . The new reformulated boundary value problem then takes the form

$$\frac{\partial}{\partial q_1} \left(K_{11} \frac{\partial \psi}{\partial q_1} + K_{12} \frac{\partial \psi}{\partial q_2} \right) + \frac{\partial}{\partial q_2} \left(K_{21} \frac{\partial \psi}{\partial q_1} + K_{22} \frac{\partial \psi}{\partial q_2} \right) = -J \omega, \tag{3.5.1}$$

$$\frac{\partial}{\partial q_1} (J U_1 \omega) + \frac{\partial}{\partial q_2} (J U_2 \omega) = 0, \tag{3.5.2}$$

with boundary conditions on $\gamma_1, \gamma_2, \gamma'_0$ and γ''_0

$$\gamma'_0 : \quad \psi(q_1, 0) = 0;$$

$$\gamma''_0 : \quad \psi(q_1, 1) = c = \int_0^1 v_1(\tau) d\tau = \int_0^1 v_2(\tau) d\tau;$$

$$\gamma_1 : \quad \psi(0, q_2) = \int_0^{q_2} v_1(\tau) d\tau; \tag{3.5.3}$$

$$\omega(0, q_2) = g(q_2);$$

$$\gamma_2 : \quad \psi(x_d, q_2) = \int_0^{q_2} v_2(\tau) d\tau.$$

The approximated solution of problem (3.5.1)-(3.5.3) will be found by the iterative method. Let us take some initial approximations denoted by $\omega^0, \psi^0, \bar{u}^0$. Once $\omega^{(k-1)}, \psi^{(k-1)}, \bar{u}^{(k-1)}$; $k = 1, 2, \dots$ are known then in order to find $\omega^{(k)}, \psi^{(k)}, \bar{u}^{(k)}$, we must solve the following two problems:

a) Determine the stream function $\psi^{(k)}(q_1, q_2)$ by the vortex $\omega^{(k-1)}$ from the Poisson equation (3.5.1).

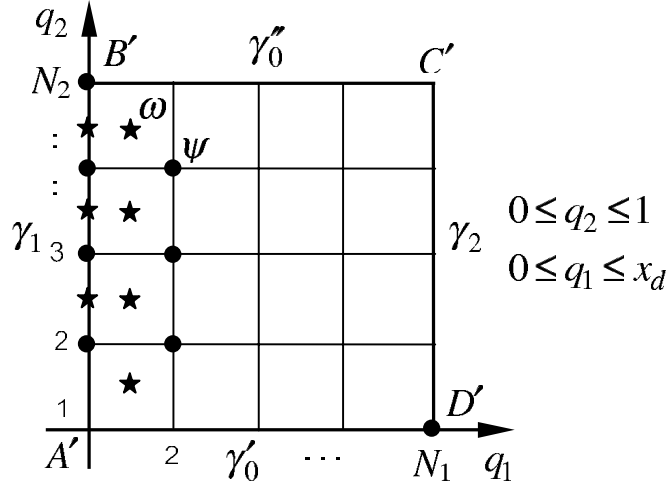


Figure 3.2: Computational domain.

b) Construct a vortex field $\omega^{(k)}(q_1, q_2)$ from the Helmholtz equation (3.5.2).

In the computational domain $A'B'C'D'$, we construct a uniform rectangular finite difference grid

$$\Omega_h = \left\{ [(q_1)_j, (q_2)_i], (q_1)_j = (j-1) * h_1, (q_2)_i = (i-1) * h_2, \right. \\ \left. i = 1, \dots, N_2; j = 1, \dots, N_1, h_1 = 1/(N_1 - 1), h_2 = 1/(N_2 - 1) \right\}.$$

The values of the stream function are approximated at the grid points. The values of the vorticity are referred at the middle of each computational cells. At the inflow boundary $q_1 = 0$, the vorticity are evaluated at the middle point between grid nodes, (see Figure 3.2).

To find approximated solution of the Poisson equation (3.5.1), we can either utilize the SOR or the Stabilizing Correction method.

The formulas of the SOR method are

$$\begin{aligned} & \frac{1}{h_1^2} \left((K_{11})_{i,j+1/2} (\psi_{i,j+1} - \psi_{i,j}) - (K_{11})_{i,j-1/2} (\psi_{i,j} - \psi_{i,j-1}) \right) + \\ & + \frac{1}{h_2^2} \left((K_{22})_{i+1/2,j} (\psi_{i+1,j} - \psi_{i,j}) - (K_{22})_{i-1/2,j} (\psi_{i,j} - \psi_{i-1,j}) \right) + \\ & + \left\{ \frac{1}{h_1 h_2} \left((K_{12})_{i,j+1/2} (\psi_{i+1/2,j+1/2} - \psi_{i-1/2,j+1/2}) - \right. \right. \\ & \quad \left. \left. - (K_{12})_{i,j-1/2} (\psi_{i+1/2,j-1/2} - \psi_{i-1/2,j-1/2}) \right) + \right. \\ & \quad \left. + \frac{1}{h_1 h_2} \left((K_{21})_{i+1/2,j} (\psi_{i+1/2,j+1/2} - \psi_{i+1/2,j-1/2}) - \right. \right. \\ & \quad \left. \left. - (K_{21})_{i-1/2,j} (\psi_{i-1/2,j+1/2} - \psi_{i-1/2,j-1/2}) \right) \right\} = -J_{ij} \omega_{ij}, \\ & \quad i = 2, \dots, N_2 - 1; j = 2, \dots, N_1 - 1, \end{aligned} \quad (3.5.4)$$

where

$$\begin{aligned}\omega_{ij} &= 0.25(\omega_{i+1/2,j+1/2} + \omega_{i+1/2,j-1/2} + \omega_{i-1/2,j-1/2} + \omega_{i-1/2,j+1/2}), \\ \psi_{i+1/2,j+1/2} &= 0.25(\psi_{i+1,j+1} + \psi_{i,j+1} + \psi_{i+1,j} + \psi_{i,j}), \\ \psi_{i-1/2,j+1/2} &= 0.25(\psi_{i,j+1} + \psi_{i-1,j+1} + \psi_{i,j+1} + \psi_{i-1,j}).\end{aligned}$$

Utilizing the Gauss–Seidel method, we get

$$\begin{aligned}\left\{ \frac{(K_{11})_{i,j+1/2} + (K_{11})_{i,j-1/2}}{h_1^2} + \frac{(K_{22})_{i+1/2,j} + (K_{22})_{i-1/2,j}}{h_2^2} \right\} \tilde{\psi}_{ij} &= \\ &= \frac{(K_{11})_{i,j+1/2} \psi_{i,j+1}^{(k,s-1)} + (K_{11})_{i,j-1/2} \tilde{\psi}_{i,j-1}}{h_1^2} + \\ &+ \frac{(K_{22})_{i+1/2,j} \psi_{i+1,j}^{(k,s-1)} + (K_{22})_{i-1/2,j} \tilde{\psi}_{i-1,j}}{h_2^2} + \\ &+ \{ \dots \}^{(k,s-1)} + J_{ij} \omega_{ij}^{(k-1)},\end{aligned}$$

where the expression in the curl brackets corresponds to the expression in the curl brackets in formula (3.5.4), $\tilde{\psi}_{ij}$ are intermediate values of the stream function at grid points. As an initial guess, for $s = 1$, we set $\psi_{ij}^{(k,0)} = \psi_{ij}^{(k-1)}$. The values, $\psi_{ij}^{(k,S)}$ are defined as

$$\psi_{ij}^{(k,S)} = \omega \tilde{\psi}_{ij} + (1 - \omega) \psi_{ij}^{(k,s-1)}, \quad s = 1, 2, \dots, S,$$

where ω is the over relaxation parameter. If the following convergence criteria

$$\left\| \psi_{ij}^{(k,S)} - \psi_{ij}^{(k,S-1)} \right\| \leq \varepsilon,$$

is satisfied, we set $\psi^{(k)} = \psi^{(k,S)}$.

The Stabilizing Correction method consists of two steps:

The first step: We utilize the implicit approximation of partial derivative in q_1 -direction

$$\begin{aligned}\frac{\tilde{\psi}_{ij} - \psi_{ij}^{(k,s-1)}}{\Delta t} &= \left[\frac{\partial}{\partial q_1} K_{11} \frac{\partial \tilde{\psi}}{\partial q_1} \right]_{ij}^h + \left[\frac{\partial}{\partial q_2} K_{22} \frac{\partial \psi^{(k,s-1)}}{\partial q_2} \right]_{ij}^h + \\ &+ \left[\frac{\partial}{\partial q_1} K_{12} \frac{\partial \psi^{(k,s-1)}}{\partial q_2} \right]_{ij}^h + \left[\frac{\partial}{\partial q_2} K_{21} \frac{\partial \psi^{(k,s-1)}}{\partial q_1} \right]_{ij}^h + J_{ij} \omega_{ij}^{(k-1)}, \\ &i = 2, \dots, N_2 - 1; \quad j = 2, \dots, N_1 - 1.\end{aligned}$$

To approximate the partial derivatives in the square brackets, we apply the central second order finite differences. The resulting tridiagonal system of equation is then solved by the ‘‘Sweep method’’ (see for example N. N. Yanenko (1971))

The second step: This step is a correction step and it helps to improve the stability.

$$\frac{\psi_{ij}^{(k,s)} - \tilde{\psi}_{ij}}{\Delta t} = \left[\frac{\partial}{\partial q_2} K_{22} \frac{\partial \psi^{(k,s)}}{\partial q_2} \right]_{ij}^h - \left[\frac{\partial}{\partial q_2} K_{22} \frac{\partial \psi^{(k,s-1)}}{\partial q_2} \right]_{ij}^h,$$

$$i = 2, \dots, N_2 - 1; j = 2, \dots, N_1 - 1; s = 1, 2, \dots, S.$$

If the following convergence criteria

$$\left\| \psi_{ij}^{(k,S)} - \psi_{ij}^{(k,S-1)} \right\| \leq \varepsilon,$$

is satisfied, we set $\psi_{ij}^{(k)} = \psi_{ij}^{(k,S)}$

The integral method is utilized to construct the finite difference equations for the vorticity. The equivalent integral form of equation (3.5.2) is

$$\oint_C (J U_1 \omega dq_2 - J U_2 \omega dq_1) \equiv 0,$$

where C denotes a closed curve which is homeomorphic to a circle. The contour integral is evaluated with respect to the computational cell with a middle point $((q_1)_{i+1/2, j+1/2}, (q_2)_{i+1/2, j+1/2})$ (see Figure 3.3).

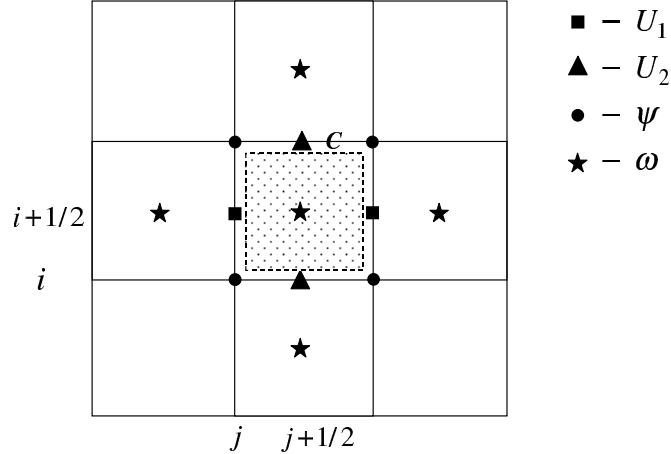


Figure 3.3: Stencil of the finite-difference equation for ω .

The mean value theorem is used to evaluate the integral with respect to cell's sides. To represent the net flow of the vorticity through the cell's sides, we take into account the sign of the contravariant components of the velocity vector U_1 and U_2 . In general, values of the vorticity are determined from the finite difference equations

$$\Lambda_1 \omega_{i+1/2, j+1/2} + \Lambda_2 \omega_{i+1/2, j+1/2} = 0, \quad (3.5.5)$$

where

$$\begin{aligned}\Lambda_1 \omega_{i+1/2, j+1/2} &= \frac{1}{h_1} \left[(JU_1 \omega)_{i+1/2, j+1} - (JU_1 \omega)_{i+1/2, j} \right], \\ \Lambda_2 \omega_{i+1/2, j+1/2} &= \frac{1}{h_2} \left[(JU_2 \omega)_{i+1, j+1/2} - (JU_2 \omega)_{i, j+1/2} \right], \\ \omega_{i+1/2, j} &= \begin{cases} \omega_{i+1/2, j-1/2}, & U_{1, i+1/2, j} \geq 0 \\ \omega_{i+1/2, j+1/2}, & U_{1, i+1/2, j} < 0, \end{cases} \\ \omega_{i, j+1/2} &= \begin{cases} \omega_{i+1/2, j+1/2}, & U_{2, i, j+1/2} < 0 \\ \omega_{i-1/2, j+1/2}, & U_{2, i, j+1/2} \geq 0 \end{cases}.\end{aligned}$$

It is easy to see that if we know the values of the vorticity at the grid points on the inflow part of the domain boundary then we can use the finite difference equation (3.5.5) to find the values of the vorticity at the middle point of each cell in the computational domain Ω_h .

3.6 Convergence, Results and Discussions

The solution of boundary value problem (3.5.1)-(3.5.3) in a channel with the curved walls are obtained by the finite difference scheme presented in section 3.5.

3.6.1 Euler Equations with Exact Solution

In this section, we obtain the numerical solution for the test problem by using the finite difference scheme presented in section 3.5. The test problem with analytical solution is chosen, and then we perform a rigorous comparison of approximate and exact solutions.

To construct a test problem with the known solution, we use the results of G.V. Alekseev and Yu.A. Mokin (1972). They studied the steady two-dimensional flow of homogenous incompressible ideal fluid. The flow domain Ω is a plane channel $A_1 A_2 A_3 A_4$ with one curved wall $A_1 A_4$ (see Figure 3.4). They discovered the set of solutions of the Euler equations for essentially vortical flow. The function $f(x)$ is a solution of

$$\frac{d^2 f(x)}{dx^2} = c f(x), \quad (3.6.1)$$

where c is an arbitrary constant and $f(x) > 0$, $x \in [0, a]$, $f(0) = b$. Additionally, the function $f(x)$ has to be three times continuously differentiable and satisfies the requirement

$$f(x) \cdot \frac{d^2 f(x)}{dx^2} - \left(\frac{df(x)}{dx} \right)^2 = c_1 < 1, \quad (3.6.2)$$

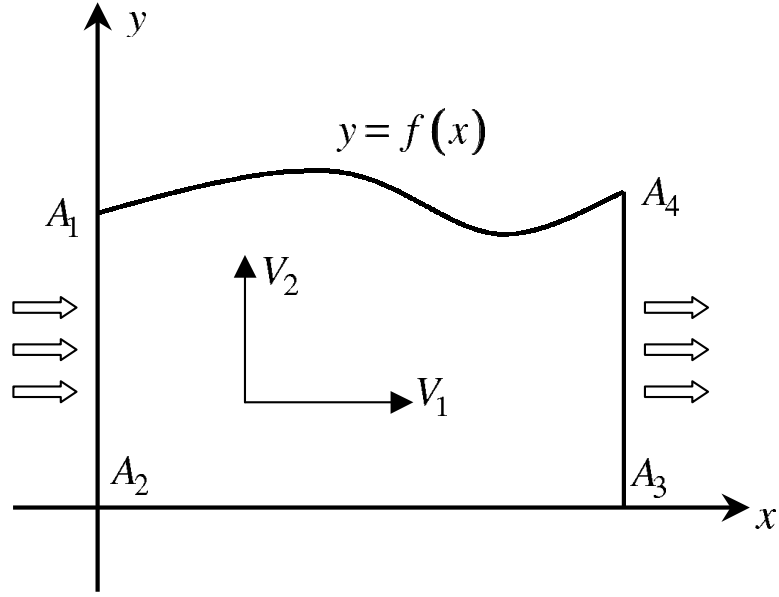


Figure 3.4: Flow domain of the test problem.

where c_1 is a constant. For an arbitrary constant $c_2 > 0$, the solution of the Euler equations has a form

$$\begin{aligned} v_1(x, y) &= \frac{c_2 f(x)}{f^2(x) - c_1 y^2}; \\ v_2(x, y) &= \frac{c_2 y f'(x)}{f^2(x) - c_1 y^2}; \\ P(x, y) &= P_0 - \frac{\rho c_2^2}{2(f^2(x) - c_1 y^2)}, \end{aligned} \quad (3.6.3)$$

where P_0 is an arbitrary constant. From formulas (3.6.3), we can find the vorticity and the Bernoulli function,

$$\begin{aligned} \omega(x, y) &= -cc_2 y f(x) \frac{f^2(x) + c_1 y^2}{(f^2(x) - c_1 y^2)^2}, \\ H(x, y) &= \frac{P_0}{\rho} + cc_2^2 \frac{y^2 f^2(x)}{2(f^2(x) - c_1 y^2)^2}. \end{aligned}$$

If $c_1 = -\sigma^2 < 0$ then, by using equation (3.6.3), it is easy to find formulas for the stream function and vorticity,

$$\begin{aligned} \psi(x, y) &= \frac{c_2}{\sigma} \arctan \frac{\sigma y}{f(x)}, \\ \Delta \psi &= -\frac{cc_2}{4\sigma} \sin \left(\frac{4\sigma}{c_2} \psi \right). \end{aligned}$$

The general solution of equation (3.6.1) for $c < 0$ is

$$f(x) = K_1 e^{i\sqrt{c}x} + K_2 e^{-i\sqrt{c}x},$$

where $i^2 = -1$ and constants K_1 and K_2 have to be real and satisfy the nonlinear system

$$\begin{aligned} -4cK_1K_2 &= c_1, \\ K_1 + K_2 &= b. \end{aligned}$$

In a particular case where

$$c = -\left(\frac{\sigma}{b}\right)^2,$$

it follows that

$$f(x) = b \cos \frac{|\sigma|}{b}x, \quad x \in \left[0, \frac{\pi}{2} \frac{b}{|\sigma|}\right]. \quad (3.6.4)$$

We consider the test problem with parameters

$$\sigma = 1, \quad a = 0.5, \quad b = 1, \quad c_2 = 4.$$

For this set of parameters, the analytical solution of the Euler equations is

$$\begin{aligned} f(x) &= \cos(x), \\ \psi(x, y) &= 4 \arctan \left(\frac{y}{\cos(x)} \right), \\ \omega(x, y) &= \sin(\psi(x, y)). \end{aligned} \quad (3.6.5)$$

If $0 < c_1 = \sigma^2 < 1$ then, by using equation (3.6.3), it is easy to find formulas for the stream function and vorticity,

$$\psi(x, y) = \frac{c_2}{2\sigma} \ln \frac{f(x) + \sigma y}{f(x) - \sigma y}, \quad (3.6.6)$$

$$\Delta\psi = \frac{cc_2}{4\sigma} \sinh \left(\frac{4\sigma}{c_2} \psi \right). \quad (3.6.7)$$

The general solution of equation (3.6.1) for $c > 0$ is

$$f(x) = K_1 e^{\sqrt{cx}} + K_2 e^{-\sqrt{cx}}, \quad (3.6.8)$$

where the constants K_1 and K_2 have to satisfy the following system

$$\begin{aligned} K_1 + K_2 &= b, \\ 4cK_1K_2 &= c_1. \end{aligned}$$

In a particular case where

$$b^2 = \frac{\sigma^2}{c},$$

it follows that

$$f(x) = b \cosh(\sqrt{cx}), \quad x \in [0, a].$$

We consider the second test problem with parameters

$$\sigma = 0.5, \quad a = 1, \quad b = 1, \quad c_2 = 1, \quad c = c_1 = \sigma^2 = 0.25.$$

For this set of parameters, the analytical solution (3.6.6),(3.6.7) and (3.6.8) of the Euler equations is the following

$$\begin{aligned} f(x) &= \cosh(0.5x), \\ \psi(x, y) &= \ln \left(\frac{\cosh(0.5x) + 0.5y}{\cosh(0.5x) - 0.5y} \right), \\ \omega(x, y) &= 0.125 \sinh(2\psi(x, y)). \end{aligned} \quad (3.6.9)$$

The algorithm developed in section 3.5 is then implemented to these test problems. Table 3.1 and 3.2 show the infinity norm of absolute errors which are obtained from the grid systems having $N1 \times N1$ nodes. With these values, the resulting rate of convergence is estimated. The rate of convergence is defined as follows:

$$m = \frac{1}{\ln 2} \ln \left(\frac{err1}{err2} \right),$$

where *err1* and *err2* are errors which correspond to grid systems with $N1 \times N1$ and $N2 \times N2$ nodes, respectively. It is observed that the convergence rate is approximately equal to two. This confirms that finite difference scheme developed in section 3.5, is of second-order accuracy.

Table 3.1: Absolute errors of stream function and vorticity and rate of convergence for test problem (3.6.5).

| Grid | ψ -error $\times 10^5$ | Rate | ω -error $\times 10^5$ | Rate |
|----------------|-----------------------------|------|-------------------------------|--------|
| 11 \times 11 | 5.5261 | – | 4.7549 | – |
| 21 \times 21 | 1.0365 | 2.41 | 1.2056 | 1.9797 |
| 41 \times 41 | 0.2590 | 2.00 | 0.3167 | 1.9287 |

Table 3.2: Absolute errors of stream function and vorticity and rate of convergence for test problem (3.6.9).

| Grid | ψ -error $\times 10^5$ | Rate | ω -error $\times 10^5$ | Rate |
|----------------|-----------------------------|------|-------------------------------|------|
| 11 \times 11 | 2.8226 | – | 1.6577 | – |
| 21 \times 21 | 0.3962 | 2.83 | 0.2842 | 2.54 |
| 41 \times 41 | 0.1031 | 1.94 | 0.1067 | 1.41 |

Figures (3.5)-(3.10) illustrate the distribution of the pressure field for two geometries of channel. Which are given by (3.6.5) and (3.6.9).

Figures (3.5) and (3.6) present the pressure contours in a physical domain. Solid lines correspond to numerical solution and dashed lines corresponds to analytical solution given by equations (3.6.3).

The pressure along the lower boundary as a function of x is shown in figure (3.7) and (3.8). The solid line corresponds to numerical solution and analytical solution corresponds to circle signs.

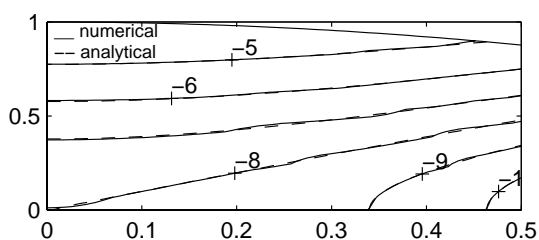


Figure 3.5: Pressure contours for solution (3.6.5)

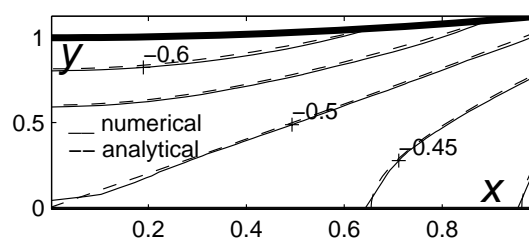


Figure 3.6: Pressure contours for solution (3.6.9)

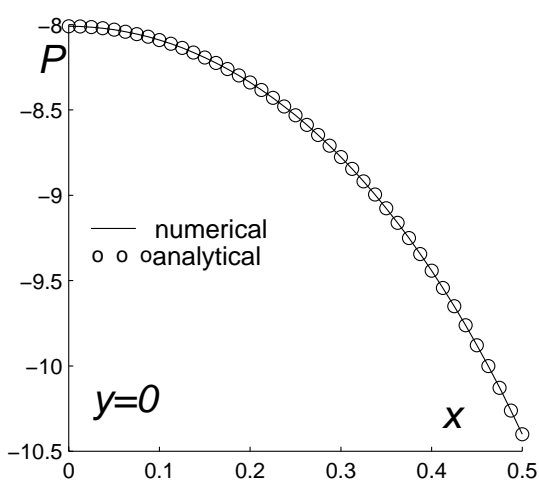


Figure 3.7: Pressure along lower boundary for solution (3.6.5)

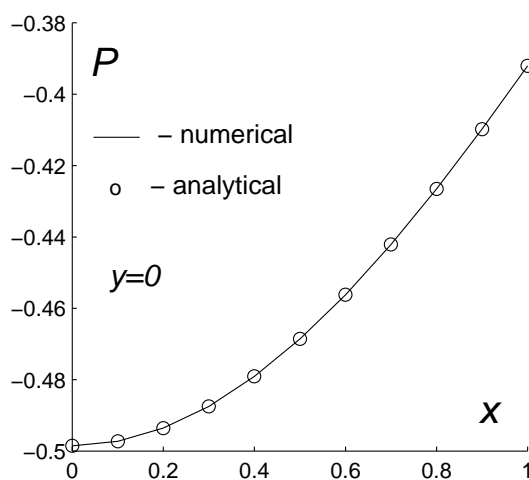


Figure 3.8: Pressure along lower boundary for solution (3.6.9)

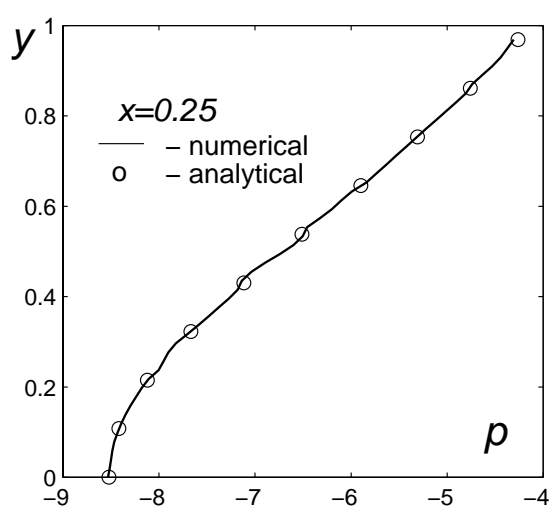


Figure 3.9: Pressure along section $x = 0.25$ for solution (3.6.5)

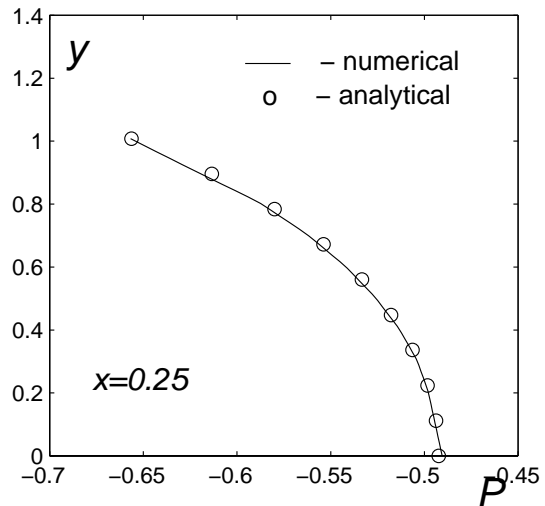


Figure 3.10: Pressure along section $x = 0.25$ for solution (3.6.9)

Figures (3.9) and (3.10) illustrate the pressure at the section $x = 0.25$. The solid line corresponds to numerical solution and analytical solution corresponds to circle signs.

To find the solution which corresponds to analytical solution (3.6.5), we use an uniform grid of 41×41 nodes. In the case of analytical solution (3.6.9), we use grid with 11×11 nodes. It is observed the very good agreement between computational and analytical solutions.

3.6.2 Flowing Through a Channel with Curved Walls

The numerical method developed in section 3.5 will now be applied to study an internal flow of an ideal incompressible fluid in a two-dimensional channel with curved walls.

3.6.2.1 Geometry of Channel and Boundary Conditions

The channel geometry and boundary conditions are shown in Figure 3.11. The equations of the impermeable walls Γ'_0 , Γ''_0 are

$$y_\alpha(x) = \begin{cases} y_\alpha & ; & x < x\alpha_1, \\ y_\alpha + h_\alpha [1 + \sin z(x)] & ; & x\alpha_1 \leq x \leq x\alpha_2, \\ y_\alpha & ; & x > x\alpha_2, \end{cases}$$

where $\alpha = d$ in the case of lower boundary and $\alpha = t$ in the case of the top boundary of channel. The function $z(x)$ is defined by the equation

$$z(x) = \frac{\pi}{2(x\alpha_2 - x\alpha_1)} [2(K_\alpha + 1)x - (2K_\alpha + 1)x\alpha_1 - x\alpha_2], \quad K_\alpha = 1, 3, 5, \dots \quad (3.6.10)$$

The numbers of troughs and crests of boundary in the interval $(x\alpha_1, x\alpha_2)$ will be determined by the choice of K_α in equation (3.6.10). The value h_α determines the vertical sizes of troughs and crests. The normal component of the velocity vector and vorticity are specified at the inflow part of boundary γ_1 :

$$\text{a) } U_{1in}(y) = C_{in} = \text{const}, \quad (3.6.11)$$

$$\omega_{in}(y) = a_\omega \sin\left(K \frac{y - y_d}{y_t - y_d} \pi\right); \quad K = 1, 2, \dots \quad (3.6.12)$$

$$\text{b) } U_{1in}(y) = C_{in}(y - y_d)(y_t - y), \quad (3.6.13)$$

$$\omega_{in}(y) = a_\omega \sin\left(K \frac{y - y_d}{y_t - y_d} \pi + \varphi\right). \quad (3.6.14)$$

The impermeable boundaries, γ'_0 and γ''_0 are enforced by condition $\bar{u} \cdot \bar{n} = 0$. The parameters C_{in} , K and φ are chosen such that the consistency of boundary conditions holds

$$\omega_{in}(y_d) = - \left. \frac{\partial U_1}{\partial y} \right|_{y=y_d}; \quad \omega_{in}(y_t) = - \left. \frac{\partial U_1}{\partial y} \right|_{y=y_t},$$

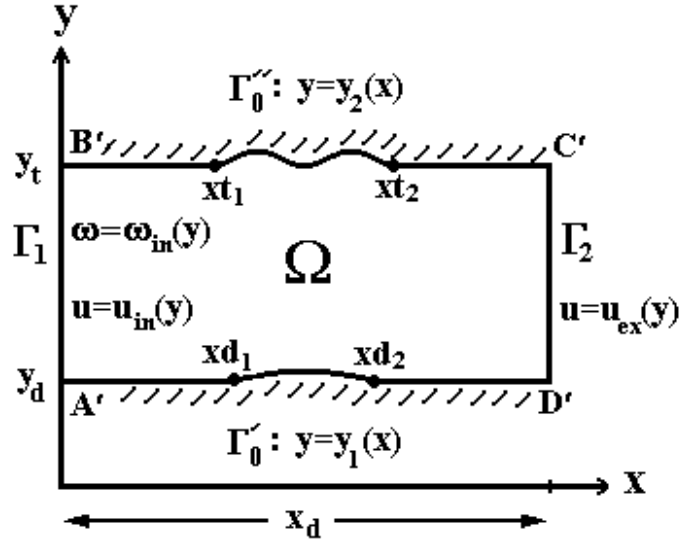


Figure 3.11: Sketch of channel with curved walls.

The normal component of the velocity vector is specified at the outflow part boundary γ_2 :

- a) $U_{1out}(y) = C_{out} = \text{const}$,
- b) $U_{1out}(y) = C_{out}(y - y_d)(y_t - y)$.

3.6.2.2 Estimation of Errors of Finite Difference Method

A criterion for assessing the quality of a numerical method is a theoretical error estimate of the form:

There exist a positive constant h_0 , $C = C(h_0)$ and $m = m(h_0)$, all are independent of h , such that for all $h \leq h_0$

$$\|u^h - P_h(u)\|_{\Omega_h} \leq Ch^m, \quad (3.6.15)$$

where $P_h(u)$ is a projection of the exact solution of the differential problem onto a set of grid functions given on Ω_h , u^h is a solution of a finite difference scheme on the mesh Ω_h and h is a parameter of grid Ω_h . In case of $h \rightarrow 0$, it means that the distance between two neighboring grid points tends to zero.

Numerical methods are usually applied to problems for which the exact solution is unknown, which is the usual situation. This means that the error, $u^h - P_h(u)$, in the numerical solution, u^h , can not be determined directly, and therefore an indirect estimate of its magnitude has to be used. We follow the results of J. Miller *et al.* (1996) and use two algorithms to estimate C and m in equation (3.6.15).

The first algorithm is useful in a case when two numerical solutions can be computed on two different grids. It is assumed that the order of convergence

is known to be approximately m . The algorithm then provides an approximate value for the error constant C . Let u denote the exact solution of the problem and $h \in R^h$, $R^h = \{h : \underline{h} \leq h \leq \bar{h}\}$, R^h is the range of h in which numerical solution can be computed. Choose any convenient value h_1 such that $h_1, h_1/4 \in R^h$. The first step is to use the numerical method to compute the two numerical solutions of the problem for the two grids Ω_{h_1} and $\Omega_{h_1/4}$. Denoting these approximate solutions by u^{h_1} and $u^{\frac{h_1}{4}}$ respectively, we compute the norm of difference on the grid Ω_{h_1} between u^{h_1} and the linear interpolant $\tilde{u}^{\frac{h_1}{4}}$, namely

$$D = \|u^{h_1} - \tilde{u}^{\frac{h_1}{4}}\|_{\Omega_{h_1}} = \max_{i,j \in \Omega_{h_1}} |u_{ij}^{h_1} - \tilde{u}_{ij}^{\frac{h_1}{4}}|. \quad (3.6.16)$$

Using the triangle inequality and equation (3.6.16), we obtain

$$D \geq \|u^{h_1} - u\|_{\Omega_{h_1}} - \|\tilde{u}^{\frac{h_1}{4}} - u\|_{\Omega_{h_1}} \geq \|u^{h_1} - u\|_{\Omega_{h_1}} - C_m \left(\frac{h_1}{4}\right)^m \approx C_m(1 - 4^{-m})h_1^m.$$

We can set

$$C_m^* = \frac{Dh_1^{-m}}{1 - 4^{-m}}, \quad (3.6.17)$$

to be the computed approximation to the unknown error constant.

The second algorithm is useful in a case where three numerical solutions can be computed on three different grids. It provides us with approximations of both the order of convergence m and the error constant C_m . A computed estimate of m is obtained the first by computing the three numerical solutions u^{h_1} , $u^{\frac{h_1}{2}}$ and $u^{\frac{h_1}{4}}$ on the grid Ω_{h_1} , $\Omega_{\frac{h_1}{2}}$ and $\Omega_{\frac{h_1}{4}}$ respectively, where h_1 is chosen so that $\frac{h_1}{2}, \frac{h_1}{4} \in R^h$. Let $\tilde{u}^{\frac{h_1}{2}}, \tilde{u}^{\frac{h_1}{4}}$ denote the piecewise linear interpolation of $u^{\frac{h_1}{2}}, u^{\frac{h_1}{4}}$ on Ω_{h_1} . We compute the norms of differences

$$D_1 = \|u^{h_1} - \tilde{u}^{\frac{h_1}{2}}\|_{\Omega_{h_1}}, \quad D_2 = \|\tilde{u}^{\frac{h_1}{2}} - \tilde{u}^{\frac{h_1}{4}}\|_{\Omega_{\frac{h_1}{2}}}, \quad D = \|\tilde{u}^{\frac{h_1}{2}} - \tilde{u}^{\frac{h_1}{4}}\|_{\Omega_{h_1}},$$

on the appropriate grids. Using the triangle inequality, equation (3.6.15), we obtain

$$\frac{D_1}{D_2} \approx \frac{Ch_1^m(1 - 2^{-m})}{C\left(\frac{h_1}{2}\right)^m(1 - 2^{-m})} \approx 2^m.$$

We can set

$$m^* = \log_2 \frac{D_1}{D_2},$$

to be the computed approximation to the unknown value of the order of convergence. Using this computed value of m and the above value of D , we apply the previous algorithm to obtain from equation (3.6.17) the computed approximation

$$C_{m^*}^* = \frac{Dh_1^{-m^*}}{1 - 4^{-m^*}}. \quad (3.6.18)$$

Table 3.3: Computed error parameters, sensitivity.

| | $\ \circ\ _\infty$ for ω | $\ \circ\ _{L_2}$ for ω | $\ \circ\ _\infty$ for Ψ | $\ \circ\ _{L_2}$ for Ψ |
|---------|---------------------------------|--------------------------------|-------------------------------|------------------------------|
| D | 0.072670 | 0.106638 | 0.004000 | 0.005258 |
| D_1 | 0.043100 | 0.064757 | 0.003200 | 0.004258 |
| D_2 | 0.032598 | 0.058317 | 0.000900 | 0.001510 |
| m^* | 0.402927 | 0.151116 | 1.830075 | 1.495407 |
| C^* | 0.567747 | 0.887257 | 1.044313 | 0.530618 |
| C_1^* | 0.591400 | 1.024007 | 1.070421 | 0.582140 |
| C_2^* | 0.591400 | 1.024007 | 1.070421 | 0.582140 |

Without computing further numerical solutions of the problem, it is now possible to test the sensitivity, relative to changes in h , of the computed error constant $C_{m^*}^*$. Using the analogous argument to the one which is used to obtain equation (3.6.17) from equation (3.6.15), we see that each of the quantities

$$C_1^* = \frac{D_1 h_1^{-m^*}}{1 - 2^{-m^*}} \quad \text{or} \quad C_2^* = \frac{D_2 (h_1/2)^{-m^*}}{1 - 2^{-m^*}},$$

may be taken as computed approximates to the error constant. The values C_1^* or C_2^* may not be close to the value $C_{m^*}^*$ in equation (3.6.18), but if $C_1^* \approx C_{m^*}^*$ or $C_2^* \approx C_{m^*}^*$ then it can be concluded, that m^* and $C_{m^*}^*$ are insensitive to variations in h between h_1 and $h_1/4$.

We now use these two algorithms to find approximations to the error parameters m and C for finite difference scheme applied to the “flowing-through” problem. We choose $h_1 = 5 \cdot 10^{-2}$ (grid in computational domain consists of 21×21 grid points in both directions q_1 and q_2). To estimate the quantities D , D_1 , D_2 , we will use discrete analogues of L_2 and infinity norms

$$\|u^h - u^{\frac{h_1}{4}}\|_{L_2} = \left(\sum_{i,j \in \Omega_h} h \left(u_{ij}^h - \tilde{u}_{ij}^{h/4} \right)^2 \right)^{1/2}, \quad \|u^h - u^{\frac{h_1}{2}}\|_\infty = \max_{i,j \in \Omega_h} \left| u_{ij}^h - \tilde{u}_{ij}^{h/2} \right|.$$

The algorithm developed in section 3.5 is then implemented to the equations(3.5.1) and (3.5.2) with boundary conditions (3.6.11)-(3.6.12). The results of our computations are summarized in Table 3.3. The geometry of the channel is determined by the values of parametrs $y_d = 0$, $y_t = 1$, $xt_1 = xd_1 = 1$, $xt_2 = xd_2 = 2$, $xd = 3$, $h_d = 0.01$ and $K_d = 1$. In Table 3.3, we analyze the data for boundary conditions (3.6.1) and (3.6.2) with parameters $U_{in}(y) = 1$, $a_\omega = 0.1$ and $K = 1$. The first column of the table refers to the quantities whose computed values are shown in the corresponding rows.

The results obtained with four uniform grids Ω_{h_1} , $\Omega_{h_1/2}$, $\Omega_{h_1/4}$, $\Omega_{h_1/8}$ for the pressure distribution at the line $x = 1.5$ are shown in Figure 3.12. We can see that all four curves are close to each other. The analysis of results in Table

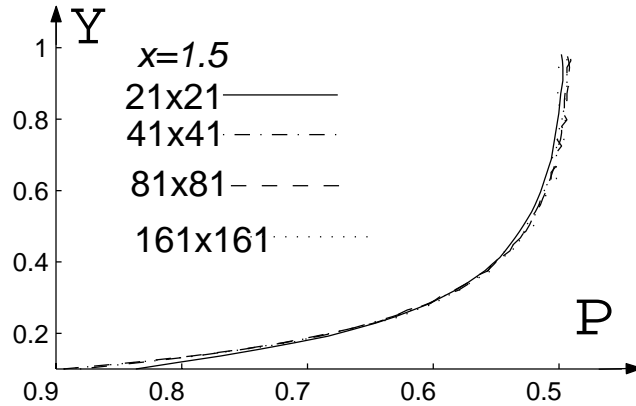


Figure 3.12: Pressure at line $x = 1.5$. Numerical solutions computed on four grids with $h_1 = 1/20$, $h_2 = h_1/2$, $h_3 = h_1/4$, $h_4 = h_1/8$.

3.3 and Figure 3.12 illustrates the convergence of the finite difference method under consideration.

3.6.2.3 Numerical Results

Figures 3.13-3.36 illustrate the distribution of the pressure field and the streamlines for varied geometries of channel and boundary conditions. Figures 3.13-3.24 illustrate the computation results for channel with straight upper wall. Geometry of the lower wall is chosen so that the relative height of contraction h_d , between $x_{d1} \leq x \leq x_{d2}$, is 0.1. Total length of channel x_d is 3.0. To find the solution, we use a uniform grid of 81×81 nodes. In each case, the iterative process converges with tolerance $\varepsilon_\omega = 10^{-6}$, $\varepsilon_\psi = 10^{-6}$. Figures 3.13-3.18 present the pressure contours in a physical domain. Boundary conditions for vorticity at the inflow part of boundary are prescribed by equation

$$\omega(y) = a_\omega \sin(Ky\pi). \quad (3.6.19)$$

Figure 3.13 corresponds to the potential flow (the vorticity at the inflow boundary is vanish, $a_\omega = 0$). Figure 3.14 corresponds to the case $a_\omega = 0.1$, $K = 1.0$. Oscillations of pressure contours on Figures 3.13 and 3.14 occur due to the interpolation program in MATLAB. Figure 3.15 corresponds to the case $a_\omega = 1.0$, $K = 1.0$. Figure 3.16 corresponds to the case $a_\omega = 1.0$, $K = 2.0$. In this last case, we have positive and negative values of the vorticity at entrance. Figure 3.17 corresponds to the case $a_\omega = 5.0$, $K = 1.0$. Figure 3.18 corresponds to the case $a_\omega = 5.0$, $K = 2.0$. The levels of isolines (or isobars) in each figure are labelled by vector v . In Figures 3.17 and 3.18, only seven isolines which are equally distributed between maximal and minimal values of the pressure field are drawn.

Figures 3.19 and 3.20 illustrate the streamlines (or trajectories) of fluid flow for two particular cases of boundary conditions for the vorticity at the inflow part of the domain boundary. Figure 3.19 corresponds to the case $a_\omega = 5.0, K = 1.0$ and Figure 3.20 corresponds to the case $a_\omega = 5.0, K = 2.0$. It is clear that nonzero value of vorticity at entrance corresponds to nonzero angle between the direction of inlet velocity vector and the direction of Ox axis.

The pressure along a lower boundary as a function of x is shown in Figures 3.21 and 3.22. Figure 3.21 corresponds to the case $K = 1.0$ and $a_\omega = 0; 0.1; 1.0$ and the results for the case the case $a_\omega = 0$ are plotted by the dash-dotted line. The dashed line in Figure 3.21 represents the pressure for the case $a_\omega = 0.1$. The solid line in Figure 3.21 represents the pressure for the case $a_\omega = 1.0$. The absolute values of the pressure peaks near the points $x = 1.0, x = 1.5$, and $x = 2.0$ increase together with increasing magnitude a_ω , of the vorticity given at the entrance. Figure 3.22 shows the pressure along the lower boundary for two cases corresponding to $a_\omega = 1.0, K = 1.0$ and $a_\omega = 1.0, K = 2.0$. We can see the increase in the pressure peaks near the points $x = 1.0, x = 1.5$, and $x = 2.0$ with increasing values of the parameter K , from 1.0 to 2.0.

Figures 3.23 and 3.24 illustrate the behavior of the pressure at the section $x = 1.5$ for different boundary conditions for the vorticity. Figure 3.23 illustrates the function

$$P = P(x, y)|_{x=1.5}, \quad (3.6.20)$$

for three different values of a_ω and $K = 1.0$ in equation (3.6.19). The solid line in Figure 3.23 corresponding to the case $a_\omega = 0$ represents the case of potential flow of an ideal incompressible fluid. The dashed line represents the function (3.6.20) for the case $a_\omega = 0.1$. The dash-dotted line shows the result for the case $a_\omega = 1.0$. In the case $a_\omega = 1.0$ function (3.6.20) has a local extreme at the middle of channel, $0.4 \leq x \leq 0.6$. In Figure 3.24, we represent function (3.6.20) for the case $a_\omega = 1.0, K = 1.0; 2.0$. In the case $K = 2.0$, we can observe two local maximums in the intervals $0.3 \leq y \leq 0.45$, $0.85 \leq y \leq 0.95$ and a local minimum in the intervals $0.5 \leq y \leq 0.7$ where the vorticity sign changes.

Figures 3.25-3.36 show the computational results for a channel with a straight upper wall. Geometry of the lower wall is chosen so that the relative height of contraction h_d , between $x_{d1} \leq x \leq x_{d2}$, is 0.6. Total length of channel x_d is 3.0. We use the uniform grid of 81×81 . Figures 3.25-3.30 present the pressure contours in a physical domain. Figures 3.25 corresponds to the potential flow with zero vorticity. Figure 3.26 corresponds to the case $a_\omega = 0.1, K = 1.0$. Figure 3.27 corresponds to the case $a_\omega = 1.0, K = 1.0$. Figure 3.28 corresponds to the case $a_\omega = 1.0, K = 2.0$. Figure 3.29 corresponds to the case $a_\omega = 5.0, K = 1.0$. Figure 3.30 corresponds to the case $a_\omega = 5.0, K = 2.0$. The levels of isolines (or isobars) in each figure are labelled by vector v . In Figures 3.29 and 3.30, only seven isolines which are equally distributed between the maximal and minimal values of the pressure field are drawn.

Figures 3.31 and 3.32 illustrate the streamlines (or trajectories) of fluid flow for two particular cases of boundary conditions for the vorticity at the inflow part of the domain boundary. Figure 3.31 corresponds to the case $a_\omega = 5.0, K =$

1.0 and Figure 3.32 corresponds to the case $a_\omega = 5.0, K = 2.0$. Behavior of streamlines are very similar to behavior of streamlines in the case $h_d = 0.1$ as shown in Figures 3.19 and 3.20.

The pressure along a lower boundary as a function of x is shown in Figures 3.33 and 3.34. Figure 3.33 corresponds to the case $K = 1.0$ and $a_\omega = 0; 0.1; 1.0$. The results for the case $a_\omega = 0$ are plotted by the solid line. The dash-dotted line in Figure 3.33 represents the pressure $P(x, 0)$, for the case $a_\omega = 0.1$. The dashed line in Figure 3.33 represents the pressure for the case $a_\omega = 1.0$. The absolute values of the pressure peaks near the point $x = 2.5$ increase together with increasing magnitude a_ω of the vorticity given at the entrance. Figure 3.34 shows the pressure along the lower boundary for two cases corresponding to $a_\omega = 1.0, K = 1.0$ and $a_\omega = 1.0, K = 2.0$. We can see increasing in the pressure peak near the point $x = 2.5$ with increasing values of the parameter K from 1.0 to 2.0. Also we observe that in Figure 3.33, the value of the local extreme in the middle region of the bump is less than the one in the downstream region, but in Figure 3.21, we observe the opposite behavior, that is, the value of local extreme in the middle region of the bump is larger than the one in the downstream region.

Figures 3.35 and 3.36 illustrate the behavior of the pressure at the section $x = 1.5$ for different boundary conditions for the vorticity. Figure 3.35 illustrates the function (3.6.20) for three different values of a_ω and $K = 1.0$ in equation (3.6.19). The solid line in Figure 3.35 corresponding to the case $a_\omega = 0$ represents the case of potential flow of an ideal incompressible fluid. The dashed line represents the function (3.6.20) for the case $a_\omega = 0.1$. The dash-dotted line shows function (3.6.20) for the case $a_\omega = 1.0$. In the case $a_\omega = 1.0$ the function (3.6.20) has a local extreme at the region $0.7 \leq y \leq 0.8$. In Figure 3.36, we represent function (3.6.20) for the two cases $a_\omega = 1.0, K = 1.0$ and $a_\omega = 1.0, K = 2.0$. In the case $K = 2.0$, we can observe local maximum in the interval $0.65 \leq y \leq 0.75$ and a local minimum in the interval $0.75 \leq y \leq 0.85$.

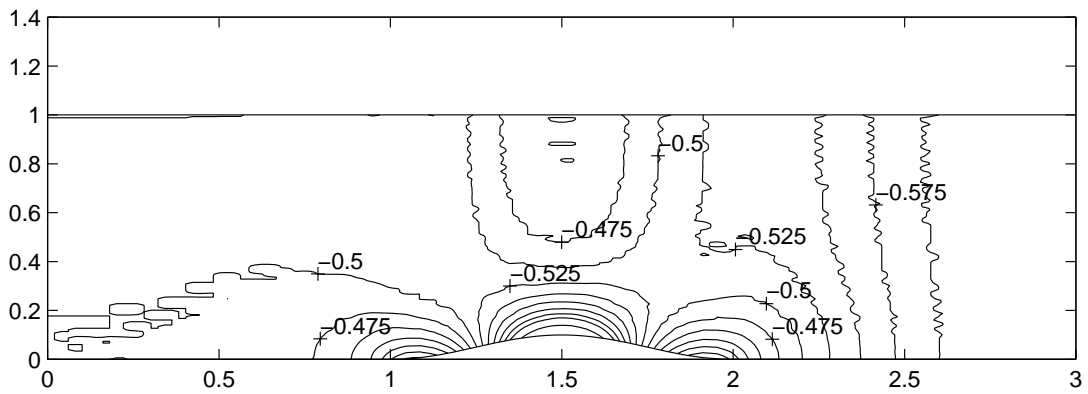


Figure 3.13: Pressure contours for $a_\omega = 0$, $K = 1$, $v = [-0.325 - 0.35 - 0.375 - 0.4 - 0.425 - 0.45 - 0.475 - 0.5 - 0.525 - 0.55 - 0.575 - 0.6 - 0.625 - 0.65 - 0.675 - 0.7 - 0.8 - 0.9 - 1.0]$.

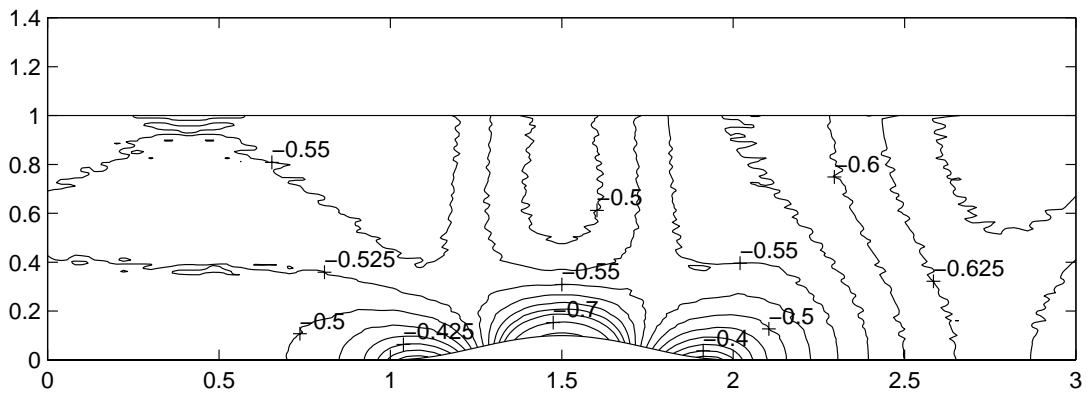


Figure 3.14: Pressure contours for $a_\omega = 0.1$, $K = 1$, $v = [-0.325 - 0.35 - 0.375 - 0.4 - 0.425 - 0.45 - 0.475 - 0.5 - 0.525 - 0.55 - 0.575 - 0.6 - 0.625 - 0.65 - 0.675 - 0.7 - 0.8 - 0.9 - 1.0]$.

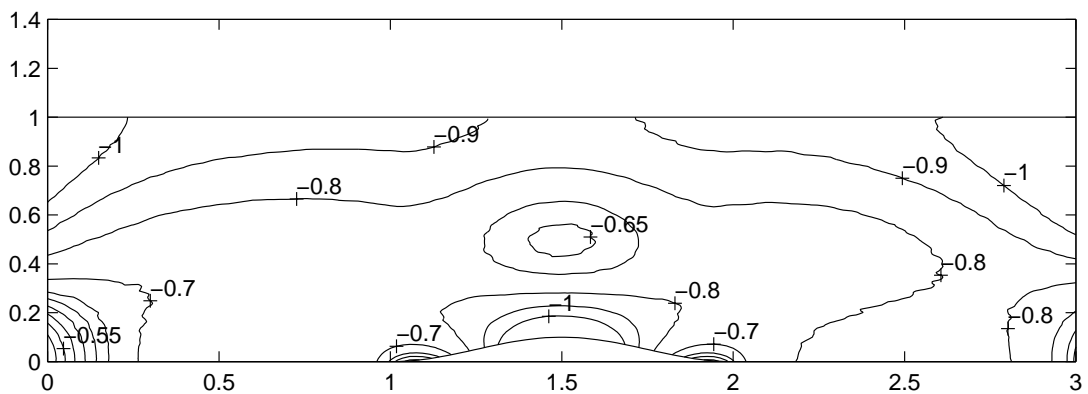


Figure 3.15: Pressure contours for $a_\omega = 1.0$, $K = 1$, $v = [-0.325 - 0.35 - 0.375 - 0.4 - 0.425 - 0.45 - 0.475 - 0.5 - 0.525 - 0.55 - 0.575 - 0.6 - 0.625 - 0.65 - 0.675 - 0.7 - 0.8 - 0.9 - 1.0]$.

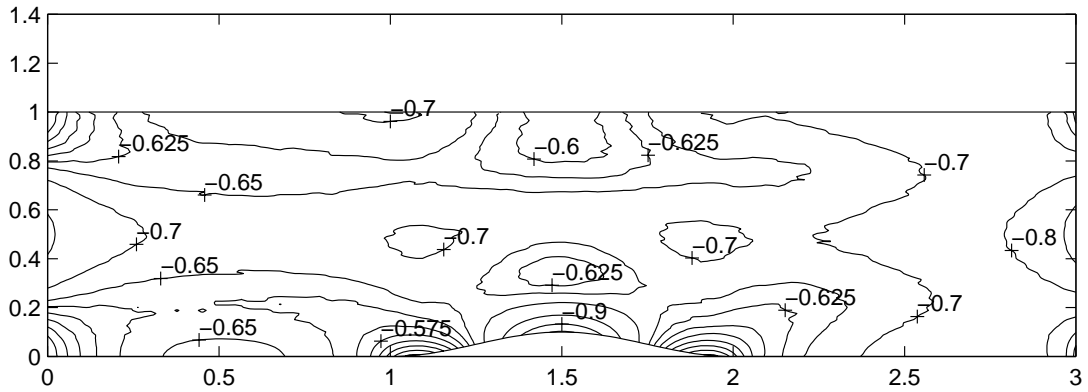


Figure 3.16: Pressure contours for $a_\omega = 1.0$, $K = 2$, $v = [-0.325 \ -0.35 \ -0.375 \ -0.4 \ -0.425 \ -0.45 \ -0.475 \ -0.5 \ -0.525 \ -0.55 \ -0.575 \ -0.6 \ -0.625 \ -0.65 \ -0.675 \ -0.7 \ -0.8 \ -0.9 \ -1.0 \ -1.1 \ -1.2 \ -1.3]$.

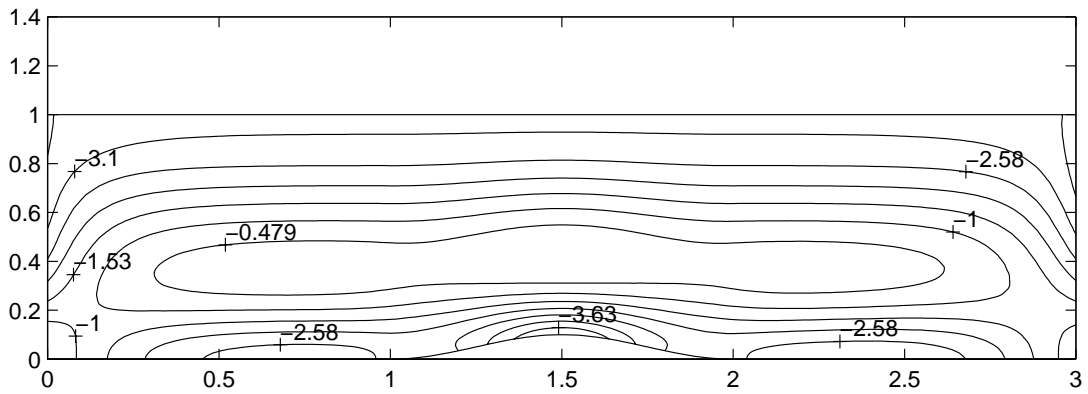


Figure 3.17: Pressure contours for $a_\omega = 5.0$, $K = 1$.

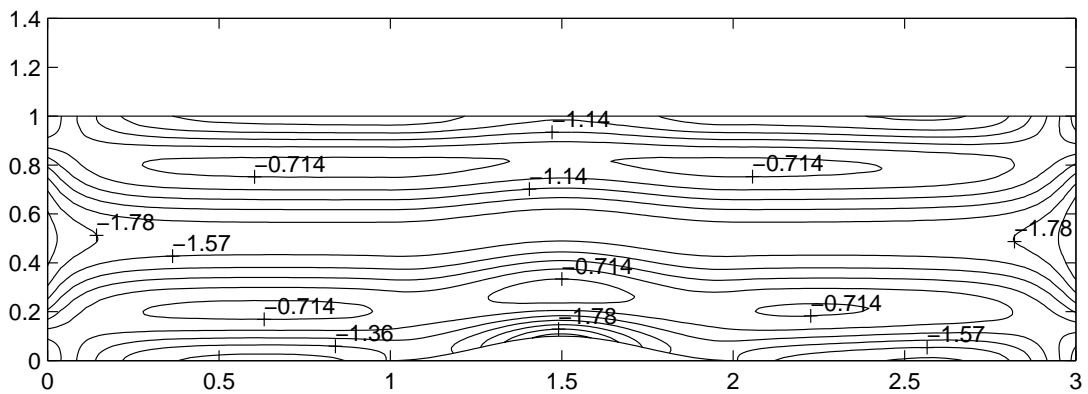


Figure 3.18: Pressure contours for $a_\omega = 5.0$, $K = 2$.

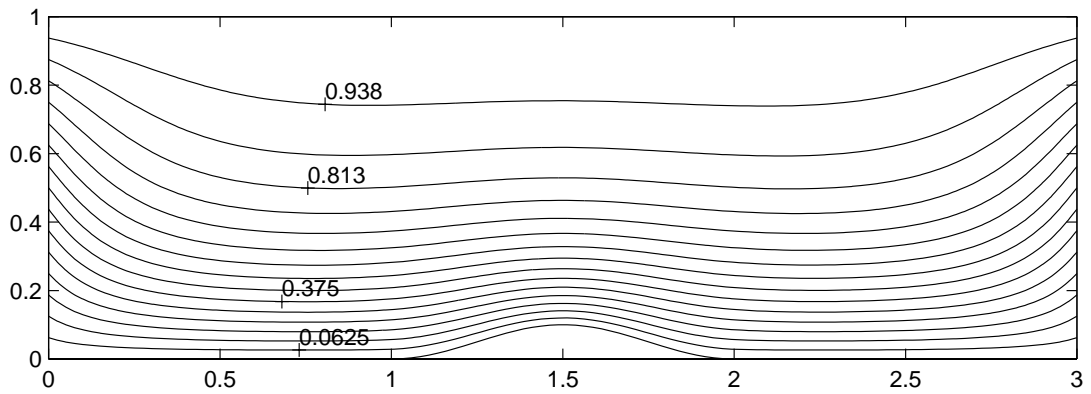


Figure 3.19: Isolines $\psi = \text{constant}$ for the values of the levels vary from 0 to 1.0 with interval 0.0625. $a_\omega = 5.0$, $K = 1$.

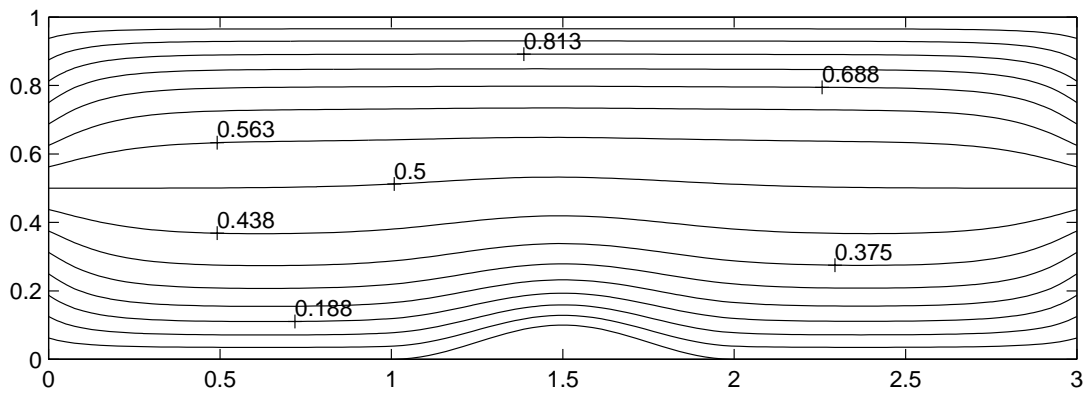


Figure 3.20: Isolines $\psi = \text{constant}$ for the values of the levels vary from 0 to 1.0 with interval 0.0625. $a_\omega = 5.0$, $K = 2$.

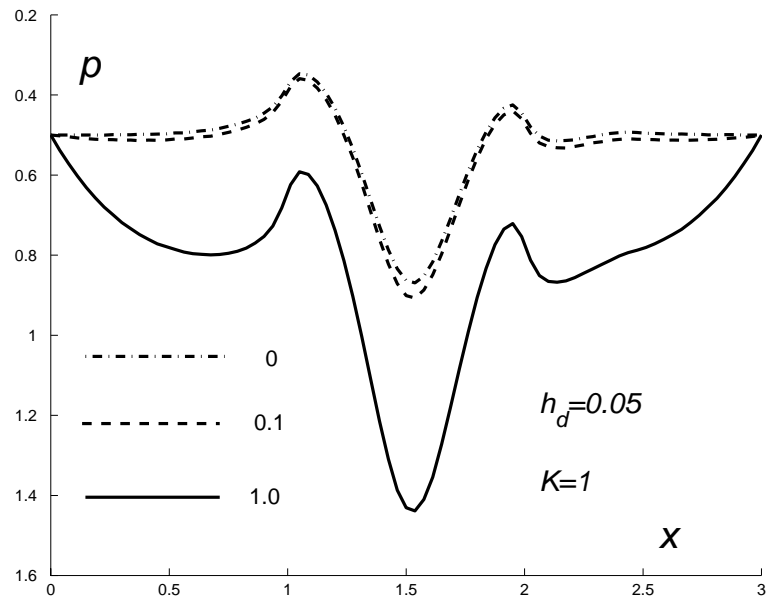


Figure 3.21: The pressure along lower boundary of channel with $x_d = 3.0$, $x_{d1} = 1.0$, $x_{d2} = 2.0$, $h_d = 0.05$. $a_\omega = 0.0; 0.1; 1.0$; $K = 1$.

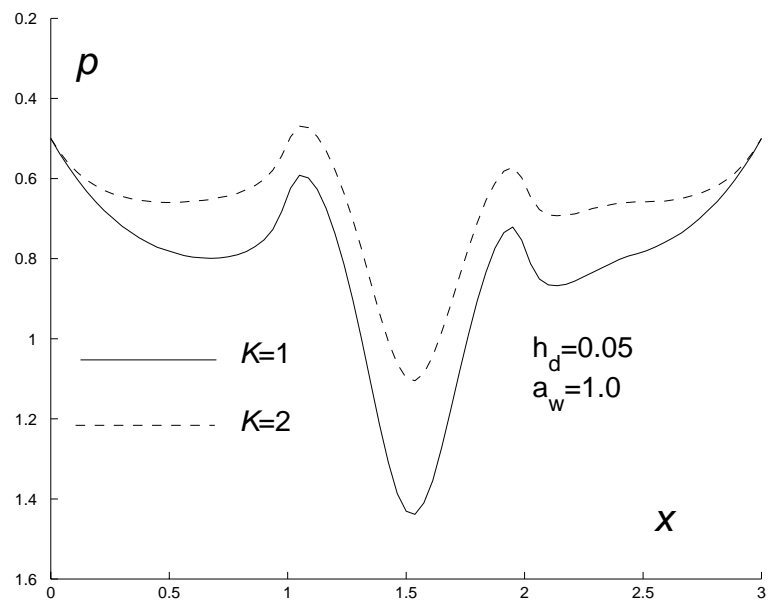


Figure 3.22: The pressure along lower boundary of channel with $x_d = 3.0$, $x_{d1} = 1.0$, $x_{d2} = 2.0$, $h_d = 0.05$. $a_\omega = 0.1$; $K = 1; 2$.

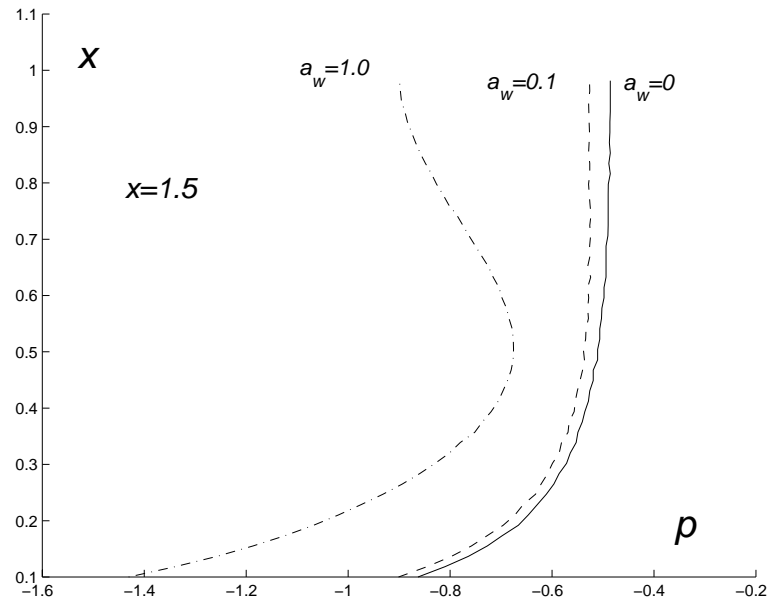


Figure 3.23: The pressure along section $x = 1.5$ of channel with $x_d = 3.0$, $x_{d1} = 1.0$, $x_{d2} = 2.0$, $h_d = 0.05$. $a_w = 0.0; 0.1; 1.0$ $K = 1$.

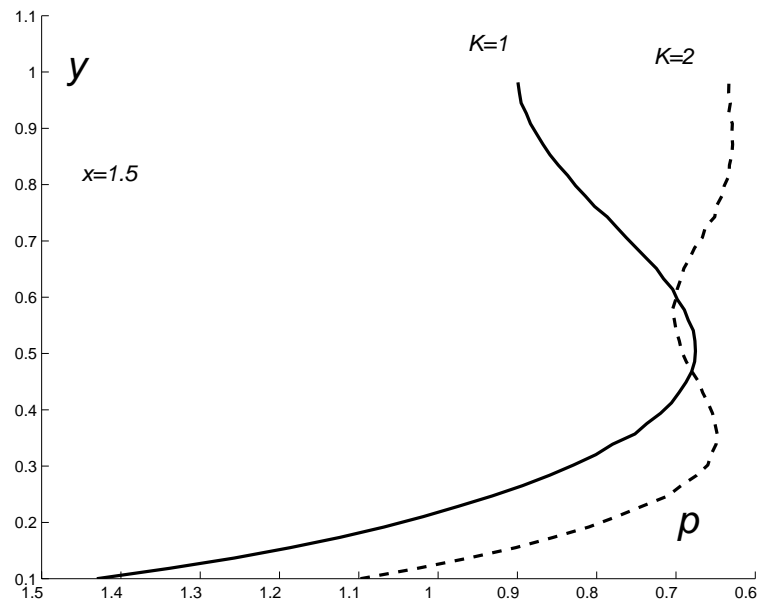


Figure 3.24: The pressure along section $x = 1.5$ of channel with $x_d = 3.0$, $x_{d1} = 1.0$, $x_{d2} = 2.0$, $h_d = 0.05$. $a_w = 1.0$ $K = 1; 2$.

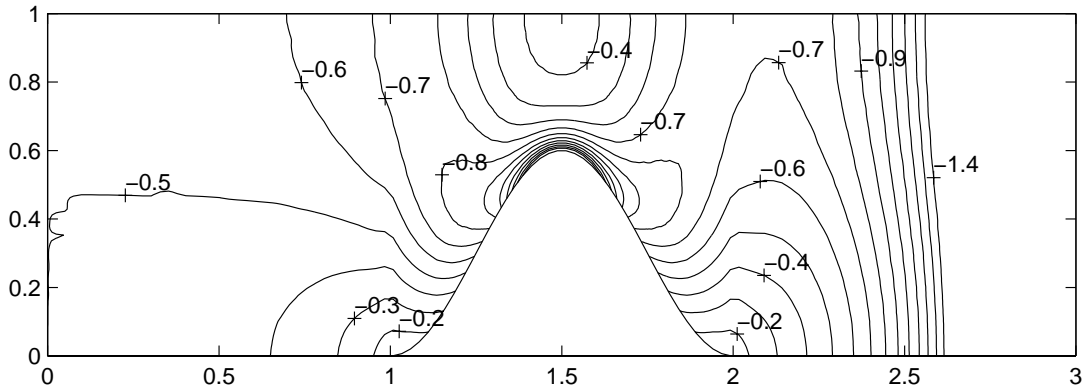


Figure 3.25: Pressure contours for $a_\omega = 0.0$, $K = 1$, $v = [-0.1 - 0.2 - 0.3 - 0.4 - 0.5 - 0.6 - 0.7 - 0.8 - 0.9 - 1.0 - 1.1 - 1.2 - 1.3 - 1.4]$.

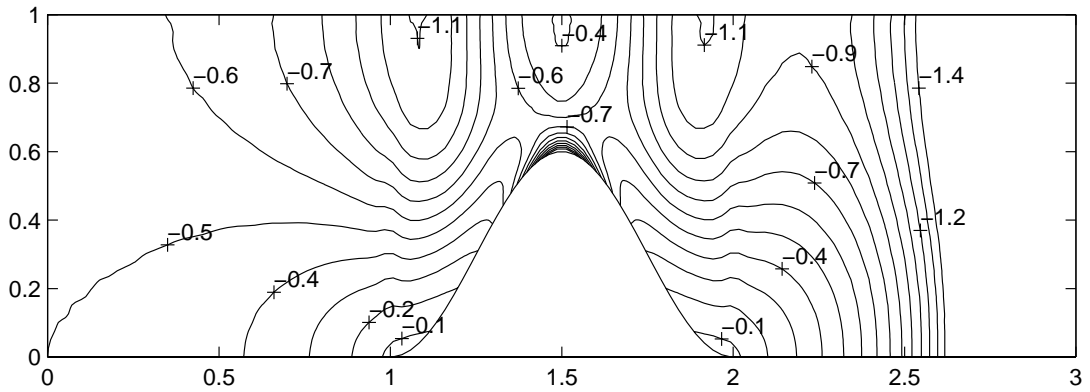


Figure 3.26: Pressure contours for $a_\omega = 0.1$, $K = 1$, $v = [-0.1 - 0.2 - 0.3 - 0.4 - 0.5 - 0.6 - 0.7 - 0.8 - 0.9 - 1.0 - 1.1 - 1.2 - 1.3 - 1.4]$.

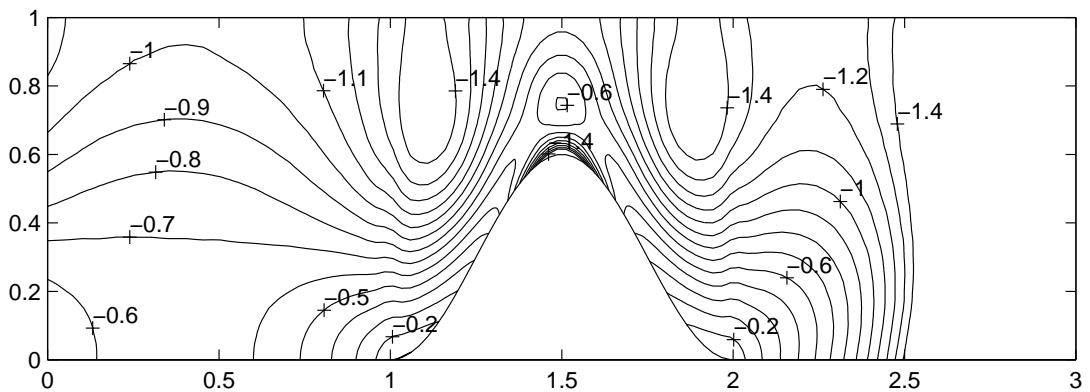


Figure 3.27: Pressure contours for $a_\omega = 1.0$, $K = 1$, $v = [-0.1 - 0.2 - 0.3 - 0.4 - 0.5 - 0.6 - 0.7 - 0.8 - 0.9 - 1.0 - 1.1 - 1.2 - 1.3 - 1.4]$.

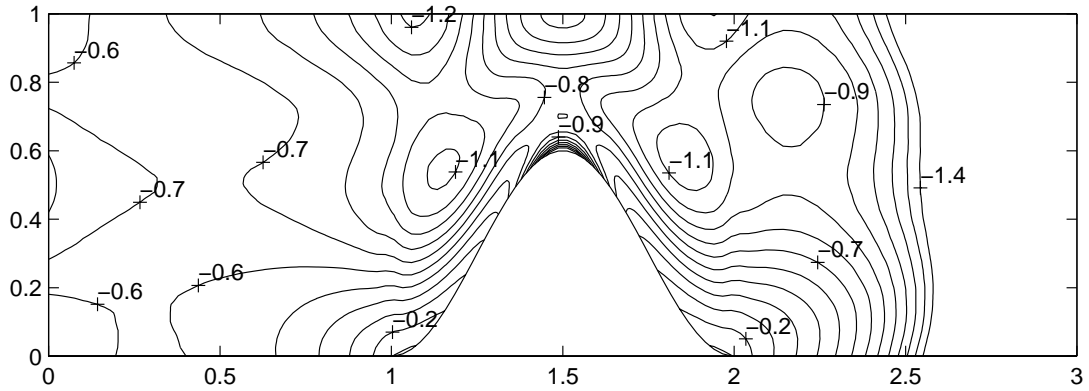


Figure 3.28: Pressure contours for $a_\omega = 1.0$, $K = 2$, $v = [-0.1 - 0.2 - 0.3 - 0.4 - 0.5 - 0.6 - 0.7 - 0.8 - 0.9 - 1.0 - 1.1 - 1.2 - 1.3 - 1.4]$.

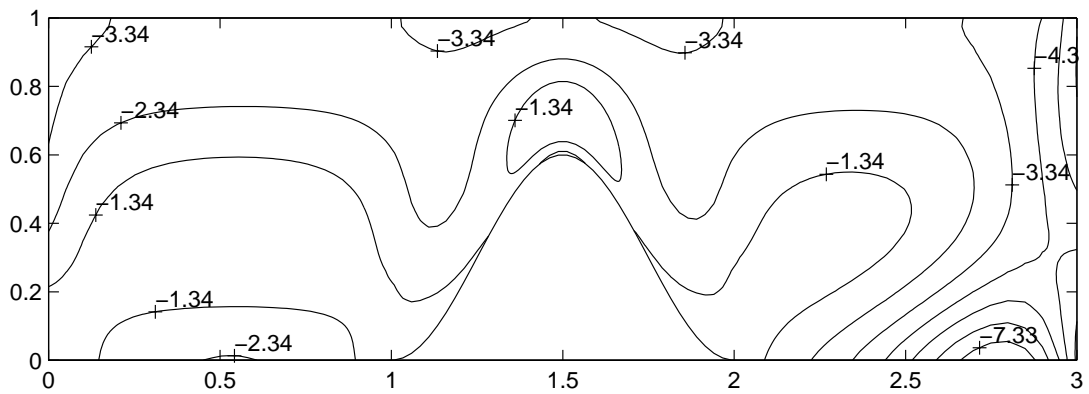


Figure 3.29: Pressure contours for $a_\omega = 5.0$, $K = 1$.

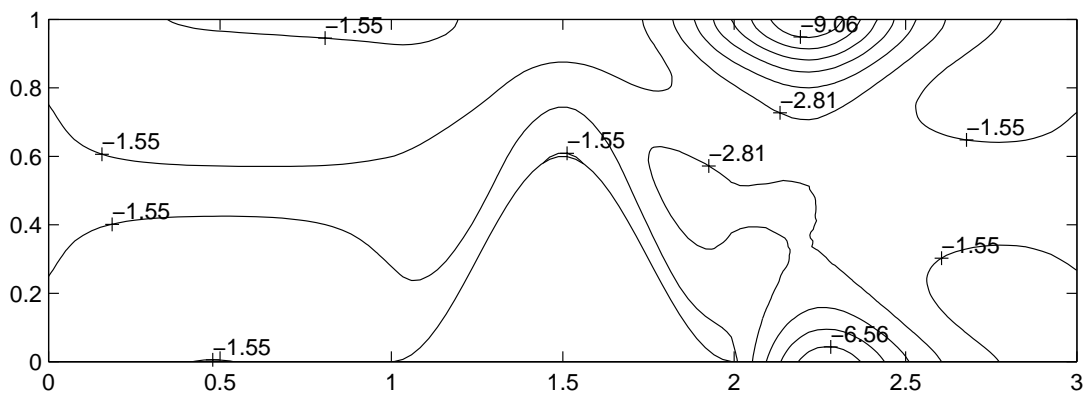


Figure 3.30: Pressure contours for $a_\omega = 5.0$, $K = 2$.

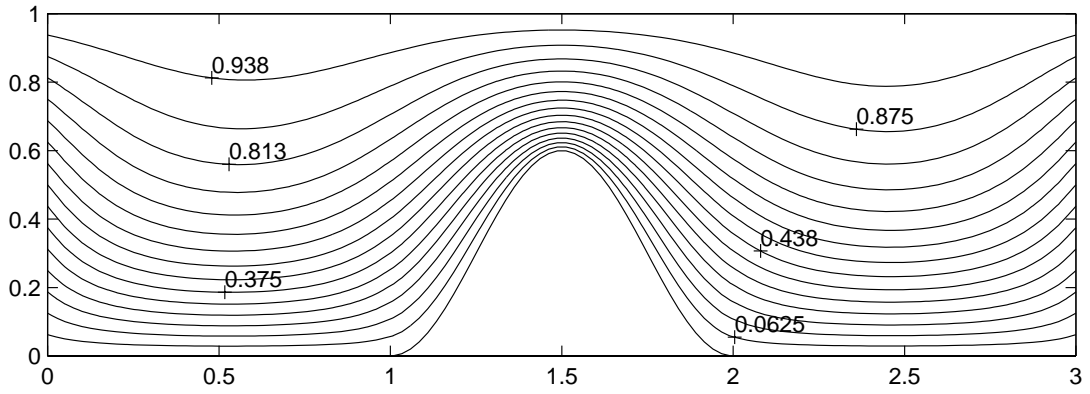


Figure 3.31: Isolines $\psi = \text{constant}$ for the values of the levels vary from 0 to 1.0 with interval 0.0625. $a_\omega = 5.0$, $K = 1$.

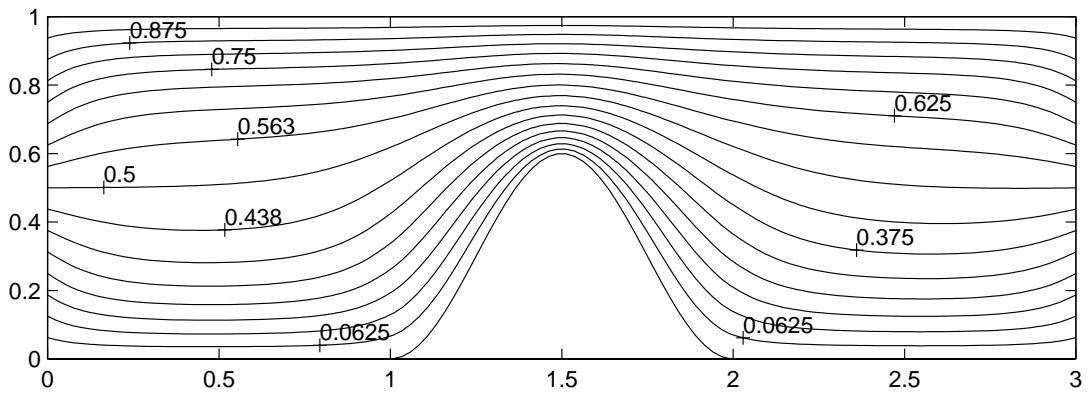


Figure 3.32: Isolines $\psi = \text{constant}$ for the values of the levels vary from 0 to 1.0 with interval 0.0625. $a_\omega = 5.0$, $K = 2$.

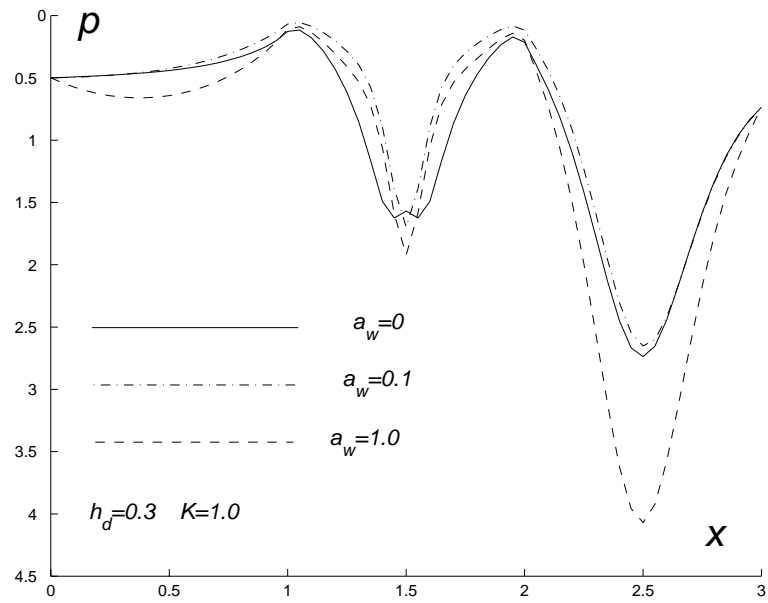


Figure 3.33: The pressure along lower boundary of channel with $x_d = 3.0$, $x_{d1} = 1.0$, $x_{d2} = 2.0$, $h_d = 0.3$. $a_w = 0$; 0.1 ; 1.0 ; $K = 1$.

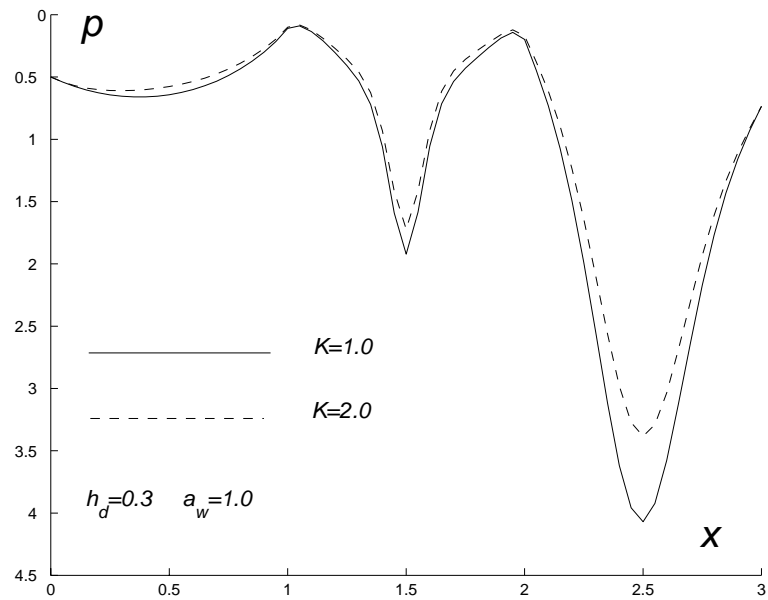


Figure 3.34: The pressure along lower boundary of channel with $x_d = 3.0$, $x_{d1} = 1.0$, $x_{d2} = 2.0$, $h_d = 0.3$. $a_w = 1.0$; $K = 1$; 2 .

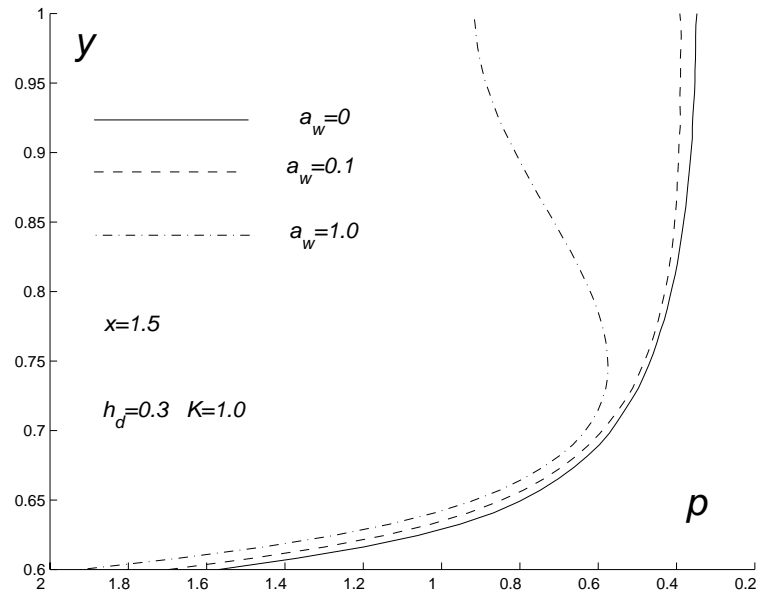


Figure 3.35: The pressure along section $x = 1.5$ of channel with $x_d = 3.0$, $x_{d1} = 1.0$, $x_{d2} = 2.0$, $h_d = 0.3$. $a_\omega = 0; 0.1; 1.0$, $K = 1$.

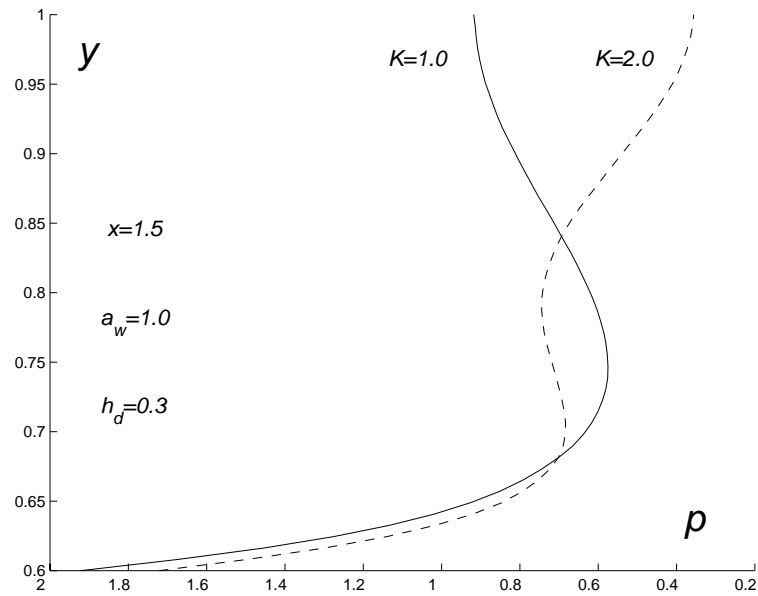


Figure 3.36: The pressure along section $x = 1.5$ of channel with $x_d = 3.0$, $x_{d1} = 1.0$, $x_{d2} = 2.0$, $h_d = 0.3$. $a_\omega = 1.0$, $K = 1; 2$.

3.7 Conclusions

The finite difference algorithms are constructed in this Chapter for steady two-dimensional ‘flowing-through’ problem in which the governing equations are the inviscid Euler equations. These algorithms are essential for boundary value problems in which at the inflow parts of boundary, the normal component of the velocity vector and the tangent components of the vorticity are given, and on the outflow parts, only the normal component of the velocity vector is known. The values of the normal component of velocity are given on the impermeable boundaries.

The vorticity-stream function form of the Euler equations has been exploited to construct the numerical algorithm. The algebraic mapping techniques with one-dimensional stretching functions are used to establish in the correspondence between points in the irregular physical domain and points in the regular computational domain. The algebraic equations produced by discretising the Euler equations in vorticity-stream function form are essentially nonlinear for vortical flow. The appropriate iterative process is suggested in section 3.5. An outer iteration decouples the Poisson equation for stream function and the Helmholtz equation for vorticity. At each step of the outer iteration, a linear system of equations is solved by the SOR or the Stabilizing Correction methods. The Helmholtz equation for vorticity has a hyperbolic character. The marching algorithm based on upwind approximation of convective terms is applied to obtain the downstream development of the vorticity field.

The convergence of the numerical algorithm to exact solution is shown for the test problem with the analytical solution in section 3.6.2. The analytical solution corresponds to essentially the vortical flow with nonlinear dependence of the stream function on the vorticity. For a two-dimensional curved channel, the rate of convergence of numerical method is found by comparison of numerical solutions on a sequence of grids.

The introduction of generalized curvilinear coordinates in section 3.4 allows utilizing the developed numerical algorithm to a large variety of domain geometries.

Chapter IV

Conclusions

The goal of the research is to develop numerical algorithms which yield approximated solutions of the “flowing-through” problems in which the governing equations are the steady Euler equations and to demonstrate the convergence, the accuracy, and the efficiency. The basic goal has been achieved.

Chapter 1 consists of the purpose and background of the research, mathematical formulation of flowing-through problems, some review of literatures and survey of the thesis.

In Chapter 2, the finite difference algorithms for approximate solution of “flowing-through” problem 2 and “flowing-through” problem 3 is proposed. These algorithms are applicable for the boundary value problems such that, at the inflow part of boundary, all components of the velocity vector are known and at the outflow part of the boundary, the normal component of the velocity vector or the values of the pressure are known. The Euler equations are expressed in terms of new unknown functions which are the flow angle (angle between the direction of the velocity vector and direction of the Ox axis) and the modulus of the velocity vector. The new independent variables are used to transform the physical domain to the canonical computational domain. The iterative method is then developed to solve the governing equations. The convergence of algorithm is demonstrated by the comparison of results on a sequence of grids. Numerical results for the two-dimensional duct flow through α degree elbow channel and channel with curved walls are presented and compared with the results in similar cases.

In Chapter 3, the finite difference algorithms for approximate solution of the “flowing-through” problem 3 are proposed. These algorithms are useful for boundary value problem in which on the inflow parts of boundary, the normal component of the velocity vector and the tangent components of the vorticity are known and at the outflow part of boundary, the normal component of velocity vector is known. The Euler equations in $\psi - \omega$ form are transformed to generalized curvilinear coordinates. The staggered grid and the upwind differences are successfully employed to construct the finite difference algorithms. The convergence of numerical algorithm is confirmed in the test problem with analytical solution. The computational techniques in the numerical experiment enable us to determine the realistic estimate of error constant and the order of convergence of numerical algorithms developed in this thesis. Numerical calculations are performed for the two-dimensional inviscid flow through a

channel with curved walls. The proposed schemes are confirmed to be efficient for a wide range of parameters. Strong dependence of the pressure field on the boundary conditions for the vorticity is shown.

The major points of the thesis can be summarized as follows:

- 1) The finite difference algorithms for solving two-dimensional steady “flowing-through” problem of an ideal incompressible fluid are developed.
- 2) The capability of applying numerical algorithms developed in this thesis to a complex geometry is provided by newly-derived Euler equations in terms of new unknowns which are the flow angle and the velocity modulus and in terms of new independent variables which are similar to the stream function and the potential.
- 3) The program by MAPLE V is developed to perform all transformations of governing equations of this algorithm.
- 4) The applicability of numerical algorithms developed in this thesis to arbitrary complex geometries is provided by transforming the Euler equations in $\psi - \omega$ form to generalized curvilinear coordinates using contravariant velocities.
- 5) The computational techniques used in the experimental investigation for the error of a finite difference scheme are presented.
- 6) The accuracy and efficiency are confirmed by examining several flow problems and by comparing the research results with the results obtained from the analytical solutions and other available results as well.

The final remark of the research is that “Numerical Algorithms for Flowing-Through Problem of an Ideal Incompressible Fluid” are intended to be used as tools for studying flow phenomena and for helping design of a flow device.

References

References

- Alekseev G.V., Mokin Yu. A. (1972) **Dinamika Sploshnoi Sredu** 12: 5-13.
- Antontsev, S.N., Kazhikhov, A.V. and Monakhov, V.N. (1990) **Boundary Value Problems in Mechanics of Nonhomogeneous Fluids**. Netherlands.
- Batchelor, C.K. (1970) **An Introduction to Fluid Dynamics**. Cambridge: Cambridge University Press.
- Boris, J.P. and Book, D.L. (1973). **J. Comput. Phys.** 11: 38-69.
- Chorin, A.J. and Marsden, J.E. (1997). **A Mathematical Introduction to Fluid Mechanics**. Springer-Verlay, Heidelberg.
- Courant, R., Isaacson, E. and Rees, M. (1952). **Comm. Pure Appl. Math.** 5: 243-255.
- Di Perua, R.J. and Majda, A. (1987). Concentration in regularizations for 2D incompressible flow. **Comm. Pure Appl. Math.** 40: 511-547.
- Di Perua, R. J. and Majda, A. (1988). Reduced Hausdorff dimension and concentration-cancellation for two dimensional incompressible flow. **J. Amer. Math. Soc.** 1: 59-95.
- Douglas, J. and Gunn, J.E. (1964). A General Formulation of Alternating Direction Implicit Methods, Part I, Parabolic and Hyperbolic Problems. **Numerische Mathematik** 6: 428-453.
- Douglas, J. and Rachford H.H. (1956). On the numerical solution of heat conduction problems in two and three space variables. **Trans. Amer. Math. Soc.** 82: 4231-4239.
- Gunter, N.M. (1927). **Izvestiya Physico-Matematicheskogo Instituta imeni V.A.Steklova** 2(1): 1-168.
- Ebin, D. and Marsden, J. (1970) Groups of diffeomorphisms on the motion of an incompressible fluid. **Ann. of Math.** 92: 102-163.
- Euler, L. (1755). **Memoires de l'Academic des Science**. Berlin.
- Harten, A. (1983). **J. Comput. Phys.** 49: 357-393.
- Hirsch, C. (1990). **Numerical computation of internal and external flows**. New York: John Wiley.

- Hoffman, J.D. (1992). **Numerical methods for engineers and scientists**. America: McGraw Hill & Sons.
- Jameson, A. (1983a). **Appl. Math. Comput.** 13: 327-356.
- Jameson, A. (1983b). **Mech. and Aero. Engrg Report 1651**. Princeton Univ.
- Kato, T. (1967). On classical solutions of the two-dimensional non-stationary Euler equations **Arch. Rational. Mech. and Analysis**. 25(3): 188-200.
- Kato, T. (1972). Non Stationary Flows on viscous and Ideal Fluid in \mathbb{R}^3 . **J. Funct. Anal.** 9: 296-809.
- Kato, T. and Ponce, G. (1988). Commutator Estimates and Navier-Stokes Equations. **Commun. Pure Appl. Math.** 41: 893-907.
- Kazhikhov, A.V. and Ragulin, V.V. (1980). Nonstationary problems on ideal fluid flow through the bounded domain. **Dokl. Akad. Nayk USSR**. 250(6): 1344-1347.
- Kotchin, N.E. (1956). On one existence theorem in hydrodynamics. **Prikladnaya matematika i mekb** 20(2): 153-172.
- Ladyzhenskaya, O.A. (1971). On solvability in small of nonstationary problems for incompressible ideal and viscous fluids and vanishing viscosity **Zapiski Nauch. Seminarov LOMI Akad Nauk SSSR** 21: 65-78.
- Lamb, H. (1932). **Hydrodynamics**, 6th Ed. Cambridge University Press, UK.
- Landau, L.D. and Lifshitz, E.M. (1968). **Fluid Mechanics**. Pergamon Press, Oxford, UK.
- Lax, P.D. (1972). **SIAM Regional Conference Series in Applied Mathematics**, vol. 11, Philadelphia.
- Lax, P.D. and Wendroff, B. (1960). Systems of conservation laws **Comm. Pure Appl. Math.** 13: 217-237.
- Lax, P.D. and Wendroff, B. (1964). **Comm. Pure Appl. Math.** 17: 381-398.
- Lichtenstein, L. (1929). **Grundlagen der Hydromechanics**. Berlin.
- MacCormack, R.W. (1969). The effect of viscosity in hypervelocity impact cratering. **AIAA Paper**. 69-354.
- Marchioro, C. and Pulvirenti, M. (1994). **Mathematical Theory of Incompressible Nonviscous Fluids**. Springer-Verlag, New York, Inc.

- Miller, J.J., O'Riordan, E. and Shishkin, G. I. (1996). Fitted Numerical Methods for Singular Perturbation Problems. **World Scientific Publishing Co.** Singapore, New Jersey, London, Hong Kong.
- Osipov, I.L. Pashenko, V.P. and Shippillin, A.V. (1978). Calculation of inviscous gas flow within channel with essential change of geometry. **Comm. Math. Phys.** 18: 964-973.
- Peyret, R. and Taylor, T.D. (1983). **Computational Methods for Fluid Flow.** Berlin: Springer-Ser.
- Poinsot, T.J. and Lele, S.K. (1992). **J. Comput. Phys.** 101: 104-129.
- Quartapelle, L. (1993). **Numerical Solution of the Incompressible Navier-Stokes Equations.** Berlin. Germany.
- Roache, R.J. (1976). **Computational Fluid Dynamics.** Hermosa Publishers, Albuquerque.
- Roberts, T.W. Swanson, R.C. and Sidilkover, D. (1999). **J. Comput. Fluids.** 28: 427-442.
- Serrin, J. (1959). Mathematical Principles of Classical Fluid Mechanics. **Handbook der Phys.** 8: 125.
- Shikin, E.V. (1995). **Handbook and Atlas Curves.** Boca Raton, New York, london and Tokyo Press.
- Strikwerda, J.C. (1977). **Comm. Pure Appl. Math.** 30: 797-805.
- Swann, H.S. (1970). The convergence with vanishing viscosity of nonstationary Navier-Stokes flow to ideal in R_3 . **Trans. Amer. Math. Soc.** 157(3): 373-398.
- Temam, R. (1975). On the Euler Equation of Incompressible Perfect Fluids. **J. Funct. Anal.** 20(1): 32-43.
- Temam, R. (1976). Local Existence of C^∞ Solution of the Euler Equations of Incompressible Perfect Fluids. **Lecture Notes in Mathematics** 565: Springer-Verlay, Newyork.
- Temam, R. (1986). Remarks on the Euler Equations in Nonlinear Functional Analysis and Its Applications (Browder, F. Ed.). **AMS Proceedings of Symposium in Pure Mathematics** 45: 429-480.
- Van Leer, B. (1977). **J. Comput. Phys.** 23: 276-299.
- Van Leer, B. (1979). **J. Comput. Phys.** 32: 101-136.
- Wolibner, W. (1933). **Math. Zs.** B. 37: 698.

- Yanenko, N.N. (1971) **The Method of Fractional Step: The solution of problems of mathematical physics in several variables.** New York, Berlin and Heidelberg: Springer-Verlag.
- Yudovich, V.I. (1963). Non-Stationary flow on an Ideal Incompressible Liquid. **USSR Comput. Math. Math.Phys.** 3: 1407-1456.
- Yudovich, V.N. (1964). Two-dimensional nonstationary problem of ideal incompressible fluid flow through the given domain. **Mat. Sbornik** 4(4): 562-588.

Appendix

Appendix A

Examples of MAPLE Program.

A.1 The MAPLE program for transformation the Euler equations. See equations (2.2.10)-(2.2.14) in Chapter 2.

```
> restart;
> eq1:=u(x,y)*diff(u(x,y),x)
      +v(x,y)*diff(u(x,y),y)
      +diff(p(x,y),x);
> eq2:=u(x,y)*diff(v(x,y),x)
      +v(x,y)*diff(v(x,y),y)
      +diff(p(x,y),y);
> eq3:=diff(u(x,y),x)+diff(v(x,y),y);
> eq4:=simplify(diff(eq1,y)-diff(eq2,x));
> eq4:=subs(u(x,y)
      =w(x,y)*cos(q(x,y)),v(x,y)
      =w(x,y)*sin(q(x,y)),eq4);
> eq4:=simplify(eq4);
> eq3:=subs(u(x,y)
      =w(x,y)*cos(q(x,y)),v(x,y)
      =w(x,y)*sin(q(x,y)),eq3);
> eq:=simplify(eq3);
> eq4:=subs(diff(w(x,y),x,y)
      =wxy,diff(q(x,y),x,y)
      =qxy,diff(w(x,y),x,x)
      =wxx,
      diff(w(x,y),y,y)=wyy,diff(q(x,y),x,x)
      =qxx,diff(q(x,y),y,y)
      =qyy,
      diff(w(x,y),x)=wx,diff(w(x,y),y)
      =wy,diff(q(x,y),x)
      =qx,
      diff(q(x,y),y)=qy,eq4);
> eq3_x:=diff(eq3,x);
> eq3_y:=diff(eq3,y);
> eq3_x:=subs(diff(w(x,y),x,y)
      =wxy,diff(q(x,y),x,y)
```

```

      =qxy,
diff(w(x,y),x,x)=wxx,diff(w(x,y),y,y)
      =wyy,diff(q(x,y),x,x)
      =qxx,
diff(q(x,y),y,y)=qyy,diff(w(x,y),x)
      =wx,diff(w(x,y),y)
      =wy,
diff(q(x,y),x)=qx,diff(q(x,y),y)
      =qy,eq3_x);
> eq3_y:=subs(diff(w(x,y),x,y)
      =wxy,diff(q(x,y),x,y)
      =qxy,
diff(w(x,y),x,x)=wxx,diff(w(x,y),y,y)
      =wyy,diff(q(x,y),x,x)
      =qxx,
diff(q(x,y),y,y)=qyy,
> diff(w(x,y),x)=wx,diff(w(x,y),y)
      =wy,diff(q(x,y),x)
      =qx,
diff(q(x,y),y)=qy,
> eq3_y);
> SolutionSet:=solve({eq3_x=0,eq3_y},{wxy,qxy});
> assign(SolutionSet);
> wxys;
> qxys;
> simplify(subs(qxy=qxys,wxy=wxys,eq3_x));
> simplify(subs(qxy=qxys,wxy=wxys,eq3_y));
> eq4:=simplify(subs(qxy=qxys,wxy=wxys,eq4));
> eq3_1:=subs(diff(w(x,y),x,y)
      =wxy,diff(q(x,y),x,y)
      =qxy,
diff(w(x,y),x,x)=wxx,diff(w(x,y),y,y)
      =wyy,diff(q(x,y),x,x)
      =qxx,
diff(q(x,y),y,y)=qyy,diff(w(x,y),x)
      =wx,diff(w(x,y),y)
      =wy,
diff(q(x,y),x)=qx,diff(q(x,y),y)
      =qy,eq3);
> eq3_2:=simplify(wx*eq3_1*sin(q(x,y)));
> eq11:=subs(wx^2*cos(q(x,y))*sin(q(x,y))=dd,eq3_2);
> sol:=solve(eq11,dd);
> simplify(subs(dd=sol,eq11));
> eq41:=subs(wx^2*cos(q(x,y))*sin(q(x,y))=dd,eq4);
> eq41:=simplify(subs(dd=sol,eq41));

```

```
> eq41:=collect(eq41,w);
> eq3_3:=simplify(wy*eq3_1*cos(q(x,y)));
> eq12:=subs(wy^2*cos(q(x,y))*sin(q(x,y))=dd,eq3_3);
> sol:=solve(eq12,dd);
> eq42:=subs(wy^2*cos(q(x,y))*sin(q(x,y))=dd,eq41);
> eq42:=simplify(subs(dd=sol,eq42));
> eq5:=sort(eq42,[w,wx,wy,qx,qy]);
> eqrr:=simplify(w(x,y)*qx*cos(q(x,y))*eq3_1);
> eqrr:=subs(w(x,y)*wx*qx*cos(q(x,y))^2=dd,eqrr);
> sol:=solve(eqrr,dd);
> eq11:=subs(w(x,y)*wx*qx*cos(q(x,y))^2=dd,eq5);
> eq11:=simplify(subs(dd=sol,eq11));
> eq5:=simplify(eq11);
> eqrr:=simplify(w(x,y)*qy*sin(q(x,y))*eq3_1);
> eqrr:=subs(w(x,y)*wx*qy*cos(q(x,y))*sin(q(x,y))=dd,eqrr);
> sol:=solve(eqrr,dd);
> eq11:=subs(w(x,y)*wx*qy*cos(q(x,y))*sin(q(x,y))=dd,eq5);
> eq11:=simplify(subs(dd=sol,eq11));
> eq5:=simplify(eq11);
```


A.2 The MAPLE program for transformation the Euler equations from coordinates (x, y) to (φ, ψ) . See equations (2.2.23)-(2.2.29) in Chapter 2.

```

> restart;
> dqdf:=diff(q(f,p),f);
> dqdp:=diff(q(f,p),p);
> eq_x:=-c*w(f,p)^3*sin(q(f,p))*dqdp+w(f,p)^2*cos(q(f,p))/sf(f,p)
    *dqdf;
> eq_y:=c*w(f,p)^3*cos(q(f,p))*dqdp+w(f,p)^2*sin(q(f,p))/sf(f,p)
    *dqdf;
> eqdyy:=c*w(f,p)*cos(q(f,p))*diff(eq_y,p)+sin(q(f,p))/sf(f,p)
    *diff(eq_y,f);
> eqdxx:=-c*w(f,p)*sin(q(f,p))*diff(eq_x,p)+cos(q(f,p))/sf(f,p)
    *diff(eq_x,f);
> eq:=simplify(eqdxx+eqdyy);
> hx:=-c*w(f,p)*sin(q(f,p))*diff(sin(q(f,p))/sf(f,p),p)
    +cos(q(f,p))/sf(f,p)*diff(sin(q(f,p))/sf(f,p),f);
> hy:=c*w(f,p)*cos(q(f,p))*diff(cos(q(f,p))/sf(f,p),p)
    +sin(q(f,p))/sf(f,p)*diff(cos(q(f,p))/sf(f,p),f);
> hxy:=simplify(sf(f,p)^2*(hx-hy));
> eq4:=simplify(sf(f,p)*eq);
> mx:=-c*w(f,p)*sin(q(f,p))*diff(cos(q(f,p))*w(f,p),p)
    +cos(q(f,p))/sf(f,p)*diff(cos(q(f,p))*w(f,p),f);
> my:=c*w(f,p)*cos(q(f,p))*diff(sin(q(f,p))*w(f,p),p)
    +sin(q(f,p))/sf(f,p)*diff(sin(q(f,p))*w(f,p),f);
> mxy:=simplify(mx+my);
> simplify(eqm4);
> eq4;
> l1:=c^2*w(f,p)*sf(f,p)*diff(w(f,p)^3*diff(q(f,p),p),p);
> l2:=diff(w(f,p)^2/sf(f,p)*diff(q(f,p),f),f);
> l2:=simplify(l2);
> l1:=simplify(l1);
> eq4_1:=simplify(l1+l2);
> eq4-eq4_1;

```

A.3 The MAPLE program for transformation the Euler equations. See equations (2.3.11)-(2.3.16) in Chapter 2.

```

> FI:=fs(x,y,f,p):
> p_x:=w(x,y,f,p)*cos(q(x,y,f,p))*diff(w(x,y,f,p)
      *cos(q(x,y,f,p)),x)+
      w(x,y,f,p)*sin(q(x,y,f,p))*diff(w(x,y,f,p)*cos(q(x,y,f,p)),y)+
      diff(pr(x,y,f,p),x);
> p_y:=w(x,y,f,p)*cos(q(x,y,f,p))*diff(w(x,y,f,p)
      *sin(q(x,y,f,p)),x)
      +w(x,y,f,p)*sin(q(x,y,f,p))*diff(w(x,y,f,p)*sin(q(x,y,f,p)),y)
      +diff(pr(x,y,f,p),y);
> eq_cont:=diff(w(x,y,f,p)*cos(q(x,y,f,p)),x)+diff(w(x,y,f,p)
      *sin(q(x,y,f,p)),y);
> eq_cont:=subs(diff(q(x,y,f,p),x)=diff(q(x,y,f,p),f)*1/FI
      *cos(q(x,y,f,p))-diff(q(x,y,f,p),p)*c*w(x,y,f,p)*sin(q(x,y,f,p)),
      diff(q(x,y,f,p),y)=diff(q(x,y,f,p),f)*1/FI*sin(q(x,y,f,p))
      +diff(q(x,y,f,p),p)*c*w(x,y,f,p)*cos(q(x,y,f,p)),
      diff(w(x,y,f,p),x)=diff(w(x,y,f,p),f)*1/FI*cos(q(x,y,f,p))
      -diff(w(x,y,f,p),p)*c*w(x,y,f,p)
      *sin(q(x,y,f,p)),diff(w(x,y,f,p),y)
      =diff(w(x,y,f,p),f)*1/FI*sin(q(x,y,f,p))+diff(w(x,y,f,p),p)*c
      *w(x,y,f,p)*cos(q(x,y,f,p)),eq_cont):
> eq_cont:=simplify(eq_cont);
> p_x:=subs(diff(q(x,y,f,p),x)=diff(q(x,y,f,p),f)*1/FI
      *cos(q(x,y,f,p))
      -diff(q(x,y,f,p),p)*c*w(x,y,f,p)*sin(q(x,y,f,p)),
      diff(q(x,y,f,p),y)=diff(q(x,y,f,p),f)*1/FI*sin(q(x,y,f,p))
      +diff(q(x,y,f,p),p)*c*w(x,y,f,p)*cos(q(x,y,f,p)),
      diff(w(x,y,f,p),x)=diff(w(x,y,f,p),f)*1/FI*cos(q(x,y,f,p))
      -diff(w(x,y,f,p),p)*c*w(x,y,f,p)
      *sin(q(x,y,f,p)),diff(w(x,y,f,p),y)
      =diff(w(x,y,f,p),f)*1/FI*sin(q(x,y,f,p))+diff(w(x,y,f,p),p)*c
      *w(x,y,f,p)*cos(q(x,y,f,p)),diff(pr(x,y,f,p),x)
      =diff(pr(x,y,f,p),f)
      *1/FI*cos(q(x,y,f,p))-diff(pr(x,y,f,p),p)*c*w(x,y,f,p)
      *sin(q(x,y,f,p)), p_x):
> p_x:=simplify(p_x);
> p_y:=subs(diff(q(x,y,f,p),x)=diff(q(x,y,f,p),f)*1/FI
      *cos(q(x,y,f,p))
      -diff(q(x,y,f,p),p)*c*w(x,y,f,p)*sin(q(x,y,f,p)),
      diff(q(x,y,f,p),y)=diff(q(x,y,f,p),f)*1/FI*sin(q(x,y,f,p))
      +diff(q(x,y,f,p),p)*c*w(x,y,f,p)*cos(q(x,y,f,p)),
      diff(w(x,y,f,p),x)=diff(w(x,y,f,p),f)*1/FI*cos(q(x,y,f,p))
      -diff(w(x,y,f,p),p)*c*w(x,y,f,p)
      *sin(q(x,y,f,p)),diff(w(x,y,f,p),y)

```

```

=diff(w(x,y,f,p),f)*1/Fl*sin(q(x,y,f,p))+diff(w(x,y,f,p),p)*c
*w(x,y,f,p)*cos(q(x,y,f,p)),diff(pr(x,y,f,p),y)
=diff(pr(x,y,f,p),f)
*1/Fl*sin(q(x,y,f,p))+diff(pr(x,y,f,p),p)*c*w(x,y,f,p)
*cos(q(x,y,f,p)), p_y):
> p_y:=simplify(p_y);
> px_1:=subs(diff(w(x,y,f,p),p)=w_p,diff(q(x,y,f,p),f)
=q_f,diff(w(x,y,f,p),f)=w_f,diff(q(x,y,f,p),p)
=q_p,diff(pr(x,y,f,p),p)=pr_p,diff(pr(x,y,f,p),f)=pr_f,p_x);
> py_1:=subs(diff(w(x,y,f,p),p)=w_p,diff(q(x,y,f,p),f)
=q_f,diff(w(x,y,f,p),f)=w_f,diff(q(x,y,f,p),p)
=q_p,diff(pr(x,y,f,p),p)=pr_p,diff(pr(x,y,f,p),f)=pr_f,p_y);
> p_p:=px_1*sin(q(x,y,f,p))-py_1*cos(q(x,y,f,p));
> p_f:=px_1*cos(q(x,y,f,p))+py_1*sin(q(x,y,f,p));
> p_f:=simplify(p_f);
> dpdf:=solve(p_f=0,pr_f);
> p_p:=simplify(p_p);
> dpdp:=solve(p_p=0,pr_p);
> eq_cont:=subs(diff(w(x,y,f,p),p)=w_p,diff(q(x,y,f,p),f)
=q_f,diff(w(x,y,f,p),f)=w_f,diff(q(x,y,f,p),p)=q_p,eq_cont);
> sol_1:=solve(eq_cont=0,w_f);
> dpf:=subs(w_f=sol_1,dpdf);
> dpf:=simplify(dpf);

```

Curriculum Vitae

FIRST NAME: Peiangpob

LAST NAME: Mounnamprang

SEX: Female

NATIONALITY: Thai

DATE OF BIRTH: 8 January 1959

EDUCATION BACKGROUND:

- M. A. in Teaching Mathematics, April 1985, Kasatsart University, Bangkok, Thailand.

WORK EXPERIENCE:

- Lecturer in Mathematics at Rajabhat Petbureewittayalongkorn Institutes, Pathumthani, Thailand. 1985-2001.
- Teaching Assistant, School of Mathematics, Suranaree University of Technology, Nakhon Ratchasima, Thailand.

PUBLICATIONS:

- N. P. Moshkin and P. Mounnumprang, "On Numerical Algorithm for the Steady Euler Equations for Flowing-Through Problem", Proc. The Fourth Annual National Symposium on Computational Science and Engineering (ANSCSE'2000), March 27-29, 2000, Kasetsart University, Bangkok, Thailand, pp. 56-64.
- P. Mounnumprang and N. P. Moshkin, "A Numerical Method for solving the Incompressible Euler Equations for Flowing-Through Problem", Proc. The First National Symposium on Graduate Research (GRS-I), June 10-11, 2000, Chiangmai University, Chiangmai, Thailand, pp. 260-266.
- N. P. Moshkin and P. Mounnumprang, "Numerical Simulation of Ideal Incompressible Fluid Flows Through Bounded Domain When Tangent Components of Vorticity are Given on the Inflow Parts of the Domain Boundary", Proc. The Fifth Annual National Symposium on Computational Science and Engineering (ANSCSE'2001), June 19-20, 2001, Bangkok Conventional Center (BCC), Central Plaza, Thailand, pp. 141-149.